

Induction of autophagy by non-structural protein 6 in important animal and human coronaviruses

By

Tyler Josh Daubrah-Scott

Thesis submitted to the University of Nottingham for the degree of Master of Research in Veterinary Science (MRes)

School of Veterinary Medicine and Science

The University of Nottingham

2024

Abstract

Coronaviruses (CoVs) are known to interfere and modulate host-cell processes to promote viral replication and evade immunity. A key role presented in available literature is that CoVs can modulate autophagy, a process critical to homeostatic maintenance. This thesis investigates the role of non-structural protein 6 (NSP6) of coronaviruses, including FCoV, the cause of feline infectious peritonitis virus (FIP), human CoV-OC43 (HCoV-OC43) and serve acute respiratory syndrome CoV 2 (SARS-CoV-2) in the manipulation of autophagy. Bioinformatic analysis, including Clustal Omega multiple sequence alignment and transmembrane prediction tools, showed that NSP6 has relatively few conserved domains and transmembrane regions across the viral species, potentially suggesting functional similarities may be preserved through structural adaptations, rather than sequence conservation.

Restriction digest cloning was employed to clone the NSP6 protein of the three viral species into a pCAGGS_mCherry vector, enabling protein expression analysis to investigate its effects on autophagy. Immunoblotting and indirect immunofluorescence showed an increase in production of autophagosomes when cells expressed NSP6, whilst also appearing to impair autophagic flux, observed by the accumulation of LC3-II and p62/SQSTM1, respectively. NSP6 appeared to have an effect mTOR signalling, which is a critical regulator of autophagy induction. Additionally, NSP6 was observed to co-localise with BST-2, indicating a potential interaction that could aid in the evasion of innate immunity by coronaviruses.

This study concludes that NSP6 may have a role in the modulation of autophagy, which could enhance viral survival and replication. In addition, co-localisation with BST-2 suggests that NSP6 may also play a role in evading host immunity and enhancing the viral survival in cells. Future studies could include analysis of NSP6 in autophagy knockout cell lines (e.g. ATG5 KO) and exploring the broader implications

of potential interactions between NSP6, BST-2 and the autophagy pathway, providing an insight into host immune evasion.

Acknowledgements

I would like to express my deepest gratitude to my supervisors, Dr Stephen Dunham, Dr Robert Stott-Marshall, Dr Christopher Coleman and Dr Toshana Foster for their amazing support and guidance throughout the entirety of this MRes project. I greatly appreciate the feedback and input into many aspects of my research, ensuring the best possible outcomes were achieved.

I would also like to extend my thanks to the A43 lab group and OneVirology for providing an outstanding working environment, one which I very much looked forward to being in daily!

Finally, I would like to thank my family and friends, especially those I have made more recently, for their encouragement and understanding throughout the whole of this MRes journey!

Author's Declaration

I declare that the work in this thesis was carried out in accordance with the regulations of the University of Nottingham. The work is original and has not been submitted for any other degree at the University of Nottingham or elsewhere.

NAME: Tyler J. Daubrah-Scott

Signature and Date: 

25.09.2024

Contents:

ABSTRACT **1**

ACKNOWLEDGEMENTS **3**

AUTHOR'S DECLARATION **4**

CONTENTS: **5**

FIGURE LIST **9**

TABLE LIST: **10**

ABBREVIATIONS: **11**

1. INTRODUCTION **16**

1.1 Coronaviruses 16
1.1.1 Overview of Coronaviruses 16
1.1.2 Genomic Organisation and Viral Proteins 17

1.2 Viral Replication 25
1.2.1 Viral Binding/Attachment 25
1.2.2 Clathrin-Mediated Endocytosis 27
1.2.3 Viral Fusion 27
1.2.3.1 Viral Replication-Transcriptase Complex 28
1.2.3.2 Viral RNA Synthesis 28
1.2.4 Viral Assembly and Release 29

1.3 Epidemiology and zoonotic potential of coronavirus infections 30
1.3.1 Epidemiology overview 30
1.3.2 Antigenic variation in coronavirus infections 33

1.4 Response to Viral Infection 34
1.4.1 Innate Immunity Overview 34
1.4.1.1 Pathogen Recognition 34
1.4.1.2 Cytokines 35
1.4.1.3 Complement System 37
1.4.1.4 Acute Phase Proteins 40
1.4.2 Dendritic Cells 40
1.4.3 Adaptive Immunity Overview 41
1.4.3.1 T Lymphocytes and Cell-mediated Immunity 41
1.4.3.2 B Cells and Humoral Immunity 42
1.4.4 Overview of autophagy 46

1.5 Drug Therapies and Vaccine Strategies in Coronavirus Infections 50

1.5.1 Therapeutic Management of Hospitalised Coronavirus patients 50
1.5.1.1 Immunomodulatory therapies 51
1.5.2 Vaccine Landscape 53

1.6 The Interactions of Coronavirus NSP6 with Autophagy 53
1.6.1 Overview 53
1.6.2 The Effect of NSP6 on Autophagosome Production 54
1.6.3 The Effect of NSP6 on Autophagic Flux and mTOR Activity 54
1.6.4 The Effect of NSP6 on BST-2/Tetherin 55

1.7 Hypothesis 55

1.8 Aims/Objectives 56

2 METHODS 57

2.1 Restriction Ligation Cloning of NSP6 into pCAGGS_mCherry Vector 57
2.1.1 NSP6 constructs in pUC57 vector 57
2.1.2 PCR 57
2.1.3 Agarose Gel Electrophoresis 58
2.1.4 PCR product purification 59
2.1.5 Restriction digest 59
2.1.6 Gel Purification 60
2.1.7 Ligation 60
2.1.8 Transformation 60
2.1.9 Plasmid MiniPrep 61
2.1.9.1 Test Digest Screening 61
2.1.10 DNA Sequencing 61
2.1.11 DNA MaxiPrep 62
2.1.11.1 DNA quantification 62

2.2 Bioinformatics 62
2.2.1 Sequence Retrieval and Analysis 62
2.2.2 Multiple Alignment 63
2.2.3 Transmembrane Prediction 63

2.3 Cell Culture 64
2.3.1 Cell Culture 64
2.3.2 Continuous Cell Lines 64
2.3.4 Cell line maintenance 64
2.4.1 Transient Transfection 65
2.4.1.1 Preparation of cell lines for Transfection 65
2.4.1.2 Transient Transfection of A549 Cell Line 66
2.4.2 Post-Transfection Drug Treatment 66

2.5 Fluorescent Imaging 67
2.5.1 Fixing Co-Transfected Cells 67
2.5.1.1 Fixing cells for Immunofluorescence 67
2.5.1.2 Antibodies 67
2.5.2 Mounting 68
2.5.3 Widefield microscopy 69

2.6 Protein Expression Analysis and Immunoblotting 69
2.6.1 Preparation of Cell Lysate 69
2.6.3 Polyacrylamide Gel Electrophoresis 69
2.6.3 Western Blotting/ PVDF Membrane Transfer 70
2.6.4 Membrane Blocking 71
2.6.5 Antibody Incubation 71
2.6.6 Chemiluminescence 72
2.6.7 Gel Imaging 73
2.6.8 Gel Analysis and Protein Quantification 73

3. RESULTS 74

3.1 Multiple Sequence alignment 74

3.2 Transmembrane prediction analysis 76

3.3 Restriction digest cloning of NSP6 into a pCAGGS-mCherry vector 81

3.4 Chemical manipulation of autophagy 84
3.5.1 Indirect immunofluorescence detection of autophagosomes 84
3.5.2 Western blot analysis of autophagy 85

3.5 NSP6 enhances the accumulation of autophagosomes 87
3.5.1 Immunofluorescent analysis 87
3.6.2 Western blot results 89

3.6 NSP6 overexpression interferes with autophagic flux 90

3.7 NSP6 modulates mTOR activity 92

3.8 NSP6 co-localises with BST-2/Tetherin 93

4 DISCUSSION 95

4.1 Modulation of autophagy by NSP6 in coronavirus infection 95

4.2 Analysis of bioinformatics 96
4.2.1 Clustal Omega multiple alignment analysis of nucleotides 96
4.2.2 Clustal Omega multiple analysis of protein sequences 96
4.2.3 Transmembrane prediction analysis 97

4.3 Restriction digest cloning of NSP6 into a mammalian expression vector 98

4.4 Protein expression analysis 99
4.4.1 Chemical manipulation of autophagy in A549 cells 99
4.4.2 NSP6 influences the accumulation of autophagosomes 100
4.4.3 NSP6 interferes with autophagic flux 103
4.4.4 Modulation of mTOR activity by NSP6 103
4.4.5 Co-localisation of NSP6 with BST-2/Tetherin 104

4.5 Broader implications of autophagy and immune modulation by NSP6 in coronaviruses 106

4.6 Future directions.....107

5. CONCLUSION.....109

REFERENCES.....110

Figure list

Figure 1: Orthocoronavirinae Subfamily.....17

Figure 2: Genomic structure of coronaviruses.....19

Figure 3: Diagram of the SARS-CoV-2 virion.....22

Figure 4 Coronavirus lifecycle and replication process.....26

Figure 5: The complement system and its three pathways of activation: alternative, classical, and lectin......40

Figure 6: The autophagy pathway.....45

Figure 7: Gel transfer stack.....71

Figure 8: Multiple sequence alignment of NSP6 using Clustal Omega.....76

Figure 9: Transmembrane prediction analysis.....81

Figure 10: Preparation of mCherry-tagged NSP6 expression constructs.....84

Figure 11: Indirect immunofluorescence of autophagy chemical manipulation..85

Figure 12: Chemical manipulation of autophagy western blot.....87

Figure 13: Immunofluorescent analysis of GFP-LC3 expression when co-transfected with mCherry-NSP6.....88

Figure 14: Western blot analysis of autophagosome accumulation when NSP6 transfected into cells.....90

Figure 15: Western blot analysis of the effect NSP6 has on autophagic flux.....91

Figure 16: Western blot analysis of mTOR activity when NSP6 is expressed in cells.....92

Figure 17: Indirect immunofluorescent analysis of BST-2-HA and mCherry-NSP6.....94

Table list:

Table 1: The five types of mammalian immunoglobulins: IgG, IgA, IgM, IgD, IgE......44

Table 2: **Oligonucleotide sequences for restriction digest PCR amplification**.....58

Table 3: Reagents quantities for a typical PCR amplification of NSP6 constructs into pCAGGS_mCherry vector 58

Table 4: Restriction enzyme double digestion reaction used.....59

Table 5: Test digest reaction used.....61

Table 6: NSP6 variants used and GenBank accession numbers 63

Table 7: Antibodies used for Immunofluorescence imaging.....68

Table 8: Antibodies used for Immunoblotting 72

Abbreviations:

+ssRNA	Positive sense single-stranded RNA
3CLpro	3C-like protease
6HB	Six-helix bundle
ACE2	Angiotensin-Converting Enzyme 2
AMPK	Adenosine monophosphate-activated protein kinase
AP	Adaptor protein
ATG	Autophagy related genes
BP	Base pair
BSA	Bovine serum albumin
BST-2	Bone marrow stromal antigen-2
CCP	Clathrin-coated pit
CCV	Clathrin-coated vesicle
CD4+	Cluster of differentiation 4
CD8	Cluster of differentiation 8
CFR	Case fatality rate
CoV	Coronavirus
COX2	Cyclooxygenase 2
CQ	Chloroquine
DC	Dendritic cell
DMN1/2	Dynamin ½
DMV	Double-membrane vesicle
E	Envelope
eIF4E	Eukaryotic translation initiator factor
ER	Endoplasmic reticulum

ERGIC	Endoplasmic reticulum-Golgi intermediate compartment
Exon	Exoribonuclease
fAPN	Feline aminopeptidase N
FBS	Fetal bovine serum
FCoV	feline coronavirus
FIP	Feline infectious peritonitis virus
FP	Fusion peptide
GFP	Green fluorescent protein
GI	Gastrointestinal
HCoV	Human coronavirus
HCV	Hepatitis C virus
HIV	Human immunodeficiency virus
HOPS	Homotypic fusion and protein sorting complex
HR1	Heptad repeat-1
HR2	Heptad repeat-2
HRP	Horseradish peroxidase
IBV	Infectious bronchitis virus
IFN	Interferon
IFN-1	Interferon type 1
IFNAR	IFNα-receptor
IFNGR	IFNγ-receptor
Ig	Immunoglobulin
IKKβ	I Kappa-Beta Kinase
IL	Interleukin
ISG	Interferon stimulating genes
JAK-STAT	Janus kinase signal transducer and activator of transcription

Kb	Kilobases
LC3	Light chain 3
LRTI	Lower respiratory tract infection
M	Membrane
mAb	Monoclonal antibody
MAC	Membrane attack complex
MAPK	Mitogen-activated protein kinases
MERS-CoV	Middle East respiratory syndrome coronavirus
MES	2-(N-morpholino)-ethanesulfonic acid
MHC	Major histocompatibility complex
MHV	Mouse hepatitis virus
mRNA	Messenger RNA
mTOR	Mammalian target of rapamycin
mTORC1	mTOR class 1
N	Nucleocapsid
NendoU	Endoribonuclease
NF-κB	Nucleation Factor-Kappa B
NK	Natural killer cells
NLR	Nod-like receptor
NLRP3	Nucleotide-binding domain, leucine-rich–containing family, pyrin domain–containing-3
NSP	Non-structural protein
NTD	N-terminal domain
OAS	2'-5'-oligodenylatesythetase
ORF	Open reading frame
PAMPS	Pathogen-associated molecular pattern

PBS	Phosphate buffered saline
PBS-T	Phosphate buffered saline- Tween20
PCR	Polymerase chain reaction
PE	Phosphatidylethanolamine
PFA	Paraformaldehyde
PI3KC3	Class III phosphatidylinositol 3-kinase
PLEKHM	Pleckstrin homology domain containing protein family member 1
PLpro	Papain-like protease
PP	Polyprotein
PRR	Pathogen recognition receptor
PVDF	Polyvinylidene fluoride membrane
RAB7	Ras-related protein 7
RBD	Receptor binding domain
RdRp	RNA-dependent RNA-polymerase
RIG-I	Retinoic-acid inducible gene-I-like receptor
R-rate	Reproduction rate
RT	Room temperature
RTC	Replication-transcription complex
S	Spike
S6K	Serine-6 kinase
SDS	Sodium dodecyl sulfate
SF	Serum free
sgRNA	Subgenomic RNA
SNARE	Soluble N-ethylmaleimide-sensitive fusion attachment protein
SQSTM1	Sequestosome 1
STAT-1&2	Signal transducer and activator of transcription-1&2

STX17	Syntaxin 17
TCR	T-cell receptor
TLR	Toll-like receptor
TNF	Tumour necrosis factor
TRS	Transcription-regulated sequences
UKC	ULK1 protein complex
ULK1	Ubiquitin-like kinase 1
URTI	Upper respiratory tract infection
UTR	Untranslated region
VAMP	Vesicle-associated membrane protein
WGS	Whole genome sequencing

1. Introduction

1.1 Coronaviruses

1.1.1 Overview of Coronaviruses

Coronaviruses (CoVs) are a family of positive sense single-stranded RNA (+ssRNA) viruses, that can cause mild-to-severe respiratory infections in humans (V'kovski *et al.*, 2021). In animals they have the potential to cause fatal respiratory and/or gastrointestinal (GI) illness (Tekes and Thiel, 2016). Coronaviruses have the largest viral RNA genomes described thus far, ranging from 27–32 kilobases (kb) in length (Liu, Liang and Fung, 2021). Coronaviruses have a distinct capability to cause severe global health threats, with the most notable of these being Severe Acute Respiratory Syndrome Coronavirus-2 (SARS-CoV-2/COVID-19) and Middle East respiratory syndrome (MERS-CoV, 2012). Coronaviruses belong to the Coronaviridae family, within which the subfamily, *Orthocoronavirinae* encompass four main genera: Alpha-, Beta-, Gamma-, and Delta-coronaviruses (Wang *et al.*, 2020) [Figure 1]. Beta-*Coronaviridae* encompass viruses that are prominent causes of severe human illnesses, as well as viruses responsible for the "common cold". Human coronaviruses (HCoV) account for between 15 and 30% of "common colds" in adults, with little-to-no post-illness pathologies (Liu, Liang and Fung, 2021). MERS-CoV, SARS-CoV, and SARS-CoV-2, however, all have an inherent ability to cause serious illness, with many severe cases being fatal; these viruses all arise from a bat origin and are an indicator of the cross-species transmission seen in many coronaviruses (Helmy *et al.*, 2020).

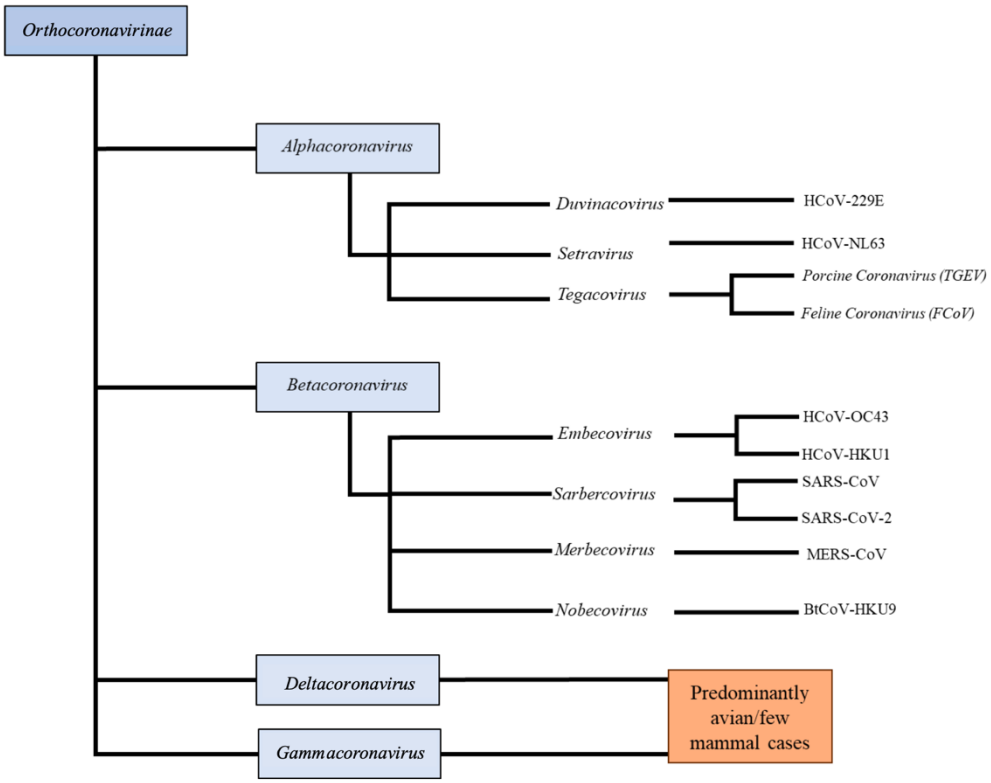

Figure 1: *Orthocoronavirinae* Subfamily

Diagram of the conceptual classifications of coronaviruses (CoV) into the four genera of the *Orthocoronavirinae* subfamily: *alphacoronavirus, betacoronavirus, gammacoronavirus*, and *deltacoronavirus*. It is based on their genetic and phylogenetic relationships. *Alphacoronaviruses* and *betacoronaviruses* predominantly infect mammals and include pathogens such as SARS-CoV-2 and MERS-CoV. Contrastingly, *gammacoronaviruses* and *deltacoronaviruses* primarily affect avian species, but mammalian cases have been observed on occasions. This figure is not to scale and is intended as a conceptual overview of evolutionary relationships. Adapted from: Payne, 2017; Zmasek *et al*., 2022.

1.1.2 Genomic Organisation and Viral Proteins

The +ssRNA genome of CoVs contain a 5' cap and 3' polyadenylate tail; it can function as a messenger RNA (mRNA) which encodes the viral replicase, subsequently, facilitating protein translation in hosts without triggering signalling cascades of innate immunity. In addition, the CoV genome serves as a template for RNA replication, with its genome being packaged into progeny virus particles. The 5’

two-thirds of the genome, the replicase gene within CoVs, comprises two long open reading frames (ORFs): 1a and 1b, which encode polyproteins (PP) 1a and 1ab. Once a co-translational process of proteolytic cleavage occurs by viral protease, 16 non-structural proteins (NSP) arise forming the replication complex (Baranov *et al.*, 2005) [Figure 2]. In addition to the ORFs encoding PP1a and 1ab, the genome also encodes accessory proteins which are linked with antagonism of host immune responses (Liu, Liang and Fung, 2021). Finally, the 4 structural proteins: spike(S), nucleocapsid (N), membrane (M), and envelope (E) comprise the full the genomic structure.

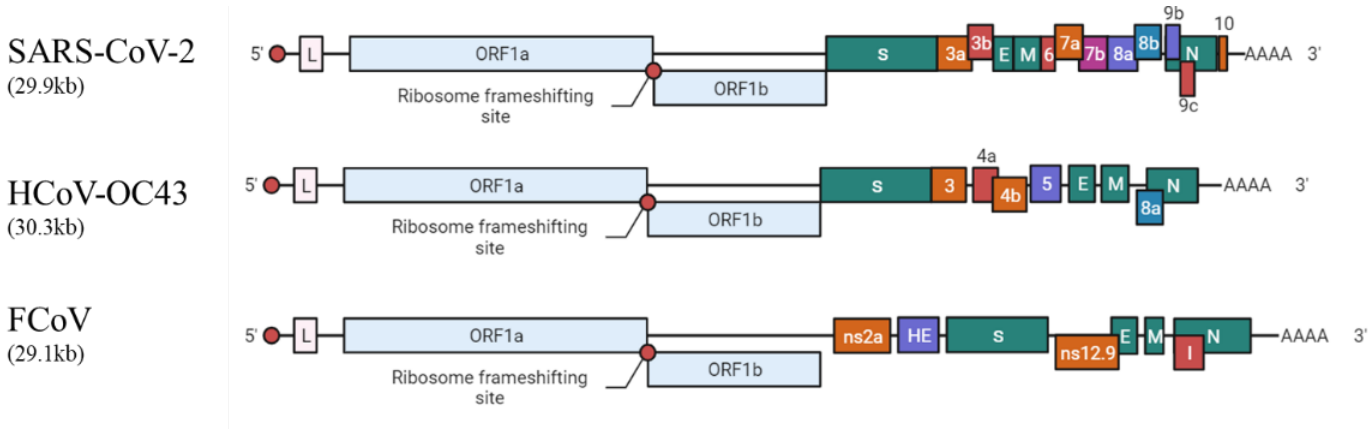

Figure 2: Genomic structure of coronaviruses

The genomic structures of three CoV variants highlighting the ORFs and structural proteins. The 5' untranslated regions (UTRs) are demonstrated by the red circles, with ORFs 1a and 1b highlighted in light blue; these encode NSPs. The ribosomal frameshifting site allows for the translation of ORF1b from ORF1a. Structural proteins are shown in green colour. Accessory proteins, such as 3a, 3b and 8a/b vary across the *betacoronaviruses* (SARS-CoV-2 and HCoV-OC43), highlighted in orange, red and blue, respectively. Additional accessory proteins are observed in SARS-CoV-2, whilst FCoV contains unique accessory proteins such as ns12.9 and n2sa. This figure is not to scale and is utilised for illustrating the genomic differences between CoV variants. Adapted from: Payne, 2017.

1.1.2.1 Structural Proteins and Morphology

Coronaviruses have a spherical structure housing four key structural proteins: S, M, E, and N; which all function to allow successful replication and the formation of progeny virions encapsidating the viral +ssRNA as seen in figure 3 (Satarker and Nampoothiri, 2020).

The S protein is an enveloped, trimeric, class I fusion glycoprotein responsible for the binding of the virus particle to host cell receptors, such as Angiotensin-Converting Enzyme 2 (ACE2) in SARS-CoV-2, which allows viral fusion to occur post-binding (Hoffmann *et al*, 2020). The spike protein possesses an ectodomain element, transmembrane moiety, and a short intracellular C-terminus. The viral ectodomain comprises two subunits: S1, which contains the receptor binding domain (RBD) and

S2, which contains heptad repeat (HR) regions which have a vital role in facilitating membrane fusion. The S protein is heavily glycosylated, which gives protection from host immune detection. Figure 3 (right), shows the spike protein S1 subunit, which has a characteristic “clove” shape, with S2 subunit forming the stem (Satarker and Nampoothiri, 2020).

The N protein is the most abundant viral protein with an important role in packaging of viral RNA and genome replication. It binds to viral RNA genome and forms a ribonucleoprotein complex which helps maintain genome stability, transcription and virion assembly (Chang *et al.*, 2014). N protein also interacts with cellular immune processes after viral entry into hosts following viral fusion, through the suppression of type I interferon (IFN–I) signalling (Wu *et al.*, 2021). Some studies suggest that the N protein has effects on inflammatory pathways, however the suggestion that N protein activates cyclo-oxygenase 2 (COX-2) in SARS-CoV-2 infection delivering a “cytokine storm” remains contested, as inflammatory markers are not as elevated compared with sepsis patients (Chen *et al.*, 2020). It also plays vital roles in the duplication of the centrosomes and degradation of viral proteins.

The E protein is a small, but integral, viroporin with multifunctional properties. The E protein is essential in viral replication as it integrates with the host membrane to facilitate the production and release of spherical viral particles (Gorkhali *et al.*, 2021). It is composed of a hydrophilic N-terminal domain (NTD), hydrophobic transmembrane domain and a hydrophilic C terminal domain which interacts with host proteins such as phospholipid scramblase 1 (PLSCR1), which is a key regulator of membrane trafficking and immune responses (Xia *et al.*, 2020). The E protein has been shown to influence viral replication and immune evasion by oligomerising to form ion channels, which alter intracellular ion homeostasis (Wilson *et al.*, 2004). Disruption of lung epithelia is a consequential feature of the E protein exacerbating lung injury in hosts (Javorsky, Humbert and Kvansakul, 2021).

The highly abundant M protein is critical in virion assembly. It comprises a short-length NTD, attached to a triple transmembrane domain, and a C-terminal ectodomain that interacts with other structural proteins (Masters, 2006). These NTDs are connected to a carboxyl terminal domain, which is N-glycosylated; these are essential for the maintenance of structural integrity of the virion and allow interactions with S and E proteins during viral assembly and budding (Satarker and Nampoothiri, 2020). This protein exists as both a long- and compact-form. The M protein is a homodimer of the N-terminal ectodomain and C terminal endodomain in different conformations; the ectodomain can undergo elongation and compression; these are key in the regulation of viral morphogenesis and budding (Neumann *et al.*, 2011). The M protein interacts with the nucleocapsid protein to stabilise ribonucleoprotein complexes in the virion. Additionally, the M protein inhibits Nucleation Factor-Kappa B (NF-kB) through an interaction with I Kappa-Beta Kinase (IKKβ), reducing COX-2 levels and reducing antiviral inflammatory responses (Kandasamy, 2021).

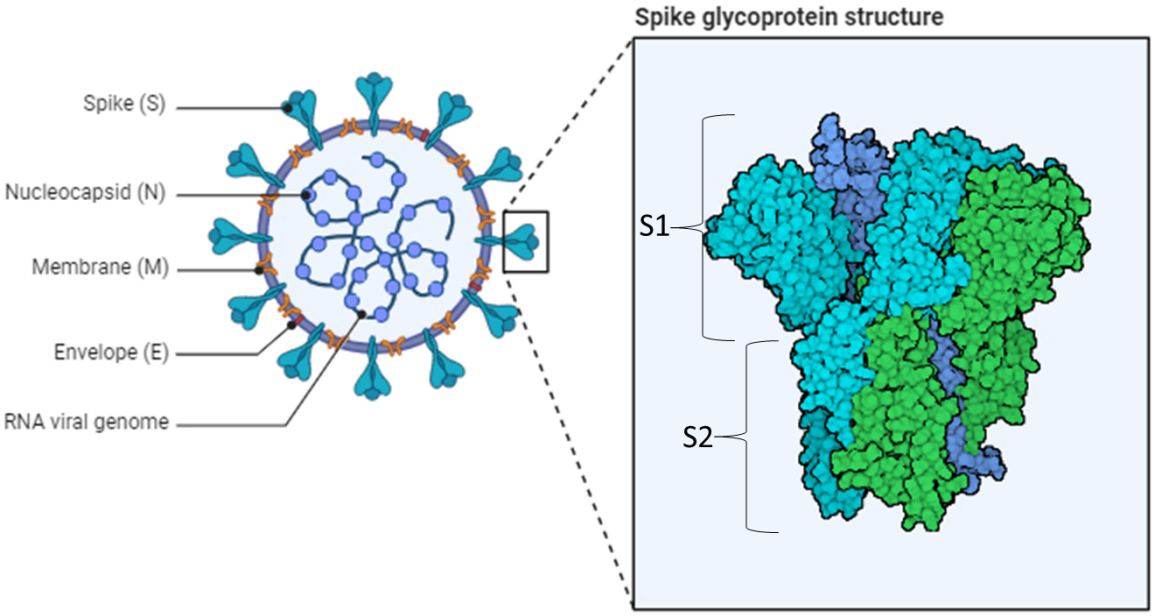

Figure 3: Diagram of the SARS-CoV-2 virion

SARS-CoV-2 virion structure comprises the spike glycoprotein (S), membrane (M), nucleocapsid (N), and envelope (E) proteins. The RNA viral genome is housed within the nucleocapsid. The structure of the S glycoprotein (right) demonstrates the two subunits: S1, key for receptor binding of the virus to ACE2 on host cells, and S2, which allows the fusion peptide to be propelled into hosts to facilitate fusion. Adapted from: Payne, 2017

1.1.2.2 Non-Structural Proteins

NSPs are encoded by ORF1a and 1b and they are the product of autoproteolytic cleavage of PP1a and 1ab via viral proteases. The 16 NSPs (NSP1–16) all perform distinct roles that provide the conditions required for viral infectivity and subsequent replication to occur (Javorsky, Humbert and Kvansakul, 2021).

NSP1 is the most N-terminal protein and acts upon translation via the suppression of host protein synthesis and IFN response, as the NSP binds to the 40S ribosomal subunit.

NSP3 contains papain-like proteases (PLpro) which allow for polyprotein processing. NSP's 3 and 4 work in tandem to produce double-membrane vesicles (DMVs) giving the sites for viral replication, playing a role alongside NSP6 to aid in autophagosome formation (Bills, Xie and Shi, 2023).

NSP5 is also known as 3C-like protease (3CLpro) and it is responsible for the activation of the NF-kB pathway, upregulating a cascade of proteolytic processing of PP1a and 1ab into 13 mature proteins.

NSP's 7 and 8 form a complex which has the ability to synthesise short RNA strands, around 6 nucleotides in length.

NSP9 is an RNA-binding protein which has been observed to mediate viral genomic RNA replication and the overall virulence of CoVs (Littler *et al.*, 2020).

NSP10 is a double-stranded RNA-binding zinc-finger protein; alongside NSP's 7, 8 and 9, it is closely related to the replication complex of NSP12, which is the RNA-dependent RNA-polymerase (RdRp).

NSP13 makes ssRNA synthesis templates from double-stranded replicative intermediates; additionally exhibiting RNA 5' triphosphatase activity, which has been linked to have a role in RNA capping (Li *et al.*, 2023).

NSP14 has exoribonuclease (Exon) activity, an enzyme which has an inherent ability to 'proof-read' the viral replicase to ensure CoV replication fidelity (Ma *et al.*, 2015). Type-I Interferon (IFN-1) is also targeted by NSP14 for lysosomal degradation.

NSP15 is an antagonist of IFN-1 and inhibits autophagosome production; it is an endoribonuclease (NendoU) meaning it can excise ssRNA and dsRNA (Otter *et al.*, 2024). NSP15 possess the ability to specifically recognise uridylates to produce 2-3'-cyclicphosphodiester products, and this prevents host innate immunity activation (Lu *et al.*, 2020).

1.1.2.2.1 NSP 6

NSP6 is a transmembrane protein with 6 to 8 predicted transmembrane domains within its structure. NSP6 has been linked in prior findings to have an inherent effect on folding, assembly and replication of CoV proteins (Bills, Xie and Shi, 2023). NSP6 is known for its role in the development of double-membrane vesicles (DMVs) as it localises to the endoplasmic reticulum (ER) membrane; NSP6 is the anchor for DMVs to connect to the ER membrane. It performs this role alongside NSPs 3 and 4. A three amino acid deletion (LSG position 105–107 and ΔSGF) and substitution (I189V) in SARS-CoV-2 NSP6 are known to influence virulence and overall transmission of progeny virions (Chen *et al.*, 2023). However, while these key sites in NSP6 of SARS-CoV-2 are well characterised, little is known whether these sites are conserved in other CoVs. The NF-κB pathway is activated and induces pro-inflammatory responses when NSP6 is polyubiquinated. NSP6 is known to activate: NLRP3-

dependent caspase-1, IL-1β/18 maturation, and impede acidification of lysosomes leading to lung epithelial cell pyroptosis (Rodrigues *et al.*, 2021). Another function of NSP6 has portrayed an inhibition of IFN-1 production through the binding of tank-binding kinase 1, preventing the phosphorylation of signal transducers and activation of transcription proteins 1 and 2 (STAT-1 & -2); a cascade which prevents IFN-1 signalling (Xia *et al.*, 2020). NSP6 is known to produce smaller autophagosomes, which downregulates canonical autophagic flux, reducing the degradation efficiency of viral components (Cottam, Whelband and Wileman, 2014).

1.1.2.3 Accessory Proteins

CoV accessory proteins are specific to each genus, with each CoV housing a different number and distribution of accessory proteins throughout the –3' end of the +ssRNA genome. The accessory proteins are either overlapping or interspaced between structural genes, which is demonstrated in figure 2. They are not required for viral replication under normal growth conditions, and are independent of the core replication cycle, unlike structural proteins (S, E, M, N) and NSPs (Fang *et al.*, 2021), accessory proteins appear to play a role in the growth and replication efficiency of coronaviruses. ORF3a of SARS-CoV-1 has been shown to promote viral assembly and subsequent budding of progeny virions through host-cell interactions, which effectively upregulate viral production, increasing viral load and overall virulence. Mutant studies have been performed using ORF3a and have shown that deletion of the gene can reduce virulence and even hinder the replicative process, due to less favourable conditions (Bianchi *et al.*, 2021). SARS-CoV-1 ORF9b has also been studied for a role in replication, it has been established that the accessory protein localises to the mitochondria and disrupts antiviral signalling. This inhibits the production of interferons, allowing a more favourable environment for enzymes, such as RdRp, to facilitate replication (Wu *et al.*, 2021).

1.2 Viral Replication

1.2.1 Viral Binding/Attachment

The S protein transitions to a state in which it overcomes the initial virus-cellular membrane repulsion; such state is termed ‘metastable’ and is the factor which allows virus-host membrane fusion. To achieve this state, transition of the S protein is enabled through two key proteolytic cleavage events, occurring post-binding with the respective receptor (ACE2 in SARS-CoV-2). The first reaction occurs at the junction of S1 and S2 subunits, with the second reaction being localised to the S2' site in the S2 subunit (Zhu *et al.*, 2021). Entry into the host cell requires target cell proteases, with Cathepsin-L and TMPRSS2 being the major two involved in S protein activation in SARS-CoV-2. TMPRSS2-mediated S protein activation occurs at the plasma membrane, whereas cathepsin-mediated activation takes place within endolysosomes, which highlights the different pathways of activation by the S protein. TMPRSS2 presence results in a cleavage of S2' at the cellular surface, exposing the fusion peptide (FP); low dissociation of S1 from S2 generates massive conformational changes in the S2 subunit (specifically within the heptad repeat 1; HR1) propelling the FP into the target host-cell membrane, initiating fusion (Belouzard *et al.*, 2012). Absence of TMPRSS2 requires an intermediary step prior to membrane fusion; internalisation of the viral-receptor bound complex into to the host cell via clathrin-mediated endocytosis generates endolysosomes, allowing the cathepsin to function within the acidic environment of the cytoplasm.

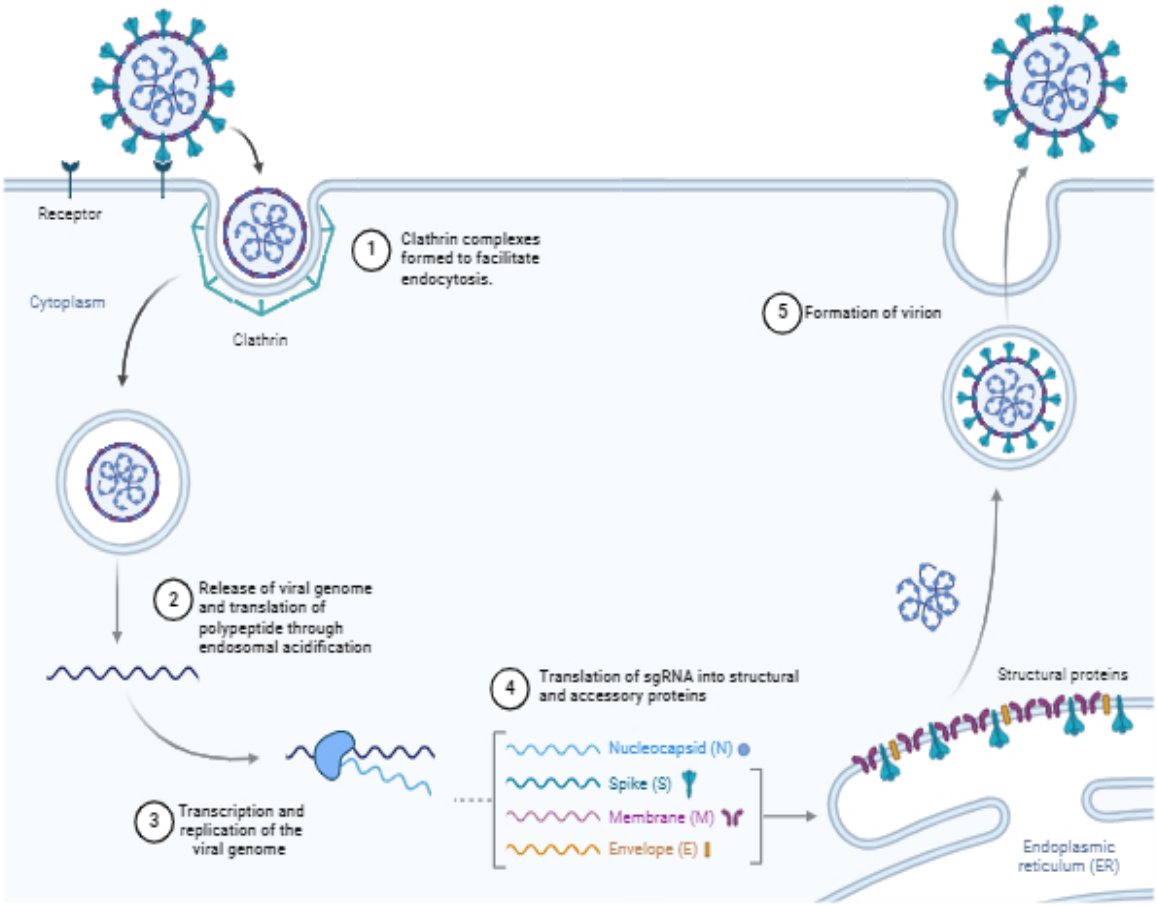

Figure 4 Coronavirus lifecycle and replication process

(1) The virus binds to the host cell receptor and is internalised through clathrin-mediated endocytosis. (2) Acidified endosomes release the viral genome into the cytoplasm allowing polyprotein translation. (3) Viral RNA transcription and replication. (4) sgRNA is translated into structural proteins (S, M, N, E) and accessory proteins in the ER. Subsequent assembly of virions occurs, and these egress the host via vesicles as an intermediary. Modified from: Trougakos et al., 2021; Savarino et al., 2003.

1.2.2 Clathrin-Mediated Endocytosis

Clathrin-mediated endocytosis acts as an alternative pathway for virus entry when there is an absence of TMPRSS2, such as lung epithelial, intestinal, and certain kidney cells. acting as an intermediate step prior to membrane fusion. When there is an absence of TMPRSS2, viral entry is unable to rely solely on membrane fusion, and requires endocytotic mechanisms (Hoffmann *et al.*, 2020). Once the virus has bound to receptors on the host cell surface, adaptor proteins (APs) are recruited and attachment to the cytoplasmic tail of the receptor occurs. Clathrin binds to, and coats, the APs to generate a Clathrin-coated pit (CCP). The viral particle is internalised, and a clathrin-coated vesicle (CCV) is formed via Dynamin 1/2 (DMN1/2) membrane scission, figure 4. Auxillin and HSC70 act to release the clathrin form the CCV, with the vesicle delivering the virus particle to early endosomes (Bayati *et al.*, 2021). As the endosome matures, the internal pH acidifies, allowing the S1 to dissociate from S2 subunit, propelling the FP into the host-target membrane; viral membrane fusion commences (Guillén *et al.*, 2005).

1.2.3 Viral Fusion

Upon conformational changes in the S2 subunit and subsequent insertion of the FP into target cells, three HR1 regions assemble into a coiled-coil trimer. Three subsequent heptad repeat 2 (HR2) regions attach to the hydrophobic groove of the HR1 trimer. The formation of this domain is known as the, stable, six-helix bundle (6HB) or fusion core (Guillén *et al.*, 2005); (White and Whittaker, 2016). The 6HB functions to bring the viral and host membranes into a readied state for fusion. The physical process of fusion is comprised of two main stages: hemifusion and pore-formation. Hemifusion is the process which allows the mixing of outer lipids from the host and virus membranes, whilst the inner lipids remain in situ (Chernomordik *et al.*, 1998) (Nikolaus *et al.*, 2011). Pore-formation is the result of localised tension from FP within the membrane, the hemifusion state undergoes a rupture and the outer lipids

mix, resulting in a complete fusion of the two membranes (Ebel, Benecke and Vollmer, 2022). The viral nucleocapsid passes through the pore formed by membrane fusion and begin to replicate within the host cell.

1.2.3.1 Viral Replication-Transcriptase Complex

The viral nucleocapsid is delivered into the host cell cytoplasm through the fusion-formed pore, where the viral replicase gene is translated from genomic RNA (Denison and Perlman, 1986). The viral replicase gene includes two ORFs: replicase 1a and replicase 1b. Figure 4 shows the translation of ORF1a into PP1a occurs as a result of the stop codon from ORF1a terminating translation, this arises from the elongating ribosome unwinding the pseudoknot, giving rise to the smaller pp1a product, which is around 440-500 kDa (Namy *et al.*, 2006). A CoV ribosomal frameshifting event of one nucleotide in the -1 direction can occur from ORF1a to ORF1b, an event that has a 25-30% frequency of occurring (Masters, 2006). The ribosomal frameshift event happens as a consequence of a heptanucleotide slippery sequence and RNA pseudoknot towards the end of ORF1a (Plant *et al.*, 2010). The ribosomal frameshifting event allows continuous translation into ORF1b, resulting in the synthesis of the larger polyprotein, pp1ab, of length between 740 and 810kDa. Autoproteolytic processing of pp1a and pp1ab results in mature products arising: 16 NSPs (NSP 1–16); as a collective NSP's form the replication-transcription complex (RTC) for coronaviral RNA synthesis (Ziebuhr, Snijder and Gorbalenya, 2000).

1.2.3.2 Viral RNA Synthesis

Assembly of the RTC gives the foundation for RNA synthesis of the CoV genome to commence. This allows viral RNA replication and the transcription of multiple sub-genomic RNAs (sgRNAs), which serve as an mRNA structure downstream of the replicase gene (Castillo *et al.*, 2023). sgRNAs consist of a leader RNA, identical to the 5' end of the genome, joined to a body RNA, which is identical to a segment of the 3' end of the genome (Miller and Koev, 2000). Use of the genomic RNA as a template

means new full-length copies of the viral genome are produced from the negative-sense genomic RNA as an intermediate template. It is a process that occurs for genomic RNA and subgenomic RNA (sgRNA) synthesis. The polymerase is able to switch templates at short motifs, known as transcription-regulated sequences (TRS), during negative-sense strand synthesis, where the leader RNA becomes fused with body RNA (Baric and Yount, 2000). These short motifs produce a 5'– nested set of negative-sense sgRNAs, utilised as templates to synthesise a –3' nested set of positive-sense sgRNAs (Miller and Koev, 2000).

1.2.4 Viral Assembly and Release

CoV viral assembly occurs in the endoplasmic reticulum-Golgi intermediate compartment (ERGIC), where the proteins translated from ribosomes in the ER (S, M and E) and the proteins translated by free ribosomes (such as N) assemble; post-translation modification occurs to modulate the functions of these structural proteins (Liu, Liang and Fung, 2021). The M protein is the catalyst for viral assembly: it provides the structure for virion formation and heterotypical interaction with other structural proteins incorporate them into the progeny virion (Neuman *et al.*, 2011). The N protein encapsidates the nucleocapsid of progeny genomes and condenses them with E proteins to drive the formation of the virion (Howley *et al.*, 2020). Once packaged, the virions are transported to the plasma membrane of host cells for exocytosis by vesicles, seen as viral egress in figure 4 (Liu, Liang and Fung, 2021). Bone marrow stromal antigen 2 (BST2/Tetherin) is an interferon-induced protein that blocks the release of enveloped viruses. SARS-CoV-2 has been demonstrated to antagonise this BST2 protein by promoting lysosomal degradation within the autophagy pathway (Neil, Zang and Bieniasz, 2008; Stewart *et al.*, 2022).

1.3 Epidemiology and zoonotic potential of coronavirus infections

1.3.1 Epidemiology overview

CoVs are significant causes of disease globally in both humans and animals. SARS-CoV-2, HCoV-OC43 and FCoV are examples of both endemic and CoVs with pandemic-potential.

1.3.1.1 HCoV-OC43

HCoVs are responsible for approximately 15% of "common colds" in humans (Liu, Liang and Fung, 2021). HCoV-OC43 is a betacoronavirus of the *Embecovirus* lineage, figure 1. The true natural origin of HCoV-OC43 is unclear, however, it is closely related to bovine coronavirus, which suggests a possible source arising from cattle as intermediate hosts (Corman *et al.*, 2018).

HCoV-OC43, is an easily transmissible CoV, but generally mild respiratory virus and laboratory testing is infrequent due to the self-limiting nature of the virus. Hereby, epidemiological data on the prevalence, impacts and fatality rates associated with HCoV-OC43 remain incomplete. HCoV-OC43 exhibits a broad respiratory tropism, with infection resulting from the binding of virus S proteins to sialic acid receptors, present on host cell surfaces. These receptors are predominantly expressed in the ciliated and non-ciliated epithelia of the respiratory tract; found particularly in bronchioles and alveoli (Hulswit *et al.*, 2018). However, whilst HCoV–OC43 primarily causes URTIs, it is also capable of infecting the lower respiratory tract in immunocompromised and older individuals. As typical in 'common colds', symptoms arise from a response by the innate immune system, such as: sore throat, headaches, increased mucus, fever and fatigue (Graat *et al.*, 2003). Symptomatic outcomes arise from the release of pro-inflammatory cytokines and other inflammatory mediators in the nasal tract (Liu, Liang and Fung, 2021). There is distinct seasonality around the prevalence of OC43 cases in the United States with notable spikes in cases between the months of December to May each year. (Gaunt *et al.*, 2010).

1.3.1.2 SARS-CoV-2

SARS-CoV-2 was the causative virus responsible for the largest global pandemic of the 21st Century. First identified in Wuhan, China, December 2019, it rapidly spread amongst a very populated local market, soon becoming prevalent in key areas of travel globally. A near-worldwide response was required to contain and control cases. SARS-CoV-2 is a betacoronavirus of the *Sarbecovirus* subgenus, figure 1. The natural host is believed to be bats, with a potential, unconfirmed, intermediary facilitating cross-species transmission (Huang *et al.*, 2023). ACE2 is the target receptor and is present on tissues in the general lung parenchyma, cardiovascular system, gastrointestinal (GI) system, and within blood vessels. Subsequent attachment and replication to receptors found on these tissues drives pro-inflammatory pathways, potentially to leading to the most severe outcomes.

SARS-CoV-2 is a highly contagious pathogen, with an estimated basic reproduction number (R_0) of 2–2.5 in the early pandemic, indicating the ease of viral transmission throughout almost all public and private settings (Petersen *et al.*, 2020). Respiratory droplet transmission was the main route of transmission, with crowded spaces and aerosol formation being key contributors to the spread of disease. Social distancing and the wearing of face masks was recommended in 2020, to aid in the prevention of viral spread. Once exposed to the virus, individuals typically begin to present symptoms after 4–5 days; despite this, many individuals were asymptomatic. Targeted community testing was used in the UK to prevent the spread of transmission by asymptomatic patients; any positive cases were isolated at home for 5–7 days and this drove a reduction in the number of cases.

The CFR for SARS-CoV-2 was estimated to be 2–3% as a global average, however, this number was significantly higher in healthcare settings and amongst those with predisposing immunosuppressive health factors. It was estimated that 6.8% of all SARS-CoV-2 infections throughout the peak of the first wave (May 2020) arose from

nosocomial settings (Read *et al.*, 2021). A mild-to-severe LRTI is characteristic of SARS-CoV-2, which can result in fatalities in some cases. The development of vaccines, such as the mRNA vaccines produced in the COVID-19 pandemic, have been critical in controlling the most severe pathologies, fatalities, and transmission of the virus, providing a vital milestone in the pandemic response globally.

1.3.1.3 Feline Coronavirus (FCoV)

FIP is a disease caused by feline coronavirus (FCoV), an alphacoronavirus of the *Tegacovirus* subgenus, Fig. 1. The target receptor for FCoV is feline aminopeptidase N ($_{f}$APN), a multifunctional enzyme predominantly found in the GI system. The main route of transmission of FCoV is the faeco-oral route; the virus is shed in faecal matter by asymptomatic felids, occurring for at least 10 months, but many years in some cases. FCoV can survive up to 7 weeks in dried faecal matter, which makes it an important reservoir for infections (Sherding, 2006). Infections are typically caused by a non-mutated form of the virus, associated with most felids remaining asymptomatic, however, upon replication in the GI tract genetic mutations can occur which allowing replication within macrophages. These mutations allow a systemic spread of the virus to target tissues, and the characteristic pro-inflammatory action which results in the clinical signs associated with FIP. The virus does not directly cause the pathologies associated with FIP, rather it is the immune reaction that is responsible (Tekes and Thiel, 2016). Severe diarrhoea, weight loss, and multi-organ failure are observed with FIP and are the reason why the disease is often fatal. Therapies have limited benefits; therefore, palliative care is typically provided to support the felid. New antiviral treatments, such as remdesivir, have shown positive outcomes and effective treatments, however, the high costs associated are a limiting factor for their usage. FCoV infections are most prevalent in young kittens, once the maternal antibodies have waned, around 6 weeks after birth; peak incidences of FIP occur between 6 months and 3 years. Risk factors such as immune impairment, increased viral load,

stress, and overcrowded environments are responsible for increased FCoV replication and the chance of mutations occurring that can cause FIP. Less than 5% of infections will mutate and have the ability to cause FIP infection. Cats are not the only felid vulnerable to FCoV infections; lions, cheetahs, cougars, leopards and lynx are all susceptible. Cheetahs are at a particularly higher risk of developing FIP (Sherding, 2006).

1.3.2 Antigenic variation in coronavirus infections

CoVs, as a family, display high levels of genetic variance, assisting in the survival and overall pathogenicity of each virus. The variation relates to changes in the antigenic structure of the spike glycoprotein. Antigenic drift is the process where there is a gradual accumulation of point mutations of the viral genome, which can result in a gradual change of the viral surface proteins (Yewdell, 2021). It is characterised by single nucleotide changes that can alter amino acid sequences of viral proteins helping to evade host immunity, which is primed to recognise any re-entering/invading pathogens. A mutation rate of $1x10^{-3}$ substitutions per base each year under natural antigenic drift occur in SARS-CoV-2 which contribute to the viruses tendency to wax and wane, explaining the observed seasonality (Wiemken *et al.*, 2023). Antigenic shifts are less prominent in CoVs than many other respiratory-prominent viruses. The segmented genome in influenza allows for reassortment of the gene segments when two types of virus strains infect the same host, which can significantly alter surface antigens (Kim, Webster and Webby, 2018). Drifts have higher prevalence in hosts with co-infections, such as other seasonal CoVs (such as HCoV-229E and HCoV-OC43). These mutations arise due to genome recombination, and the new strains pose serious global health security threats and have pandemic potential (Cameroni *et al.*, 2022). Both antigenic shift and drift are prominent factors in the need for vaccine changes being required periodically, the process driven by viral surveillance by health security bodies.

1.4 Response to Viral Infection

1.4.1 Innate Immunity Overview

The innate immune system is a host's first-line defence against pathogens, such as bacteria and viruses. The innate immune system exhibits pattern-specific responses utilising pathogen recognition receptors (PRRs) that recognise pathogen-associated molecular patterns (PAMPs) which are conserved in microbial structures. They predominantly act as a preventative measure to physically block entry and provide a first-line attack mechanism against infection/invading pathogens (Janeway *et al.*, 2001).

Innate immunity activates almost immediately upon pathogen recognition, inducing the more-specific adaptive immune system through induction by key modulators within the innate immune system; the adaptive process contains a lag-phase period activate because of this. The innate immune system comprises physical barriers (including genitourinary, gastrointestinal and respiratory tracts mucus, and tight junctions in the skin); immune cells (such as macrophages, neutrophils and basophils); pathogen recognition molecules (such as toll-like receptors, TLRs; pathogen-associated molecular patterns, PAMPs); cellular cytokine secretion (by macrophages and mast cells, triggering later immune cascades). Adaptive immunity is triggered by cytokine secretion and co-stimulatory signals, which induce B and T lymphocyte activity.

1.4.1.1 Pathogen Recognition

Innate immunity has a characteristic pro-inflammatory mechanism response to infection which is the result of germline-encoded, pathogen PRRs. Key PRRs in innate immunity are: TLRs, retinoic-acid inducible gene-I-like receptors (RIG-I receptor; RLR), and nucleotide-binding oligomerisation domain (NOD-like receptors; NLRs). These PRRs detect PAMPs, such as viral proteins and RNA, activating signal cascades that initiate the transcription of antiviral genes and production of cytokines

(e.g. IFNs; interleukins, ILs; tumour necrosis factors, TNFs) occurs as a response to these PRRs (Akira, Uematsu and Takeuchi, 2006). Cytokines enhance the innate immune response by recruiting immune cells, key in antigen-presentation and overall activation pathways that induce the adaptive immune response.

1.4.1.2 Cytokines

Cytokines are key modulators of both the innate and adaptive immune pathways, playing roles in pathogen recognition, signal transduction, inflammation and downstream signalling cascades. Cytokines, as a signal, are derived from immune cells, endothelial cells and fibroblasts. These signals trigger specific receptors which have roles in differentiation and subsequent proliferation of immune cells (Liu *et al.*, 2021). The cytokines involved in innate immunity include: ILs, IFNs and TNFs. Pathogen recognition by cells leads to the release of cytokines which act on other cells.

1.4.1.2.1 Interferons

IFNs are vital moderators of the innate immune response to infection, key in the anti-viral defences in hosts as a first-line measure in the wake of pathogenic entry. Signals released by IFNs upon infection travel to neighbouring cells where they bind to the respective IFN receptor. Subsequentially, the complex formed triggers the release of antiviral proteins that can inhibit viral proliferation. Signalling complexes are comprised into three groups: type I IFNs (IFNα and IFNβ), type II IFNs (IFN-γ) and type III IFNs (IFN-λ). All IFN signalling occurs through the Janus kinase signal transducer and activator of transcription (JAK-STAT) pathway. JAKs actively phosphorylate IFN-receptors in a regulatory mechanism (Satarker *et al.*, 2020). Active transcription of interferon stimulating genes (ISGs) results from the activation of STAT; as a preventative measure, antiviral proteins are secreted in neighbouring cells. In the CoV family, there are some specific types of ISGs which have more intrinsic antiviral activity against the virus. Such specific ISGs include: TRIM25 (which

ubiquitinates the RIG-I protein, controlling viral proliferation); IFITM family (block viral entry through the inhibition of endosomal and viral membrane interactions); 2′-5′-oligodenylatesythetase (OAS; degrades viral RNA, inhibiting replication) (Gea-Mallorquí, 2021). Type I IFNs are secreted in nearly all cell types following viral infection (inclusive of dendritic cells (DCs) and macrophages); once secreted, they bind to IFNα-receptor (IFNAR) on neighbouring cells. Type I IFNs enhance the activity of NK cells, vital as an inducer of the adaptive immunity pathway through their antigen presentation capabilities (Kim and Shin, 2021). Type II IFNs are secreted by NK, helper T cells, and CD8 T cells promoting macrophage activation and subsequent adaptive immunity activation. They bind to the IFNγ-receptor (IFNGR), activating the JAK-STAT pathway, increasing the expression of MHC which leads to further antigen presentation downstream (Platanias, 2005). Type III IFNs signal through the IL-28/IL-10R2 pathway situated on epithelial cells and some immune cells (e.g. leukocytes); this IFN provides antiviral capabilities at physical barriers (such as the respiratory and gastrointestinal tracts), without an over-characterised inflammatory response (Hm *et al.*, 2019).

1.4.1.2.2 Other Cytokines

In addition to IFNs, there are other cytokines that are essential in the regulation of inflammation and immunity. Two of the most notable examples of these are: TNFs and ILs. TNFα is the main type of TNF produced by macrophages and DCs and is an important pro-inflammatory cytokine in the regulation of inflammation, playing a key role in tissue damage prevention, aiding the removal of damaged organelles and viral proteins/particles. It performs many other key functions such as: increasing endothelial cell adhesion molecules, activates downstream immune pathways, involved in the recruitment of further immune cells, and stimulates the recruitment of further cytokines (e.g. ILs) (Croft, 2009). ILs are cytokines critical in regulating inflammation and autophagy. Innate immunity utilises to three key ILs: IL-1, IL-6,

and IL-12. IL1α and IL-1β are pro-inflammatory cytokines produced by macrophages and DCs; they bind to the IL-1 receptor which activates NF-κB and MAPK pathways inducing pro-inflammatory genes (such as those involved in fever, endothelial cell activation, and leukocyte recruitment). NLRP3 activation also occurs, which can modulate autophagic flux (Sun *et al.*, 2022). IL-6 is a regulator of systemic inflammation in response to infection; signalling of IL-6 involves the JAK-STAT pathway, which induces pro-inflammatory gene expression, which can deliver the characteristic 'cytokine storm' observed in the most severe coronavirus infections. Autophagy-related gene expression is also enhanced by IL-6 which can lead to increased viral clearance (Wang *et al.*, 2022). IL-12 signals through the IL-12 receptor, which activates the JAK-STAT pathway. It is responsible for the differentiation of non-specific T cells into helper T cells, specifically Th1, as well as the production of IFN-γ by NK cells (Yang *et al.*, 2021).

1.4.1.3 Complement System

Complement is a system of around 30 serum proteins that play a role in host immune defences and pro-inflammatory cascades in both, innate and adaptive immunity pathways (Rus, Cudrici and Niculescu, 2005). They are series of enzymatic proteins that are sequentially activated through one of three different pathways: classical, alternative, and lectin. In each pathway, the catalyst of complement, C3, is cleaved into C3a and C3b, two fragments of differing sizes, by C3 convertase enzyme complex [figure 5]. The latter, C3b, is the largest fragment and binds to microbial surfaces to facilitate phagocytic uptake. Both fragments, alongside another key complement protein, C5, are key initiators of pro-inflammatory responses. C5 convertase also converts C3 into C3a and C3b, which act in a downstream manner as well to form the membrane attack complex (MAC). C3a and C5a are specifically known as anaphylatoxins; these have strong pro-inflammatory capabilities and interact with associated G-protein-coupled receptors C3aR and C5aR, attracting leukocytes to

the site of infection (Klos *et al.*, 2009). Other key aspects of complement include: opsonin C3b, iC3b and C3d, all of which have roles in facilitating the transport and subsequent removal of targeted debris. The MAC, seen as the terminator of the system in figure 5, with a cascade leading from C5b-C9, directly lyse the targeted pathogens and/or damaged-host cells (Xie *et al.*, 2020).

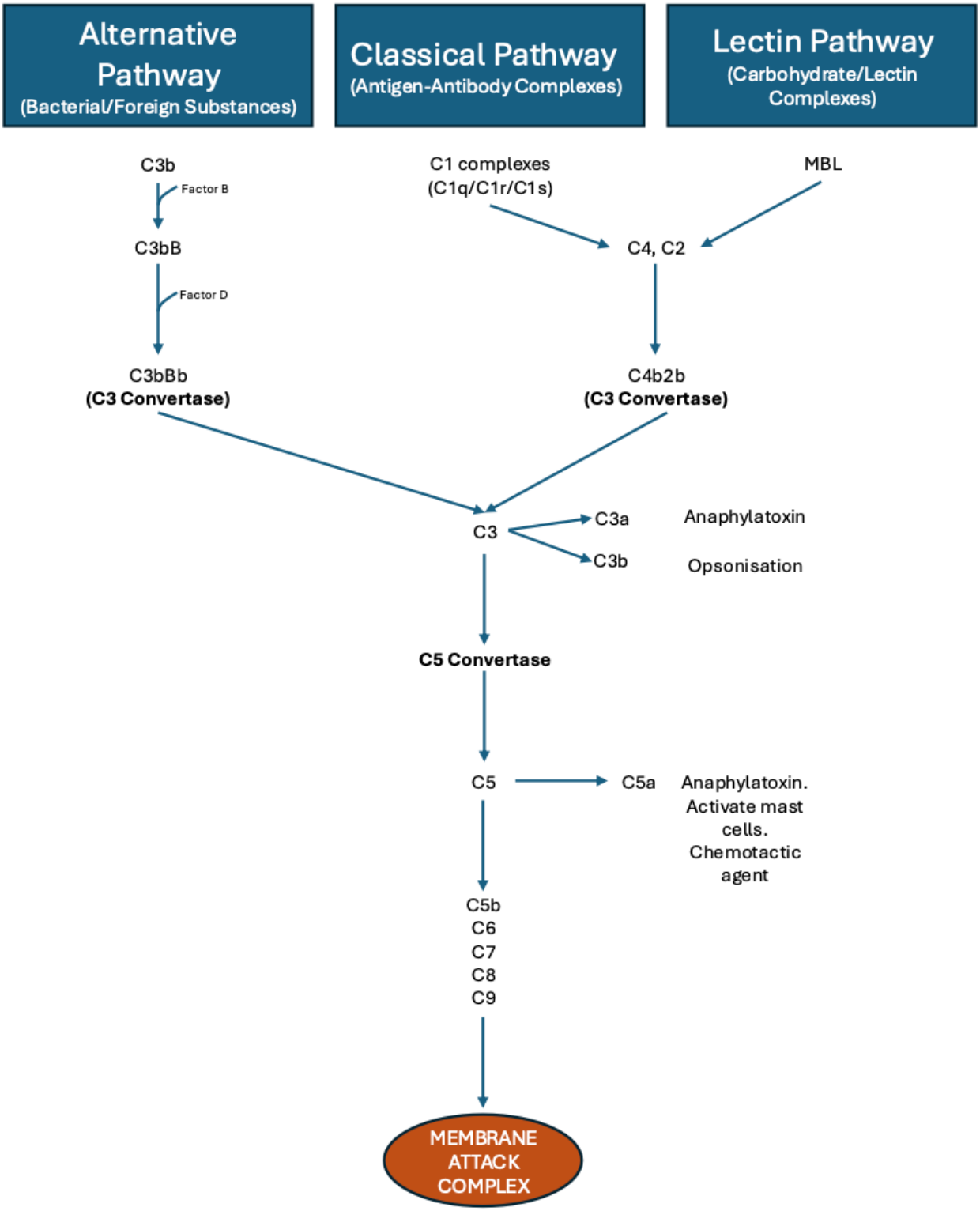
Alternative Pathway
(Bacterial/Foreign Substances)
Classical Pathway
(Antigen-Antibody Complexes)
Lectin Pathway
(Carbohydrate/Lectin Complexes)
C3b
Factor B
C3bB
Factor D
C3bBb
(C3 Convertase)
C1 complexes
(C1q/C1r/C1s)
MBL
C4, C2
C4b2b
(C3 Convertase)
C3
C3a
Anaphylatoxin
C3b
Opsonisation
C5 Convertase
C5
C5a
Anaphylatoxin. Activate mast cells. Chemotactic agent
C5b
C6
C7
C8
C9
MEMBRANE ATTACK COMPLEX

Figure 5: The complement system and its three pathways of activation: alternative, classical, and lectin.

An overview of the complement system, which has three activators: classical, alternative and lection. The key convertases, C3 and C5 are in bold, whilst the membrane attack complex is presented in orange to mark the termination of the cascade. Adapted from: Nesargikar, Spiller and Chavez, 2012.

1.4.1.4 Acute Phase Proteins

A group of plasma proteins produced by the liver that increase in numbers during the course of infection (Suffredini *et al.*, 1999). Examples of these plasma proteins include the C-reactive protein and complement components (such as C3). Opsonisation is a surface coating performed by C-reactive protein, antibodies (such as IgE) and complement proteins. Phagocytes intrinsically recognise these coating proteins from opsonisation and engulf them (Thau, Asuka and Mahajan, 2024).

1.4.2 Dendritic Cells

Dendritic cells (DCs) are a vital modulator of both the innate and adaptive immunity pathways, playing a pivotal role in presentation of foreign peptides/antigens to T lymphocytes. DCs develop in the bone marrow and are a derivative of the monocyte colony-forming cell lineage (Zanna *et al.*, 2021). These cells migrate to lymphoid tissues whilst immature, despite this, they still possess high phagocytic abilities. DCs undergo maturation once exposed to key factors of immunity, such as cytokines and PAMPs. Once matured, DCs become stimulators of T lymphocytes through the transportation and subsequent presentation of antigens to helper T cells (Nakayama, 2014). These helper T cells are key regulators of effector cell activation upstream such as: NK cells, cytotoxic T cells, B cells and eosinophils.

1.4.3 Adaptive Immunity Overview

Once activated, DCs initiate the cellular and humoral immune responses through T and B lymphocytes activation in a process occurring 4–7 days post-infection. The cellular response is a cascade mediated by the T lymphocytes; activated by DCs that have captured foreign antigens and migrated to lymphoid organs where they present these antigens to helper T cells. The humoral immune response is characterised by specific antibodies being produced by B cells. In mammals, T cells arise from the thymus, whilst B cells are derived from haematopoietic cells within the bone marrow. Upon pathogen recognition by B and T lymphocytes, cellular differentiation and proliferation derives effector cells that target the specific pathogen (Janeway *et al.*, 2001).

1.4.3.1 T Lymphocytes and Cell-mediated Immunity

T cell activation is the catalyst for cell-mediated immunity; activated T cells secrete cytokines and/or cytotoxic molecules onto neighbouring cells. T-cell receptors (TCRs) are the binding domain that initiate antigen recognition, commencing proliferation and differentiation into effector or helper T cells. TCRs have two components: a part that recognises specific cell markers and a part that inspects the MHC for foreign antigen presence (Shah *et al.*, 2021). There are two main types of T cell that have roles in intracellular immunity: helper T cells and cytotoxic T cells.

Extracellular antigens are degraded into peptides once they have been taken up by endocytosis. Endosomal fusion with vesicles containing major histocompatibility complex II (MHC-II) proteins occurs, creating a complex with the foreign peptide; these are then inserted into the plasma membrane, where helper T cells can recognise them (Rock, Reits and Neefjes, 2016). Helper T cells are characterised through their display of cluster of differentiation 4 (CD4+) on the cell surface. These cells become activated post-interaction with exogenous antigens that are associated with MHC-II molecules on the surface of APCs. Upon recognition of MHC-II molecules on

macrophages and B cells, CD4+ cells secrete many cytokines such as IL-2. These enhance the proliferation of B and T cells; in macrophages, IL-2 can stimulate the normal killing mechanisms of the cell (Luckheeram *et al.*, 2012).

Cytotoxic T cells express the CD8 glycoprotein on their cell membrane, and they are activated by presentation of foreign antigens associated with major histocompatibility complex I (MHC-I) on infected, tumour and transplant cells (nucleated cells). Upon infection by viruses or intracellular bacteria, foreign proteins are expressed in their cytoplasm; endosomes catalyse the breakdown of foreign proteins into peptides. Such proteins are transported to the endoplasmic reticulum (ER) where MHC-I proteins bind to them, once this complex is formed, they are inserted into the plasma membrane where cytotoxic (CD8) T cells can bind to them (Rock, Reits and Neefjes, 2016). Despite this cascade, complete activation of CD8 cells requires co-signals produced by helper T cells, such as IL-2. Large populations of cytotoxic T cells and cytotoxic memory cells, which are antigen specific, are produced by clonal selection. Activated CD8 cells can secrete granzymes, which digest proteins, triggering apoptosis. They also release granulysin and perforin, which are key in the destruction of infected cells (Zhang and Bevan, 2011). Memory CD8 cells have an inherent ability to give more rapid responses in the wake of re-infection by the same invading antigen in the future. T cells not only enhance the entire adaptive immunity cascade, but they provide help with immune response regulation in hosts, helping to reduce tissue damage (such as pulmonary fibrosis) in hosts.

1.4.3.2 B Cells and Humoral Immunity

Humoral immunity is characterised by antibody-mediated binding of specific B cells to antigens. Secretion of cytokines, such as IL-2, by helper T cells provide a co-stimulatory cascade for B cell activation. Like CD8 cells, clonal selection, maturation and proliferation of cells occur, however in B cells, they become plasma or memory cells (Nutt *et al.*, 2015). Antibodies, more formally known as immunoglobulins (Ig),

bind to the intrinsic antigen epitope that initiated activity of the ‘parent’ B cell. There are five main classes of Igs that exist in most mammals: IgG, IgA, IgM, IgD and IgE. The functions of these individual classes are outlined in table 1. Each Ig can bind to a specific foreign antigen and perform key immune activities such as: deactivating the antigen, prevent bacterial motility, agglutinate and precipitate antigens, activate the complement system cascade and enhance cellular phagocytosis (Schroeder and Cavacini, 2010).

The primary response to infection is modulated by plasma cells, which are mature B cells with relatively small cytoplasm and few ribosomes. Upon infection and subsequent antigen stimulation, the mature B cells transform into antibody-secreting plasma cells; such cells have a much larger cytoplasm, alongside many ribosomes which are the site of antibody synthesis (Nutt *et al.*, 2015). B cell antibody production has a short lag-phase after initial infection due to requirement for activation of B lymphocytes by the innate pathway. The antibody primarily secreted by B cells in primary infection is IgM, an activator of the complement system, which enhances the ability of the immune system to combat infection. Peak IgM blood levels are observed around 7 days post infection (Sathe and Cusick, 2024). Some B cells can produce IgG, which are antibodies with longer-lasting effects and a peak in levels about 14 days post-infection.

The secondary immune response arises in the case of re-exposure to the same foreign peptide/antigen, constituting a much swifter response (Vidarsson, Dekkers and Rispens, 2014). During a secondary immune response, IgG levels rise more rapidly and reach a higher concentration than in the primary response, remining elevated for a significantly longer period. In contrast, IgM levels follow a similar pattern to those levels observed in primary response, with only slight enhancement in magnitude or duration of the response. The more rapid and greater secondary response arises due to the recruitment of memory cells that did not mature into antibody-secreting plasma

cells in the primary infection, but they were produced in the development of the initial clone. B lymphocyte memory cells respond to small levels of antigen/foreign peptide once active (Natoli and Ostuni, 2019).

Table 1: The five types of mammalian immunoglobulins: IgG, IgA, IgM, IgD, IgE.

Immunoglobulin	**Function**
IgG	The main immunoglobulin secreted in the secondary response. The main antibody found in blood serum. Crosses the placenta
IgA	Primary form of immunoglobulin in external secretions (e.g. tears, saliva, and breast milk). First line of defence against pathogens, part of the physical barrier system of innate immunity
IgM	The first antibody released in the primary response, induces the complement system, enhancing immunity. First antibody produced by the foetus
IgD	Major function unknown
IgE	Mediator/trigger of allergic reactions/hypersensitivity

This table outlines the five main classes of Igs found in mammalian plasma, giving a brief overview of each. (Adapted from: Moser and Leo, 2010)

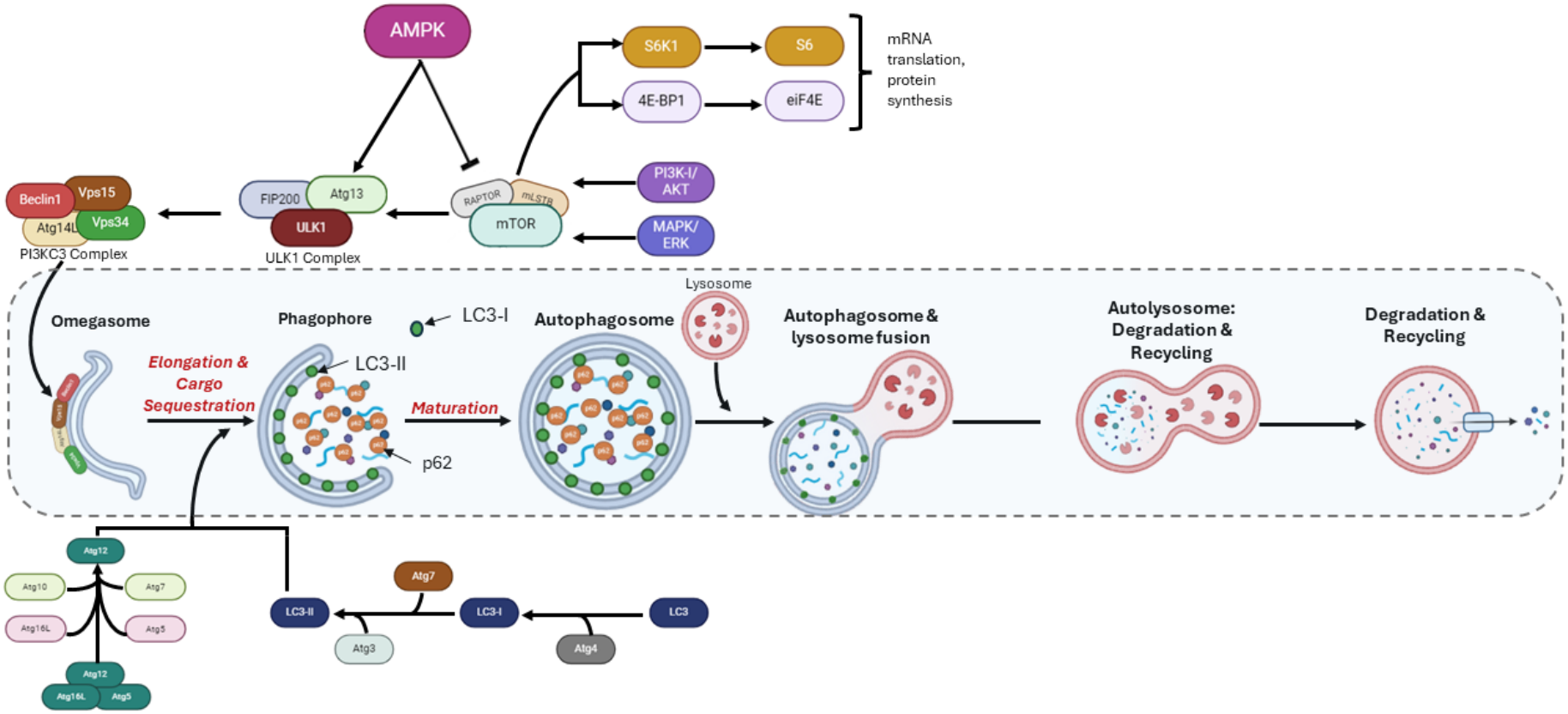

Figure 6: The autophagy pathway

The key stages of the autophagy pathway and regulatory mechanisms involved. The upstream cascades of mTOR and AMPK are displayed. Activation of AMPK and inhibition of mTOR are promotors of autophagy. Upstream of these, S6K and eIF4E are presented and these are key regulators of translation and protein synthesis. Once autophagy has been upregulated, the ULK1, PI3KC3 and Atg-12-5-16L complex being to elongate the omegasome derived from the ER. The creation of the early phagophore initiates the autophagy pathway, followed by maturation into autophagosomes, marked by LC3-I and LC3-II. Autophagosomes fuse with lysosomes and sequestered cargo is degraded; recycling of the products can then occur. Adapted from: Klionsky and Codogno, 2013; Pant et al., 2022.

1.4.4 Overview of autophagy

Autophagy is a cellular process where cells degrade and recycle damaged proteins, organelles, and aid in clearance of viral proteins, providing a short-lived provision of amino acids available post-lysosomal degradation for use in other biosynthetic processes.

Autophagy a catabolic process mediated by multiple upstream cascades. The mammalian target of rapamycin (mTOR) is a key mediator of autophagy and, when inhibited, allows for sequential interactions with ULK1 protein complex (UKC) 'initiating' the autophagy pathway. In spite of this, mTOR is not the sole mediator of autophagy– it can also be activated by other signalling cascades in response to stress situations. Such pathways include:

- → Mitophagy– damaged mitochondria are degraded, utilising the PINK1/Parkin signalling pathway (Youle *et al.*, 2011).
- → ER-phagy– damaged ER turnover by autophagy. Mediated by ER-phagy receptors (such as RTN3L; Khaminets *et al.*, 2016)
- → Xenophagy– PRRs detect pathogen-associated structures, sequestering intracellular pathogens into autophagosomes, allowing clearance (Sil, Muse and Martinez, 2018).

The class III PI3K complex is a downstream complex to ULK1 and helps in the recruitment of downstream autophagosomal proteins. Phagophore formation is the catalyst for the initiation of autophagy and subsequent autophagosome production. During elongation, the membrane of the phagophore expands into a double membrane vesicle (DMV) with the aid of key autophagy proteins. Maturation is the step where autophagosome-lysosome fusion occurs, forming autolysosomes where the breakdown of cargo is catalysed by lysosomal hydrolases. Termination of the autophagy process releases the products of lysosomal degradation into the cytoplasm for later uptake and recycling (Liang *et al.*, 2021). Canonical autophagy is vital for the

maintenance of cellular homeostasis, primarily under stress and starvation conditions (Sil, Muse and Martinez, 2018).

1.4.4.1 Initiation of Autophagy

The autophagy pathway is under constant suppression when mTOR is activated; whilst active, the downstream pathway of autophagy is suppressed. The ULK1 complex contains the proteins ULK1, ATG13 and FIP200. mTOR actively phosphorylates both FIP200 and ATG13, which inhibits the ULK1 complex and any downstream signalling cascades (Torii *et al.*, 2016). Serine 6 kinase (S6K), seen upstream of autophagy in figure 6, is a protein that is actively phosphorylated by mTOR, which promotes protein synthesis downstream. Contrastingly, in times of nutrient deprivation, starvation or stress-conditions, mTOR is inhibited and activates a downstream signalling cascade initiating canonical autophagy, in addition, the activity of S6K is significantly lower, suppressing protein synthesis (Tavares *et al.*, 2015). In addition, AMPK is an inhibitor of mTOR that can perform this action under low levels of energy; the activation of autophagy drives energy restoration (Dagon *et al.*, 2012). The ULK1 complex becomes activated and translocates to pre-autophagosomal membranes, generating omegasomes and phosphorylating, and subsequently, activating the downstream PI3KC3 complex. The downstream signalling cascade that results from mTOR inhibition and activation of the ULK1 complex initiates a secondary autophagy effector, the class III phosphatidylinositol 3-kinase (PI3KC3) complex comprising: BECLIN-1, Vps15, Vps34, and ATG14L; this complex functions to drive early phagophore formation in autophagy (Choi, Houdek and Anderson, 2018). Figure 6 presents the interactions of the autophagy pathway upon suppression of mTOR activity. PI3KC3 complex also recruits downstream autophagy proteins key for elongation, maturation and lysosomal fusion in the later stages of the pathway.

1.4.4.2 Elongation

The early phagophore is a DMV which elongates to form the autophagosome.

The origin of the early phagophore is contested, and likely depends on the cellular stress exhibited, but evidence suggests that it is primarily derived from the ER, Golgi, mitochondria, or endosomal compartments depending on the context of the trigger (Hamasaki *et al.*, 2013). Ubiquitin-like conjugation systems facilitate the elongation of the early phagophore and there are two main systems that perform this: the Atg12–Atg5-Atg16L and the Atg4B-Atg3-Atg7 complexes. The Atg4B-Atg3-Atg7 complex provides two key autophagy proteins, Atg3 and Atg7, which are crucial in the conjugation of cytosolic-LC3 (LC3-I) to phosphatidylethanolamine (PE), converting the protein into the lipidated and membrane-bound LC3-II (Kuma *et al.*, 2002). This conversion is observed in figure 6, both as a pathway interaction and upon integration into the autophagosome, where LC3-II is within the membrane compartment and LC3-I is within the cytoplasmic space.

Atg12–Atg5-Atg16L1 complex functions similarly to an E3-ubiquitin ligase enzyme which covalently lipidates the ubiquitin-like LC3, which directs the binding of LC3-II to the early phagophore membrane. This binding initiates a cascade of other autophagy proteins required for elongation and subsequent maturation into an autophagosome (Virgin and Levine, 2009).

In addition to this, conjugation by ATG12 to ATG-3 mediated (CASM) autophagy is a noncanonical LC3 lipidation cascade where ATG12-conjugated ATG3 allows direct LC3 lipidation, bypassing the need for the ATG5–ATG12-ATG16L complex. This CASM pathway plays a key role in host immune defence against intracellular pathogens as it is an upregulator of viral protein clearance by autophagy (Hooper *et al.*, 2022).

1.4.4.3 Maturation and Sequestration

Sequestosome 1 (SQSTM1), otherwise known as p62/SQSTM1, is an autophagy signalling adaptor protein which is vital for sequestering cellular debris and cargo into the autophagosome for degradation in the terminal stages of the canonical autophagy pathway. The early phagophore (a cup-shaped double membrane structure) elongates and curves around the sequestered cargo, and a fusion reaction occurs once cargo has been sequestered into the early vesicle. p62/SQSTM1 interacts with and binds to polyubiquitinated proteins and other aggregates; it possesses an LC3-interacting region which binds to LC3-II present in the autophagosome membrane compartment, allowing p62/SQSTM1 and its bound cargo to be sequestered into the DMV (Tung *et al.*, 2010). This is a functional interaction that ensures that cargo is encapsulated in the autophagosome prior to membrane closure and the formation of the double-membraned vesicle/autophagosome. The closure of the double-membraned structure has other mediators key for fusion and subsequent closure of the elongated phagophore to generate an autophagosome. Atg2 is a protein recruited by WIPI3/4 sensing of PI3P and it is a lipid transferase recruited to the elongating phagophore to transfer lipids to outer leaflets for Atg9 to deliver to the phagophore. Atg9 contains a transmembrane domain that allows the exchange of lipids delivered by Atg2 between the inner and outer leaflets of the phagophore membrane, which facilitates fusion and closure of the double-membrane (Broadbent *et al.*, 2023). SNARE proteins are also known to possess a role in the fusion of the elongated phagophore, with the intrinsic interactions yet to be fully understood, but it has been suggested that homotypic fusion by lipidated LC3 (LC3-II) is mediated by SNARE (Wang *et al.*, 2016).

1.4.4.4 Lysosomal Fusion and Degradation of Cargo

Once a complete DMV has been formed, it then fuses with lysosomes in a process facilitating the formation of autolysosomes and the degradation of sequestered cargo. In the maturation process, complete autophagosomes become decorated with key

mediators of lysosomal fusion: RAB7 and SNARE. Atg14L of the class III PI3KC complex interacts downstream in the autophagy pathway in a secondary mechanism, binding to the SNARE complex, STX17-SNAP29, and also with the vesicle-associated membrane protein 8 (VAMP8) (Chen *et al.*, 2021). The complete autophagosomes move along microtubules via motor proteins (e.g. dynein) to the lysosomes. STX17 and VAMP8 interact to localise the membranes, which allows the pleckstrin homology domain containing protein family member 1 (PLEKHM) to bind with LC3-II, RAB7 and STX17. This results in the recruitment of the homotypic fusion and protein sorting complex (HOPS) which, alongside, SNARE proteins forms a complex that tethers the autophagosome and lysosomal membranes together to allow the fusion process (McEwan *et al.*, 2015). In this, the membranes merge and draw apart to create a pore allowing the contents of the autophagosome and lysosomes to come together. Lysosomes have an acidic environment (pH 4.5–5.5) which is optimal for the lysosomal hydrolase enzymes (lysozymes) to effectively breakdown proteins, lipids, carbohydrates, and nucleic acids into monomers. The acidity within lysosomes is maintained by vacuolar ATPases, which are proton pumps situated within the lysosomal membranes (Yim and Mizushima, 2020). Monomers that result from breakdown are transported to the cytoplasm where they are recycled for use in many further biosynthetic processes. In a previous study CoVs have been shown to manipulate the autophagy process by restricting autophagic flux; achieved by limiting the size of autophagosomes, which provided a less acidified lysosome for viral survival and nutrients for optimal viral replication (Cottam, Whelband and Wileman, 2014).

1.5 Drug Therapies and Vaccine Strategies in Coronavirus Infections

1.5.1 Therapeutic Management of Hospitalised Coronavirus patients

Symptomatic cases of human CoVs are typically categorised into non-hospitalised or hospitalised patients. Those with mild-to-moderate symptoms are typically managed

with symptomatic care and supportive guidance at home (seen with HCoV-OC43 and mild SARS-CoV-2 infections), whilst those with pre-disposing factors and severe illness are treated in hospital settings to aid in more desired outcomes. Hospitalised COVID-19 patients that require oxygen therapy were administered immunomodulatory drugs (such as corticosteroids) and viral inhibitors (such as remdesivir) (Atluri, Aimlin and Arora, 2022). In spite of this, the most serious patients who required more invasive oxygen therapy followed a course of immunomodulatory drugs alongside prophylactic antibiotic therapy to provide protection against concomitant infections by opportunistic pathogens. In the case of felids, they are administered treatment if it is deemed beneficial to the animal, however, most serious cases result in palliative care or euthanasia being opted for (Izes *et al.*, 2020). More treatment options for FIP are becoming available as a result of the COVID-19 pandemic, however they are currently expensive. HCoV-OC43 is typically not treated with immunomodulatory therapies due to mildness of illness compared to more acute disease, as such, it is not a target of any current anti-viral therapies.

1.5.1.1 Immunomodulatory therapies

Immunomodulatory therapies, such as glucocorticosteroids and monoclonal antibodies (mAbs), have been used extensively since the COVID-19 pandemic with systemic inflammation presenting as the characteristic ‘cytokine storm’ observed in the most severe cases. Glucocorticosteroids, such as dexamethasone, have inhibitory effects on both the innate and adaptive immune systems; they suppress pro-inflammatory cytokine release, which reduces the activity of many immune cells (such as macrophages and helper T cells) preventing excessive immune activity (Chan, Sharif and Rochwerg, 2021). In addition to this, they bind to glucocorticoid receptors which modulates transcription factors of key pro-inflammatory molecules (such as NF-κB). Glucocorticosteroids are also renowned for their activity in reducing capillary permeability, which aids in the control of pulmonary oedema in the lungs, for

example. mAbs are another key therapeutic strategy employed in the management of severe CoV cases. They bind to the surface of the viral target, for example the spike protein, blocking viral entry into host cells. The Fc region of mAbs can attract immune cells (such as cytotoxic T cells and macrophages), leading to immune response modulation, which aids in viral clearance (Gogesch *et al.*, 2021). Examples of mAbs authorised for use in COVID-19 infection are: bamlanivimab plus etesevimab, sotrovimab and bebtelovimab (Miguez-Rey *et al.*, 2022). In felids, the use of mAbs is much less, but they can be used to aid in therapy of early FIP cases and improve survival chances (Lemmermeyer *et al.*, 2016). mAbs have been demonstrated to have increased efficacy in the early course of infection, reducing viral load, improving case outcomes, and contributing to lowered mortality rates. Resistance to mAbs can arise though antigenic drift, meaning new derivates need to be produced, which is a costly process and a limiting factor in their general usage globally.

1.5.1.2 Coronavirus Viral Inhibitors

Viral inhibitors, or anti-viral treatments, have been developed to prevent transmissibility, severe illness and increased mortality in CoV infections. In COVID-19, three antiviral therapies were made available for use; remdesivir and molnupiravir are RdRp inhibitors, whilst Paxlovid is an inhibitor of 3C-like proteases in the virus (Najjar-Debbiny *et al.*, 2023). The efficacy of these inhibitors is still an area for much more study, with remdesivir being found to have little-to-no statistically significant benefits to patient outcomes (Wang *et al.*, 2020) and can have a range of off-target effects. FIP has a much more limited number of treatments available, but recent studies on GS-441524, an RNA terminator of viral RdRp have found significant effectiveness in treatment of FIP in infected felids, whilst remaining safe in the therapeutic period (Izes *et al.*, 2020).

1.5.2 Vaccine Landscape

Vaccine development, and overall landscape, for CoVs has been subject to massive recent advances, particularly owing to the COVID-19 pandemic. Vaccines are vital for the control of pandemic-level events as they are a mechanism of controlling transmission and lowering mortality. Adaptive immune responses are much stronger in vaccinated individuals, with IgG levels rapidly rising. In SARS-CoV-2, many forms of vaccines were developed, such as: mRNA, vector-based, viral protein/adjuvant and inactivated vaccines. In the USA, the Pfizer-BioNTech (mRNA), Moderna (mRNA) and Novavax (Recombinant spike protein, adjuvant) were licenced for use (Cascella *et al.*, 2024). As reported by the UK Government in 2024, the vaccines made avaliable provided an increased protection from hospitalisation by 50 to 60% against the Omicron variant. In spite of the efficacy, the constant antigenic drift that occurs in CoVs means that there is a continual need for informed viral surveillance and monitoring to ensure the effectiveness of the vaccines against future strains. Booster doses are administered to provide this increased level of protection, and are predominantly given to those with predisposing health conditions (Shekhar *et al.*, 2021). In FCOV, the development of vaccines is currently a difficult proposition due to the mutation dynamics of the virus; vaccines available have limited efficacy, and research is continuing to provide more effective choices. HCoV-OC43 is not the target of vaccine programmes due to most infections usually being mild and self-clearing; despite this, the understanding of antigenic drift of the virus can provide invaluable knowledge to drive vaccine developments in other key CoVs (Kistler and Bedford, 2021).

1.6 The Interactions of Coronavirus NSP6 with Autophagy

1.6.1 Overview

CoV NSP6 is a transmembrane protein with a crucial role in the replication and assembly of progeny virions in the CoV lifecycle. ORF1a is the gene where NSP6 is

encoded and it is conserved across many CoVs (such as SARS-CoV-2, FCOV and HCoV-OC43). Interactions of NSP6 with the autophagy pathway in host cells has been observed previously; NSP6 has been suggested to modulate autophagy perhaps as a mechanism to modulate the process for more optimal viral replication.

1.6.2 The Effect of NSP6 on Autophagosome Production

The most widely understood effect of NSP6 on autophagy is the interference with autophagosome production. In SARS-CoV-2, NSP6 has been shown to interact with the early omegasome which forms the autophagosome later in the pathway (Cottam *et al.*, 2011). Sequential interactions with Atg proteins initiates autophagosome formation and maturation (Cottam *et al.*, 2011). Previous studies have shown that NSP6 also restricts the size of the autophagosomes formed. It was established by Cottam *et al* (2014) that the size of the autophagosomes formed in infectious bronchitis virus (IBV) infection were significantly smaller than those induced by standard stress inhibition of mTOR. This has been identified as a potential mechanism that NSP6 utilises to modulate autophagy to promote greater viral proliferation and subsequent egress.

1.6.3 The Effect of NSP6 on Autophagic Flux and mTOR Activity

Canonical autophagic flux is the rate at which cellular material is degraded and recycled through autophagy. It refers to the entire process occurring under standard conditions (such as stress and nutrient deprivation), and the subsequent degradation of autophagosomal cargo by lysosomes, generating molecules for use in further biosynthetic processes (Karsli-Uzunbas *et al.*, 2014). Whilst mTOR is active, the process of autophagy is under constant suppression; NSP6 has been hypothesised to have a role upstream in autophagy, which would potentially lead to a greater flux, generating larger numbers of autophagosomes for viral proliferation. NSP6 plays a significant role in inhibition of lysosomal acidification, a condition required for effective degradation of sequestered cargo within the autolysosome by lysosomal

hydrolases (Bills, Xie and Shi, 2023). This inhibition results in an accumulation of non-digestive autophagosomes, significantly impeding canonical autophagic flux. It has been suggested that NSP6 performs this role perhaps in a bid to evade immunity and degradation of the virus within autophagosomes, meaning they can survive in the, otherwise, acidic environment of the lysosomes (Sun, Yu, *et al.*, 2022). Survival within autophagosomes may allow the virus to have access to nutrients necessary for replication, enhancing viral survival and proliferation (Sun, Liu, *et al.*, 2022). Inhibition of lysosomal acidification can lead to higher stress levels in host cells, which drives NLRP3 activation. NLRP3 detects pathogens and stress signals and subsequently release pro-inflammatory cytokines (such as IL-1β) once caspase-1 has been activated (Rodrigues *et al.*, 2021). This cascade results in pyroptosis, which can damage neighbouring cells and tissues by inflammation; a potential mechanism for viral pathogenesis and overall transmissibility (Bergsbaken, Fink and Cookson, 2009).

1.6.4 The Effect of NSP6 on BST-2/Tetherin

BST-2/Tetherin is a protein that anchors progeny virions of enveloped viruses (such as CoVs) to the surface of host cells, restricting the release and transmissibility to neighbouring cells (Neil, Zang and Bieniasz, 2008). Transfection of Middle-East respiratory syndrome (MERS-CoV) NSP6 interfered with BST-2 activity (Dr Coleman, unpublished data). A probable conclusion for this activity was that NSP6 performs this action to allow greater viral egress and replication, driving overall replication.

1.7 Hypothesis

This study hypothesises that NSP6 modulates autophagy and interferes with host metabolic pathways including mTOR signalling, to drive CoV replication and immune evasion and that such function is conserved between different CoVs.

1.8 Aims/Objectives

The main aim of this project was to determine the potential effect of coronavirus NSP6 of FCOV, HCoV-OC43 and SARS-CoV-2 on autophagy in mammalian cell lines. This was achieved through several key objectives:

- → To analyse bioinformatics data of coronavirus NSP6 using tools such as: Clustal Omega, NCBI BLASTP, and transmembrane prediction analysis.
- → To produce coronavirus NSP6 (of FCOV, HCoV-OC43 and SARS-CoV-2) constructs expressing N-terminal mCherry tags, through restriction digest cloning.
- → To measure the induction of autophagy using immunoblotting and indirect immunofluorescence to evaluate expression of LC3.
- → To use immunoblotting to evaluate p62/SQSTM1 expression and assess the effect of NSP6 on autophagic flux.
- → To use indirect immunofluorescence to assess BST-2/tetherin expression, providing an insight into the modulation of host immune defences by NSP6.
- → To assess the effect of NSP6 on mTOR activity through immunoblotting, evaluating the expression of S6K and phosphoS6K.

2 Methods

2.1 Restriction Ligation Cloning of NSP6 into pCAGGS_mCherry Vector

2.1.1 NSP6 constructs in pUC57 vector

NSP6 constructs of FCOV, HCoV-OC43 and SARS-CoV-2 were synthesised and cloned into the pUC57 vector by GenScript, UK. The constructs were codon optimised for mammalian cell line expression and included the full-length NSP6 coding sequence. Upon receipt of the constructs, they were stored at -20°C prior to use in restriction digest cloning. To verify the cloned NSP6 sequences, the constructs were sent for Sanger sequencing (GeneWiz, UK). The sequencing results were analysed in SnapGene and were confirmed to match the expected NSP6 sequences prior to commencing further cloning applications.

2.1.2 PCR

Polymerase chain rection (PCR) was used to amplify the mCherry coding sequence from pBABE-puro mCherry_eGFP_LC3 stock plasmid (Addgene, 22418) with 5'EcoRI and 3'KpnI restriction sites added in the PCR primers, to allow cloning into the pCAGGS vector utilising the included restriction sites. This was performed for each of the three selected NSP6 sequences. Stop codons were not added to the pCAGGS_mCherry 3′ primer in order to allow expression of the fluorescent tag in frame with 3′ ligated NSP6 constructs. NSP6 constructs were amplified from the manufacturer's puc57 vector. Primer sequences are shown in table 2. The PCR reactions were performed using a 96-well BIOER Gene Explorer thermal cycler (BioER) utilising a programmed set of conditions: initial denaturation step 98ºC for 30 seconds; 30 cycles of 98ºC for 30 seconds/ melting temperature gradient of primer (10ºC gradient, table 2) for 30 seconds/72ºC for 20–30 seconds (per kb); a final 2-minute 72ºC extension was programmed to complete the reactions, with the

temperature being held at 16°C until samples removed. PCR amplification reactions were made to a 25 µl total with the reagents outlined in table 3.

Table 2*:* Oligonucleotide sequences for restriction digest PCR amplification

Oligonucleotide name	Oligonucleotide	Melting Temperature (T_m), °C	Product size (Base pairs)
EcoRI_mCherry_for	gatctaGAATTCggatctgccaccatg	55	771
mCherry_KpnI_Rev	agtatgGGTACCtcctgggccagcgga	59	
KpnI_FIP_For	actcatGGTACCatgtccggcaaggtc	54	912
FIP_NheI_Rev	agtatgGCTAGCctactggacggtggagat	53	
KpnI_OC43_For	actcatGGTACCatgagcaagagaacc	49	891
OC43_XhoI_Rev	atgagtCTCGAGctattgaaactggctcac	48	
KpnI_CoV2_For	actcatGGTACCatgtccgctgtgaag	52	900
CoV2_XhoI_Rev	atgagtCTCGAGctactggacggtggcgac	58	

Restriction sites are capitalised and underlined.

Table 3: Reagents quantities for a typical PCR amplification of NSP6 constructs into pCAGGS_mCherry vector

Reagent	Concentration
5X Q5 Reaction Buffer (NEB)	1X
10 mM deoxynucleotides (dNTPs, NEB)	200 µM
10 µM Forward Primer	0.5 µM
10 µM Reverse Primer	0.5 µM
Plasmid/Template DNA	<1000 ng
Q5 High Fidelity PCR Enzyme (NEB)	0.02 U/µl
Nuclease Free Water (NF H_2O)	to 25 µl

2.1.3 Agarose Gel Electrophoresis

Samples of the amplified PCR products were loaded into agarose gels utilising 6X purple loading dye (New England Biolabs, NEB); DNA fragments were separated by length in 1% agarose gels in TAE buffer with 0.02 µg/ml Nancy-520 (Sigma-Aldrich) to visualise the DNA bands. Electrophoresis was performed at 120V for 45–50

minutes, or until clear separation of products was seen. The band sizes were compared to those of the 1 kb DNA ladder (NEB). The gel was visualised by UV transillumination using the nucleic acid gel viewer on the iBright CL1500 (ThermoFisher Scientific), and the size of these bands was compared to the predicted virtual gel feature and known base-pair (bp) values from sequences of the constructs on Geneious Prime (Biomatters).

2.1.4 PCR product purification

PCR amplified products were purified from agarose gel(s) utilising the PCR purification protocol provided by the manufacturer (Machery-Nagel). Purified DNA was eluted in 30 µl of nuclease free (NF) H_2O and stored in a -20°C freezer until required.

2.1.5 Restriction digest

Purified PCR products were analysed by Nanodrop spectrophotometer (ThermoFisher Scientific) to measure absorbance at 260/280 nm and calculate the concentration of DNA which was used to determine the volume required to achieve 1 µg of DNA in each reaction. Each purified product was digested with 1 µl of the relevant oligonucleotide restriction enzymes, as displayed in table 4 (NEB). The digests were performed in 0.2 ml PCR tubes and were added to a preheated heat block (ThermoFisher Scientific) at 37°C and incubated for 1 hour. Digests were entirely loaded into agarose gels and gel electrophoresis performed utilising the conditions detailed previously, in section 2.1.3.

Table 4: Restriction enzyme double digestion reaction used

Reagent	Concentration
Amplified PCR DNA Product	1 µg
Forward Restriction Enzyme	1 µl
Reverse Restriction Enzyme	1 µl
10X rCutSmart (NEB)	1X
Nuclease Free Water (NF H_2O)	To 10 µl

2.1.6 Gel Purification

The agarose gel was visualised under low-level UV light box, the correct PCR product bands were excised using a sterile scalpel and placed into correspondingly labelled 1.5 ml Eppendorf tubes. The excised bands were purified using the nucleospin columns (Machery Nagel) following the manufacturer's gel clean-up protocol. Purified DNA was eluted in 30 µl of NF H_2O and DNA concentration established using a Nanodrop spectrophotometer (ThermoFisher Scientific) prior to being stored at -20ºC until required.

2.1.7 Ligation

Purified mCherry DNA insert was ligated into compatible restriction digested pCAGGS vector at 16ºC overnight in BIOER Thermal Cycler Gene Explorer. The quantity of DNA for each reaction was determined as previously outlined. Reaction for ligations typically comprised: 1 µl 10x ligase buffer (NEB), a 1:3 vector: insert concentration determined by the NEB ligation calculator (NEB Cloning), 1 µl T4 DNA ligase enzyme (NEB), and NF H_2O to achieve a final volume of 10 µl.

2.1.8 Transformation

Ligated vector and insert DNA mixes were transformed into chemically competent Stbl-3 *Escherichia coli* (ThermoFisher Scientific), aliquots of which were stored at –80ºC. Cells were thawed on ice, 30 µl aliquots were made in Eppendorf tubes, and 3 µl of ligation mix was added to an aliquot. The aliquots were incubated on ice for 30 minutes and then heat-shocked at 42ºC for 30–45 seconds prior to being placed on ice for a further 5 minutes. After such time, 170 µl of SOC growth media (NEB) was added. The cells were then incubated for 1 hour at 37ºC, in a shaking incubator at 220 RPM (ThermoFisher Scientific) prior to being spread onto LB-agar (Sigma Aldrich) plates containing 50 µg/ml ampicillin (Sigma Aldrich) and incubated at 37°C overnight.

2.1.9 Plasmid MiniPrep

The transformed plates were compared against a control plate of vector only and were verified for use if the insert+vector plate had visibly more colonies. Single bacterial colonies were inoculated into 3 ml of LB-Broth (Sigma Aldrich) with 50 µg/ml Ampicillin (Sigma Aldrich) and were incubated in a shaking incubator at 220 RPM, 37°C overnight. From the overnight culture, 2.8 ml was removed and centrifuged, which resulted in a pellet; the remaining 0.2 ml of the overnight culture was reserved for Midi/MaxiPrep once the plasmid DNA was verified. The plasmid DNA was extracted from the pellet using a Monarch MiniPrep kit (NEB), following the manufacturer's protocol. Purified plasmid DNA was eluted in 30 µl NF H_2O and stored at -20°C.

2.1.9.1 Test Digest Screening

Purified plasmid DNA was digested with the relevant restriction enzymes to ensure that the plasmid contained the desired gene after transformation. Each plasmid digest was set up as displayed in table 5. The digests were performed in 0.2 ml PCR tubes and were added to a preheated heat block (ThermoFisher Scientific) at 37°C and incubated for 1 hour. Test digests were loaded into agarose gel in line with the conditions outlined in section 2.1.3.

Table 5: Test digest reaction used

Reagent	Concentration
Amplified PCR DNA Product	1 µg
Forward Restriction Enzyme	1 µl
Reverse Restriction Enzyme	1 µl
10X rCutSmart (NEB)	1X
Nuclease Free Water (NF H_2O)	To desired volume

2.1.10 DNA Sequencing

DNA sequencing was performed to ensure that the vector had been successfully ligated and contained the desired fusion protein in frame with the NS6 sequence

(mCherry or HA). Sequencing reactions were performed using plasmid DNA at a concentration of 100 ng/µl and were subjected to Sanger sequencing using the commercially available primers used for sequencing applications RJS27 (5′- CAA GAA GGG CGA CAG TAG AC -3′) and M13 Reverse. Sequences received were analysed in both Geneious prime and SnapGene to ensure that that the sequences were as predicted.

2.1.11 DNA MaxiPrep

MaxiPrep purification of plasmid DNA was performed to provide sufficient quantities of plasmid for transient transfection into cells. Bacterial cultures remaining from those previously used for Minipreps were retrieved from storage at 5°C and inoculated into 200 ml of LB-Broth supplemented with ampicillin (50 µg/ml) and incubated at 37°C overnight with shaking at 220 RPM. DNA was purified utilising the PureYield MaxiPrep system (Promega); the entire process took place through the PureYield Maxi binding column according to the standard product protocol. Post-purification, the DNA was eluted in 1 ml of NF H_2O in a 1.5 ml Eppendorf tube.

2.1.11.1 DNA quantification

Plasmid DNA produced from the MaxiPrep purification process was quantified to ascertain the DNA concentration (ng/µl), using the method previously outlined.

2.2 Bioinformatics

2.2.1 Sequence Retrieval and Analysis

To confirm the identity of the NSP6 sequences synthesised into the puc57 plasmid constructs (obtained from GenScript), the Basic Local Alignment Search Tool (BLAST, NCBI, USA Government) database was used. These NSP6 sequences had been confirmed using full plasmid sequencing prior to cloning and further protein expression analyses, outlined in later chapters. The BLAST tool allowed for identification of the closest matching reference sequence strains, and their

corresponding GenBank accession numbers, to identify the viral strain embedded in the sequence; these are highlighted in table 6.

Table 6: NSP6 variants used and GenBank accession numbers

Virus name	Strain/isolate	GenBank Accession number	Gene analysed
FCoV (FIP)	Feline infectious peritonitis virus	WYM67007.1	ORF1ab polyprotein
HCoV-OC43	Human coronavirus OC43	AGT51686.1	Replicase polyprotein 1a
SARS-CoV-2	Wuhan-Hu-1 (NC_045512.2)	WZB22770.1	ORF1a polyprotein

2.2.2 Multiple Alignment

FASTA-format nucleotide and amino acid sequences of NSP6 and full-length CoV genomes were aligned using the Clustal Omega multiple alignment tool. This process involved pairwise alignments and the creation of a distance matrix using a neighbour-joining method (UPGMA) delivering a similarity index for the aligned sequences. First, the whole genomes from the NCBI reference sequences were aligned to assess similarities and differences across the CoV variants. Then, NSP6 sequences were aligned to determine the percentage similarity and also to identify highly conserved regions within the sequences. LB4717 was an identifier provided by GenScript when constructs were synthesised. Clustal Omega was accessed via EMBL-EBI web server (Madeira *et al*, 2024).

2.2.3 Transmembrane Prediction

Transmembrane prediction was performed using DeepTMHMM (Hallgren *et al.*, 2022) by submitting FASTA format amino acid sequences into the online machine-learning tool; the algorithm predicts the topology of alpha-helices and beta-barrel transmembrane proteins. These transmembrane proteins play a large role in cellular processes; the helices are key for membrane proteins that span the lipid bilayer, being exposed on both side of the membrane.

2.3 Cell Culture

2.3.1 Cell Culture

Complete cell culture media was prepared utilising Dulbecco's Modified Eagle Medium (DMEM, containing D-glucose and l-glutamine; Gibco, ThermoFisher Scientific), performed by adding 50 ml of One Shot Fetal bovine serum (FBS; ThermoFisher Scientific), giving a 10% final FBS concentration. 200 µg/ml gentamicin solution (Sigma) was added to complete the media preparation. The complete media was pre-warmed to 37°C prior to cell culture activities.

2.3.2 Continuous Cell Lines

The human lung adenocarcinoma 549 (A549) cell line (kindly provided by Dr Stott-Marshall) was typically cultured in T25 flasks at 37°C in a 5% CO_2 humidified incubator (ThermoFisher Scientific).

2.3.3 Cell Line Recovery

Recovery of frozen cell stocks was performed by removing cell cryovials from liquid nitrogen storage and rapidly incubating at 37°C. The cells were added slowly to 3 ml of warmed growth media; this was made up to 10 ml prior to centrifugation, which was performed at 500 x g for 8 minutes. The supernatant was carefully removed, and the pellet was resuspended in fresh growth media. Cell counts were performed using a Countess 3 automated cell counter (ThermoFisher/Invitrogen), and cells transferred into new T25 flasks. Complete media was replaced at 24 h intervals until confluency was reached. Frequent passages were performed as outlined below (section 2.1.3).

2.3.4 Cell line maintenance

Cell lines were observed at regular intervals (2 days) with an inverted light microscope. Cells were passaged once confluency of >80% was achieved, or if floating cells were observed. Cells were passaged by removing the growth media, followed by a washing step with phosphate-buffered saline (PBS). Then, 1ml of

TrypLE (Gibco, ThermoFisher Scientific) was added and incubated at 37℃ for 3–5 minutes, or until cells were visibly detached from the flask wall. TrypLE is a gentle dissociation reagent, which detaches the adherent cells from the flask bottom. Following removal of the cells from the wall of the plastic flask, 9 ml of pre-warmed, fresh complete DMEM was added to neutralise the TrypLE reagent, reaching a total volume of 10 ml in the flask. The cells were gently pipetted up and down to remove visible clumping, and one this was confirmed 9 ml of media was removed to give a 1:10 split of the cell line. The T25 flask was then topped up to 7 ml with complete DMEM, the passage number/date was written on the flask, and it was returned to the incubator at 37℃. Due to constant usage of the cell lines in transfections, the cell lines were always split 1:10, performed twice weekly to ensure that cells at an optimal working confluency (≥70%) were readily available.

2.4.1 Transient Transfection

2.4.1.1 Preparation of cell lines for Transfection

Cell lines were passaged as detailed in 2.2.3, up to the neutralisation of TrypLE dissociation enzyme, when the cells were re-suspended with 9 ml of complete DMEM and remained in the T25 flask. Ten microlitres of cells were removed from the T25 flask at this point, placed into a haemocytometer and counted as outlined in section 2.2.2. The countess calculates a total cell number, and the amount of media required to achieve desired concentrations. Typical cell concentrations seeded were:

- → 24-well plate: 0.24 x10^5 cells/well
  - Density at confluence: 0.24x10^6
- → 6-well plate: 0.3 x 10^6 cells/well
  - Density at confluence: 1.2x10^6

The plate(s) were incubated for 24 hours prior to transfection, to ensure a confluency of cells ≥80%.

2.4.1.2 Transient Transfection of A549 Cell Line

A549 cells were grown to ≥80% confluency and transfected in duplicate (at a minimum), within a 24-well plate with or without circular glass coverslips (which were pre-soaked in 100% Methanol and lined the bottom of each well) depending on whether the intended use was for fluorescent imaging (with) or immunoblotting (without). TransIT-X2 transfection delivery reagent, MIR6000 (Mirus Bio, Wisconsin, United States of America) was used to transfect cells with 1 µl of DNA (concentration: 1 µg/µl) per well of pCAGGS_mCherry-tagged constructs alongside the pCAGGS_mCherry empty vector as a negative control. For each transfection, complexes were made by adding 50 µl of serum-free (SF) media and the DNA to 1.5 µl of TransIT-X2; this was repeated for each of the mCherry-NSP6 constructs. The transfection complex was incubated at room temperature (RT) for 30 minutes to allow sufficient complexes to form. After incubation, 50 µl of each complex was added dropwise to the desired wells and was incubated for 48 hours prior to harvesting the coverslips and proceeding with either cell lysis to harvest cellular protein for immunoblotting or proceeding with the fluorescence protocol.

2.4.2 Post-Transfection Drug Treatment

Prior to the preparation of cell lysate(s) or the commencement of fluorescence protocols the transfected cells were optionally treated with either chloroquine (CQ) (Sigma Aldrich) or torin (Sigma Aldrich). CQ treatment raises lysosomal pH and inhibits the fusion of lysosomes to autophagosomes, which results in an accumulation of autophagosomes, desirable to assess the activation of autophagy in mammalian cells, providing a positive control for subsequent experiments. Torin treatment inhibits mTOR, causing an activation of the autophagy pathway, desirable to observe as a control versus potential effects that NSP6 alone, has on autophagy induction.

2.5 Fluorescent Imaging

2.5.1 Fixing Co-Transfected Cells

Coverslips within the 24-well plate containing the transfected cells were washed with PBS to remove excess media prior to being fixed with a 4% paraformaldehyde (PFA) buffer for 15–20 minutes at RT. The fixed cells were then washed three times with PBS on a desktop mini rocker (Stuart Science Equipment), each for 5 minutes to remove any excess PFA. A quenching step with 0.1M glycine was performed for 10 minutes to remove excessive background from the coverslips, before being washed three more times with PBS for 5 minutes. Fresh PBS was then added to each of the wells and the plate was stored at 4ºC until used for imaging.

2.5.1.1 Fixing cells for Immunofluorescence

The coverslips from autophagy drug-treated cells were fixed and permeabilised in methanol as an alternative to PFA. Crosslinks when PFA is utilised means that some epitopes are unavailable for antibody binding, therefore the decision was made to fix these treated cells with methanol. Media was removed from the cells before fresh 100% methanol, at -20℃ was added to the wells and placed in the freezer for 15 minutes. The wells were then washed three times with PBS for 5 minutes each to remove methanol prior to being blocked with a 5% bovine serum albumin (BSA).

2.5.1.2 Antibodies

Prior to antibody incubation the fixed cells were blocked by rocking incubation for one hour at RT in 5% BSA (Fisher, ThermoFisher Scientific, Loughborough United Kingdom) in PBS-Tween (0.1% v/v; PBS-T). Post-blocking, the wells were emptied of BSA buffer. Primary antibodies were prepared in 5% BSA, PBS-T to the dilutions outlined in table 6; 200 µl of diluted antibody buffer was added to each well, and the 24-well plate was incubated at 4ºC overnight on a rocking incubator. After overnight incubation, each well was washed three times with PBS-T on a rocking incubator for five minutes. Secondary antibodies were then prepared in 5% BSA, PBS-T to the

dilutions in table 6 and 200 µl was added to each well. The plate was incubated with rocking at RT for one hour in darkness to prevent loss of fluorescence. The cells were washed on a rocking incubator three times for 5 minutes with PBS-T in darkness and were left in fresh PBS-T prior to slide mounting.

Table 7: Antibodies used for Immunofluorescence imaging

Monoclonal Antibody	Dilution Used	Manufacturer	Product code
Primary antibodies			
Rabbit Anti-HA	1:400	Cell Signaling Technology	3274s
Mouse Anti-HA	1:400	Cell Signaling Technology	2367s
Rabbit Anti-LC3B	1:400	Cell Signaling Technology	3868s
Secondary Antibodies			
Goat Anti-Rabbit AlexaFluor 594	1:1000	Abcam	ab150080
Donkey Anti-Mouse AlexaFluor 488	1:1000	Abcam	ab150105

2.5.2 Mounting

Once the secondary antibody wash steps had been performed, counterstaining using Fluoroshield™ with DAPI mounting media (Sigma-Aldrich) was performed to stain cell nuclei. The glass coverslips were removed from each well and kept 'cell side up'. Each coverslip was then inverted to make the cells 'face down' and were mounted onto a glass microscopy slide with a drop of mounting media on its surface. Once the mounting media had set and the coverslip was fixed, excess mounting media was removed, and the coverslips were sealed with clear nail polish to preserve the quality of the slides. The slides were kept in a slide storage container at 4°C in darkness prior to examination.

2.5.3 Widefield microscopy

Widefield microscopy was used to visualise cellular proteins and structures once immunofluorescent and indirect immunofluorescent samples were fixed. Images were obtained at 40x and 100x magnification on a Leica DM5000b microscope (Leica Microsystems, USA). At 40x magnification, the samples were examined to assess overall cell morphology and generalised patterns of protein expression. Then, at 100x magnification, using immersion oil, higher-resolution images were obtained to focus on areas of protein localisation within cells. All images were obtained in a darkened room using the Leica LASX software (Leica, USA).

2.6 Protein Expression Analysis and Immunoblotting

2.6.1 Preparation of Cell Lysate

Once the transfected cells had been incubated for 48 hours the cell media was removed, and each well washed with PBS. The cells were then lysed by adding 100 µl of Laemmli (1X) LDS sample buffer (Bio-Rad). Before use, 900 µl of 2X LDS buffer was reduced with 100 µl 2-Mercaptoethanol (Sigma Aldrich) and diluted with PBS to prepare a 1X final working concentration of BOLT LDS buffer. The prepared working 1X BOLT buffer was added, and the cells were incubated at room temperature for 5 minutes, with frequent gentle agitation to completely disrupt the cells. Once agglutination was observed in cells, the lysates were then harvested into correspondingly labelled 1.5 ml microtubes and heated at 70ºC for 10 minutes, following the manufacturer's protocol. The lysates were used immediately or stored at -20°C until further use.

2.6.3 Polyacrylamide Gel Electrophoresis

A pre-made BOLT 4-12% Bis-Tris Plus gel (Invitrogen, ThermoFisher Scientific) with a 1 mm thickness and 12 pre-set wells was used. A 1X concentration of running buffer was made by diluting 50 ml of a 20X NuPAGE 2-(N-morpholino) ethanesulfonic acid (MES) sodium dodecyl sulfate (SDS) Running Buffer in 950 ml of deionised water.

Then, 400 ml of 1X running buffer was added to the gel running chamber. Each sample was loaded into the pre-allocated well; a volume of 20 µl of each lysate was typically used. A pre-stained protein colour standard ranging from 10 to 250 kDa (New England Biolabs) was added at a volume of 3 µl per well. Once all samples and standards had been loaded and the 1X running was at the designated fill line, gel electrophoresis was performed at an initial 80V for 15 minutes and then run at 150V for 45–50 minutes.

2.6.3 Western blotting/ PVDF Membrane Transfer

A 1X transfer buffer, Trans-Blot Turbo (Bio-Rad) was prepared through the dilution of 5X stock in 20% ethanol. A polyvinylidene fluoride (PVDF) membrane (Bio-Rad Laboratories) was placed in 100% ethanol for 2 minutes to charge the membrane prior to being placed into the pre-prepared transfer buffer. Trans-blot mini size transfer stacks (Bio-Rad Laboratories) were soaked in the transfer buffer prior to being arranged into the blot 'stack' as shown in figure 7; in the assembly of the stack a blot roller was used to remove excess buffer and any bubbles, from the stacks and membrane. Once the gel electrophoresis had completed, the gel casing was opened, and the gel was carefully transferred onto the PVDF membrane and blot stacks, briefly being rolled before the cassette lid was placed. The blot stack was prepared on a power blot semi-dry transfer cassette (Invitrogen, ThermoFisher Scientific) and was loaded into the docking station/power supply; the membrane transfer was run on the 'Mixed-range' setting (1.3 amps for 7 minutes).

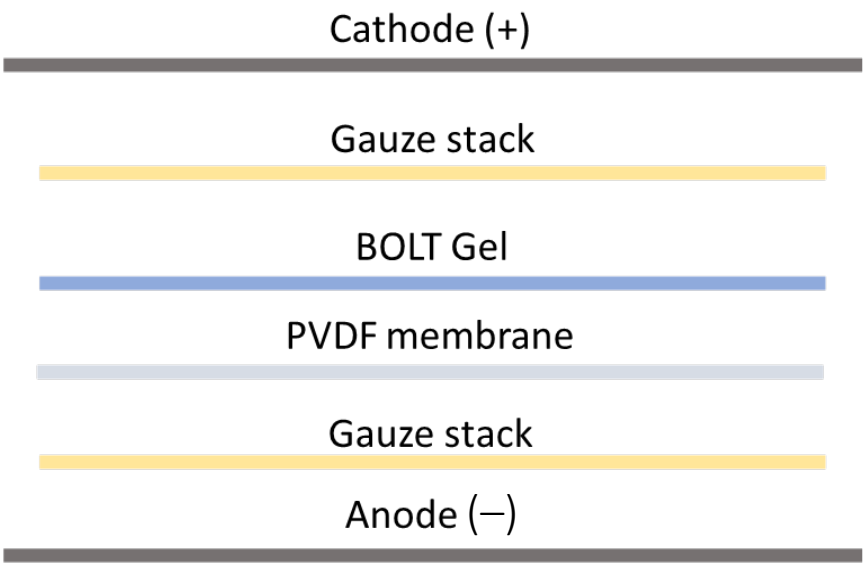

Figure 7: Gel transfer stack

Once polyacrylamide gel electrophoresis had ran, the gel was removed from the cassette and placed into a blot transfer stack, as shown. The order is: anode, gauze stack, PVDF membrane, gel, gauze stack, cathode. The stack was closed securely and docked in the transfer dock to allow blotting.

2.6.4 Membrane Blocking

A 5% milk blocking solution was prepared by adding 1.5 g of dried skimmed milk (Tesco, United Kingdom) to 30ml of PBS-T. Once protein transfer to the PVDF membrane had completed, it was removed from the stack and placed into a 50 ml tube with 5 ml of 5% milk and was incubated on a roller for 1 hour at RT. Once blocking had been completed, the PVDF membrane was cut into separate strips depending on the size of proteins of interest, to allow blots of each section with different antibodies.

2.6.5 Antibody Incubation

Once incubated with the milk block for 1 hour, the membrane was washed three times with PBS-T, rolling for 5 minutes at RT between each wash. Primary antibodies were diluted in 5% milk to optimised concentrations shown in table 7; the primary antibody incubation was performed at 4ºC overnight on a tube roller. Prior to incubation with

secondary antibodies, the membrane was washed on a roller three times for 5 minutes with PBS-T. The secondary antibodies were also diluted in 5% milk to the concentrations shown in table 7 and the incubation was performed at RT for one hour. Secondary antibodies were horseradish peroxidase (HRP)-linked to allow chemiluminescent development for blot imaging.

Table 8: Antibodies used for Immunoblotting

Monoclonal Antibody	Dilution Used	Manufacturer	Product code
Primary antibodies			
Mouse Anti-hsp90	1:5000	Invitrogen, ThermoFisher Scientific	MBH90AB
Rabbit Anti-HA	1:1000	Cell Signaling Technology	3724s
Mouse Anti-HA	1:1000	Cell Signaling Technology	2367s
Mouse Anti-P62	1:1000	Cell Signaling Technology	D5L7G
Rabbit Anti-LC3B	1:1000	Cell Signaling Technology	3868S
Secondary Antibodies			
Anti-rabbit IgG HRP-Linked	1:10000	Cell Signaling Technology	7074S
Anti-mouse IgG HRP-Linked	1:10000	Cell Signaling Technology	7076S

2.6.6 Chemiluminescence

Post-secondary antibody incubation the membrane was washed three more times with PBS-T on a rolling incubator for 5 minutes each. SuperSignal West Pico PLUS (ThermoFisher Scientific) is an HRP conjugated chemiluminescent substrate used to detect protein intensity to allow western blot analysis. The solution was prepared according to the method outlined by the manufacturer where 1 ml of stable peroxidase is mixed with 1ml of Luminol/enhancer. The membrane was incubated for 5 minutes at RT on a rolling incubator for 5 minutes.

2.6.7 Gel Imaging

The membranes were drained of any excess chemiluminescent substrate prior to being imaged. The iBright FL1500 (Invitrogen, ThermoFisher Scientific) was used to image the membrane and the chemiluminescence was observed. Images were saved as a TIF file to provide the highest quality images for protein quantification and analysis.

2.6.8 Gel Analysis and Protein Quantification

Each image obtained from the iBright system was analysed and quantified using ImageJ software (Schneider, Rasband and Eliceiri, 2012). The density of each protein band was measured using the region of interest tool which provided a pixel density for the area selected. hsp90 loading controls were used to determine an intensity ratio for each sample. Once each individual density had been measured, the quantified results were entered into an Excel spreadsheet. The hsp90 control was used to standardise the level of protein expression of each lysate. Each of the probed proteins/bands of interest was divided by the hsp90 control, and then standardised to the control lysate, giving a ratio respective to a vector only control, ensuring the measured impact on protein expression observed were a direct result of the NSP6 constructs, rather than the transfection process itself.

3. Results

3.1 Multiple Sequence alignment

Multiple sequence alignment was performed on both the nucleotide and protein sequences using the Clustal Omega algorithm to assess sequence conservation of NSP6 of FCoV, HCoV-OC43, and SARS-CoV-2. Both nucleotide (figure 8a) and protein (figure 8b) sequences of the NSP6 CoV variants (from table 6, chapter 2.2.1) were aligned to identify conserved regions that may potentially be significant to the functional properties of NSP6.

Alignment of the nucleotide sequences (figure 8a) revealed an overall conservation of around 46%, with the highest conservation being between SARS-CoV-2 and HCoV-OC43 of around 51% (fig 8b); this higher level of conservation may reflect the sequence similarity and predominant tropism of beta-CoVs.

Protein sequence alignment (figure 8c) between SARS-CoV-2 and HCoV-OC43 was around 32%, where FCoV only showed around a 28% similarity with the beta-CoVs (figure 8d). These findings highlighted a relatively low conservation between the NSP6 sequences, suggesting that the function of NSP6 may be more dependent on protein structure rather than strictly the sequence homology. Despite a generalised sequence divergence, some conserved motifs were observed (figure 8c), these include two stretches of three amino acids (highlighted in orange) and one of five amino acids, which may be functionally important. The five amino acid conservation here is situated in the N-glycosylation site (highlighted in green, figure 8c).

a)

```
FIPV            GAATTCAACATGTCCGGCAAGGT---------CAAGAGCATCTTCTACCCCATGATGACC    51
HCoV-OC43       GAATTCAACATGAGCAAGAGAACCAGACTGTTCAAAGGCACCGTGTGCTGGATCATGGCC    60
SARS-CoV-2      GAATTCAACATGTCCGCTGTGAAGAGAACCATCAAGGGAACCCACCACTGGCTGCTGCTG    60
                ***********  *                ***  * * *     *    *  **

FIPV            GCCATCGCTATTCTGTTCGCCTTCTGGCTCGAGTTCTTCATGTACACCCCCTTCACATGG    111
HCoV-OC43       TCCACCTTCCTCTTCAGCTGCATCATCACCGCCTTTGTGAAGTGGACCATGTTCATGTAT    120
SARS-CoV-2      ACCATTCTGACCTCTCTGCTGGTGCTGGTGCAGTCCACCCAGTGGTCTCTGTTCTTCTTC    120
                 ***                  *         *       **   *    ***   *

FIPV            ATCAACC---CCACCTTCGTCAGCGTGGTGCTGGCCATCACCACCCTCGTGAGCGTGCTG    168
HCoV-OC43       GTCACCA---CCAACATGTTCTCCATCACCTTCTGCGCTCTG---TGCGTGATCTCTCTG    174
SARS-CoV-2      CTCTACGAGAACGCCTTTCTGCCCTTCGCCATGGGCATCATC---GCCATGTCCGCCTTT    177
                 **  *     *  * *  *   * *     *   *           * **  *    *

FIPV            CTGGTGGCTGGCATCAAGCACAAGATGCTGTTCTTCATGAGCTTCGTGATGCCCAGCGTG    228
HCoV-OC43       GCCATGCTGCTGGTGAAGCACAAGCACCTCTACCTCACCATGTACATCACCCCCGTGCTG    234
SARS-CoV-2      GCCATGATGTTCGTCAAGCACAAGCACGCCTTTCTGTGTCTGTTTCTGCTGCCCTCTCTG    237
                    **       * *********      *   *       *   *    ***    **

FIPV            ATTCTGG---CCACAGCCCACAATGTGGTGTGGGACATGACCTACTA---CGAGTCTC--    280
HCoV-OC43       TTCACACTGCTGTACAACAACTACCTCGTGGTGTACAAGCACACCTTTAGAGGCTACG--    292
SARS-CoV-2      GCCACAGTCGCCTACTTCAACA------TGGTCTACATGCCCGCCAGCTGGGTGATGAGG    291
                              * **       **    *** *  *  *      *

FIPV            -TGCAAGTGCTGGTGGAAAACGTGAACACCACATTCCTCCCCGTGGAC---ATGCAAGGC    336
HCoV-OC43       -TGTACGCTTGGCTGT-CCTACTACGTG--CCTAGCGTGGAGTATACCTACACCGACGAG    348
SARS-CoV-2      ATCATGACATGGCTGGACATGGTGGACACCTCTCTGAGCGGCTTTAAGCTGAAGGACTGC    351
                 *         * **       *         *                    *   *

FIPV            GTGATGCTGGCTCTGTTTTGCGTGGTCGTGTTCGTGATCTGCACCATTAGATTCTTCACA    396
HCoV-OC43       GTGATCTACGGCATGCTGCTGCTCGTGGGAATGGTCTTCGTCACACTGAGAAGCATCAAC    408
SARS-CoV-2      GTGATGTACGCCAGCGCCGTGGTGCTCCTCATT---CTGATGACCGCTAGAACCGTGTAC    408
                *****    *            *  *     *     *    **    ***  * *

FIPV            TGCAAGCAGAGCTGGTTCTCTCTGTTCGCTACCACCATCTTCGTGATGTTCAACATCGTC    456
HCoV-OC43       CACGATC------------------TGTTCAGCTTCATCATGTTCGTGGGAAGACTCATC    450
SARS-CoV-2      GATGACG------------------GAGCTAGAAGGGTCTGGACACTGATGAACGTGCTG    450
                    *                         *      **       **   *   *  *
FIPV            AAGCTCCTCGGCATGATCGGCGAGCCTTGGACAGATGACCACTTTCTCCTCTGTCTGGTG    516
HCoV-OC43       AGCGTGTTCTCTCTGTGGTATAAGGGCA------------GCAATCTGGAGGAGGAAATT    498
SARS-CoV-2      ACACTGGTCTACAAGGTGTACTACGGCA------------ATGCTCTGGACCAAGCCATC    498
                *   *  **     *       *                     ***          *

FIPV            AACATGCTGACCATGCTGATCTCTCTGACCACCAAAGACTGGTTCGTGGTGTTTGCCTCC    576
HCoV-OC43       CTGCTGATGCTGGCCTCTCTGTTCGGCACATATACATGG------------ACCACCGTG    546
SARS-CoV-2      TCCATGTGGGCTCTGATCATCTCCGTGACCTCCAACTACTCCGGCGTGGTGACCACCGTG    558
                    **  *          * *     **    *                      **

FIPV            TACAAGGTCGCC------TACTACATCG---TCGTGTACGTGATGCAACCCGCCTTCGTC    627
HCoV-OC43       CTGTCCATGGCCGTGGCTAAGGTGATCGCTAAGTGGGTGGCCGTGAATGTGCTCTACTTC    606
SARS-CoV-2      ATGTTTCTGGCTAGAGGCATCGTGTTCA---TGTGCGTCGAGTATTGCCCCATCTTCTTC    615
                       * **             **          *            ** * **
```

b)

```
Percent Identity  Matrix - created by Clustal2.1


                    FIPV  HCoV-OC43 SARS-CoV-2
  1: FIPV           100.00   46.24    49.42
  2: HCoV-OC43      46.24    100.00   51.44
  3: SARS-CoV-2     49.42    51.44    100.00
```

c)

```
CLUSTAL O(1.2.4) multiple sequence alignment

LB4717-7-FIPV            EFNMSGKVKSIFYPMM-------T--AIAILFAFWLEFFMYTPFTWINPTFVSVVLAITT  51
LB4717-10-SARS-CoV-2     EFNMSAVKRTIKGTHHWLLLTILTSLLVLVQSTQWSLFFFLYENAFLP-----FAMGII-  54
LB4717-3-OC43            EFNMSKRTRLFKGTVCWIMASTFLFSCIITAFVKWTMFMYVTTNMFS------ITFCAL-  53
                         *****   : :               :    . *  *:      :       ..:

LB4717-7-FIPV            LVSVLLVAGIKHKMLFFMSFVMPSVILATAHNVV------WDMTYYESLQVLVENVNTTF  105
LB4717-10-SARS-CoV-2     AMSAFAMMFVKHKHAFLCLFLLPSLATVAYFNMVYM-PASWVMRIMTWLDMVDTSLSGFK  113
LB4717-3-OC43            CVISLAMLLVKHKHLYLTMYITPVLFTLLYNNYLVVYKHTFRGYVYAWLSYYVPSV-EYT  112
                          :  : :  :***  ::  :: * :      * :      :       *.    .:

LB4717-7-FIPV            LPVDMQGVMLALFCVVVFVICTIRFFTCKQSWFSLFATTIFVMFNIVKLLGMIGEPWTDD  165
LB4717-10-SARS-CoV-2     LK---DCVMYASAVVL-LILMTARTV-----YDDGARRV----WTLMNVLTLVYKVY-YG  159
LB4717-3-OC43            YT---DEVIYGMLLLVGMVFVTLRSI-----NHDLFSF-----IMFVGRLISVFSLWYKG  159
                               : *: .   :: ::: * * .       .           ::  *  : . :  .

LB4717-7-FIPV            HFLLCLVNMLTMLISLTTK-DWFVVFASYKVAYYI--VVYVMQPAFVQDFGFVKCVSIIY  222
LB4717-10-SARS-CoV-2     NALDQAISMWALIISVTSNYSGVVTTV-MFLARGIVFMCVEYCPIFFITGNTLQCIMLVY  218
LB4717-3-OC43            SNLEEEILLM--LASLFGTYTWTTVLS-MAVA-KVIAKWVAVNVLYFTDIPQIKIVLLCY  215
                           *   : :   : *:  .    ..     :*  :          :.     :: : : *

LB4717-7-FIPV            MACGYLFCCYYGILYWVNRFTCMTCGVYQFTVSPAELKYMTANNLSAPKTAYDAMILSFK  282
LB4717-10-SARS-CoV-2     CFLGYFCTCYFGLFCLLNRYFRLTLGVYDYLVSTQEFRYMNSQGLLPPKNSIDAFKLNIK  278
LB4717-3-OC43            LFIGYIISCYWGLFSLMNSLFRMPLGVYNYKISVQELRYMNANGLRPPKNSFEALMLNFK  275
                            **:  **:*::  :*    :  ***:: :*  *::**.::.*  **.: :*: *.:*

LB4717-7-FIPV            LMGIGGGRNIKISTVQP-    299
LB4717-10-SARS-CoV-2     LLGVGGKPCIKVATVQPG    296
LB4717-3-OC43            LLGIGGVPIIEVSQFQPG    293
                         *:*:**   *::: .**
```

d)

```
Percent Identity  Matrix - created by Clustal2.1


                        FIPV    HCoV-OC43  SARS-CoV-2
    1: FIPV             100.00   28.10      27.70
    2: HCoV-OC43        28.10    100.00     32.76
    3: SARS-CoV-2       27.70    32.76      100.00
```

Figure 8: Multiple sequence alignment of NSP6 using Clustal Omega

A) This nucleotide alignment shows the sequence conservations and differences between NSP6 variants: FCOV, HCoV-OC43, and SARS-CoV-2. B) The percentage identity matrix demonstrates a quantitative comparison of nucleotide sequence similarities. C) Protein sequence alignment of the three NSP6 variants. The conserved regions with >3 amino acids are highlighted. N-glycosylation site is highlighted in green. D) Percentage identity matrix for the protein sequence alignment.

3.2 Transmembrane prediction analysis

Transmembrane domain prediction analysis was conducted on the CoV NSP6 (FCoV, HCoV-OC43, SARS-CoV-2) sequences. Various transmembrane domain tools were used for prediction, these included DeepTMHMM, TMHMM and Protter; these

compared NSP6 structures from SARS-CoV-2, FCoV, and HCoV-OC43 (figure 9), and all of these depicted between 7 and 8 transmembrane regions across the NSP6 sequences.

The Protter tool (figure 9a) was used to generate a visual representation of the predicted transmembrane helices. The models highlighted that all three NSP6 proteins contain multiple membrane-spanning regions, consistent with their hypothesised roles in ER-associated membrane remodelling. The N-glycosylated site that is conserved in amino acid alignment is also denoted by a green symbol at the 5′ end of each NSP6.

DeepTMHMM (figure 9b) applies a posterior probability score to each amino acid residue to predict whether it resides inside, outside, or within a membrane-spanning region. This analysis revealed conserved transmembrane topologies across all three viral NSP6 proteins, however, there were differences in the lengths and positions of the specific helices.

Finally, TMHMM was used (figure 9c) to compare transmembrane region predictions. This produced highly similar results to DeepTMHMM, which further implies the point that there are between 7 and 8 predicted transmembrane regions in all three sequences, although minor variations in the helices.

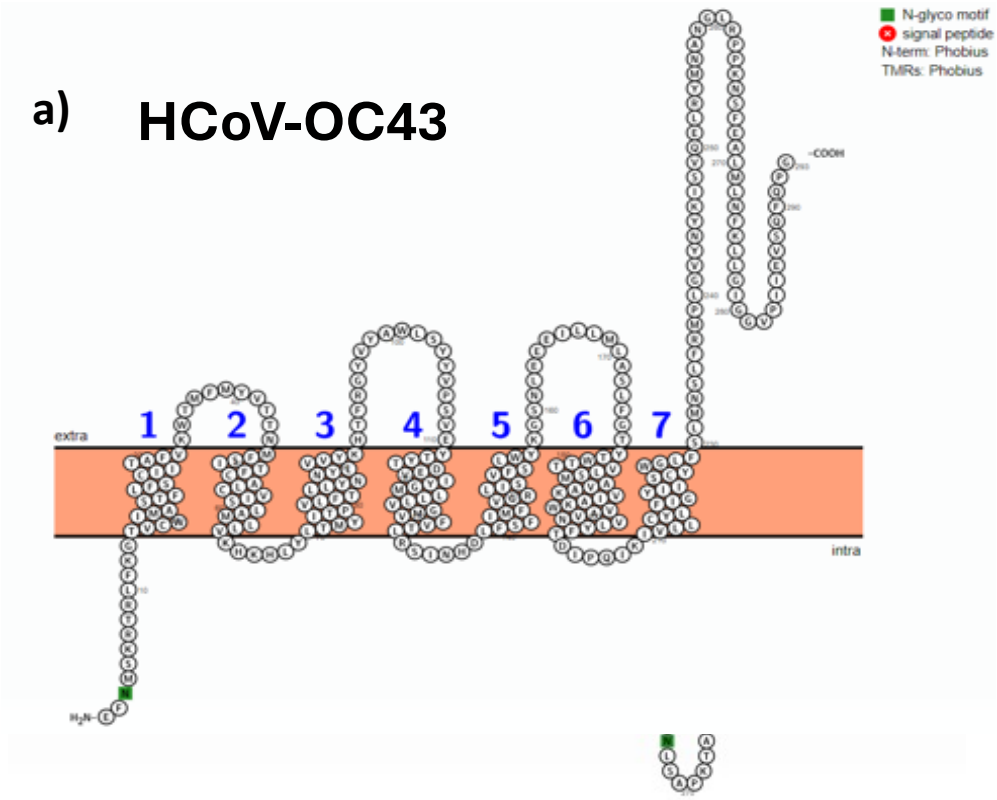
a)
HCoV-OC43
N-glyco motif
signal peptide
N-term: Phobius
TMRs: Phobius
extra
intra
1
2
3
4
5
6
7
-COOH
H2N-

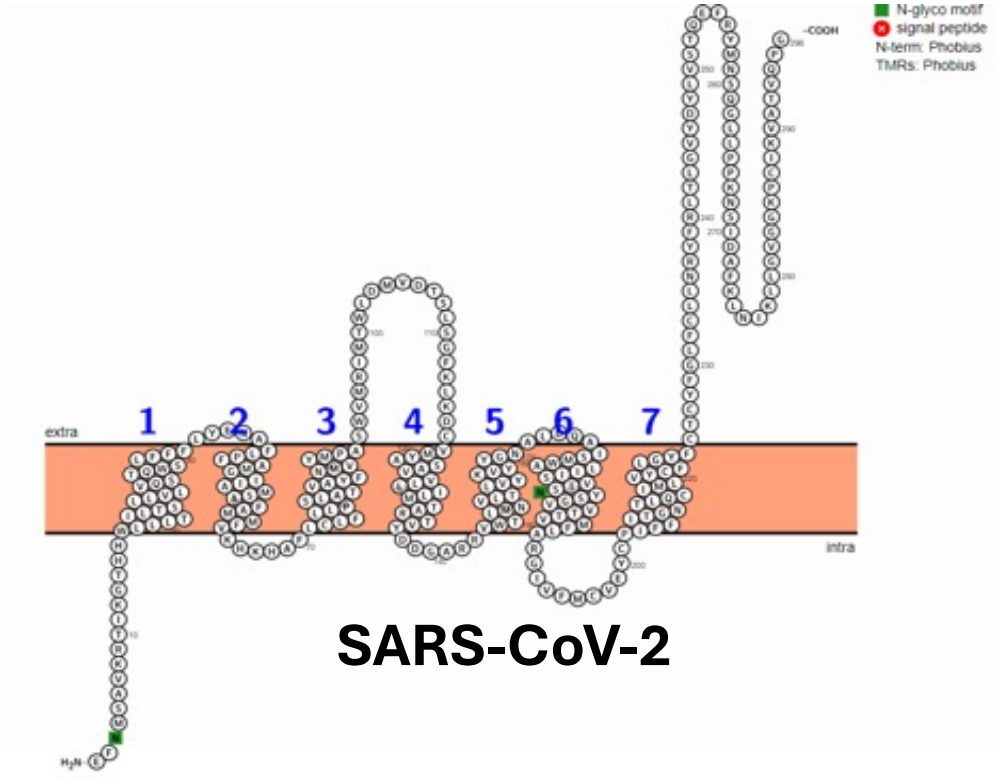
N-glyco motif
signal peptide
N-term: Phobius
TMRs: Phobius
extra
intra
1
2
3
4
5
6
7
-COOH
H2N-
SARS-CoV-2

b)

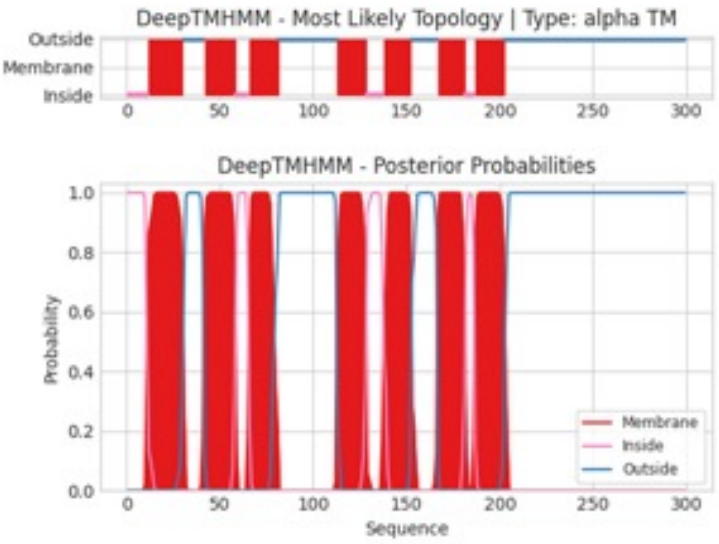

FCoV

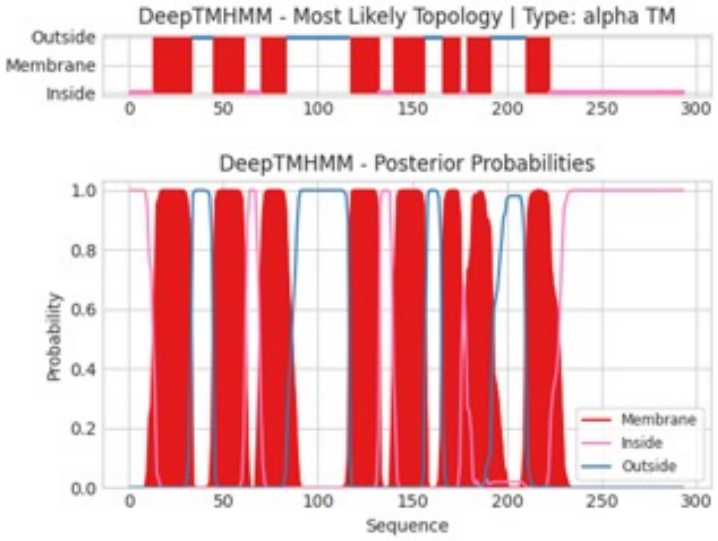

HCoV-OC43

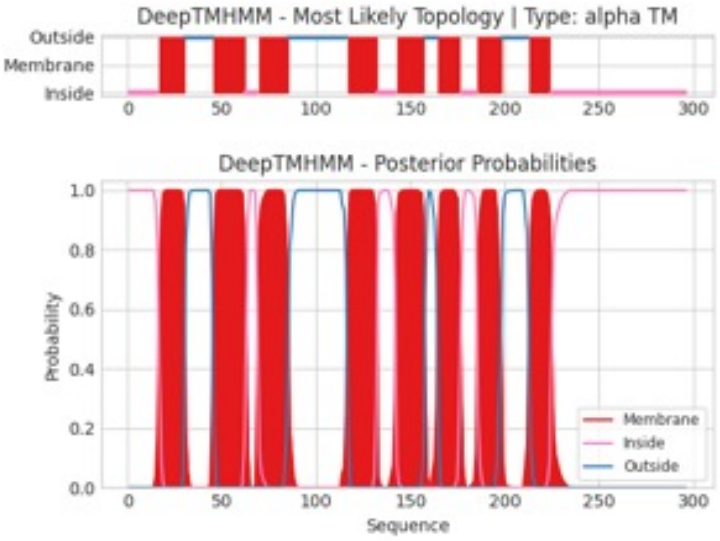

SARS-CoV-2

c)

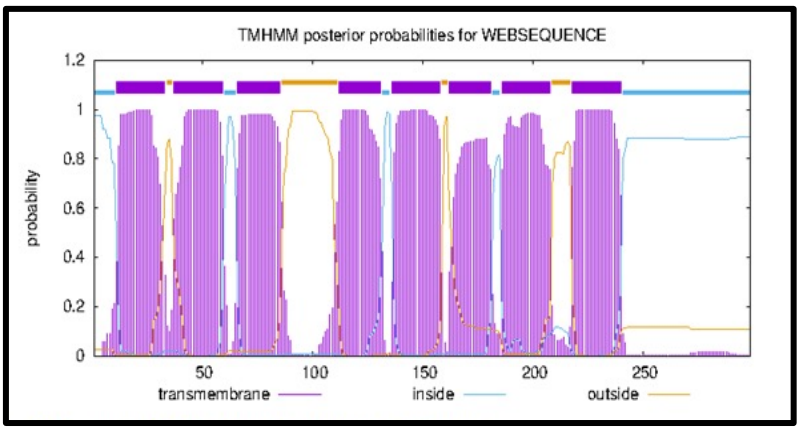

FCoV

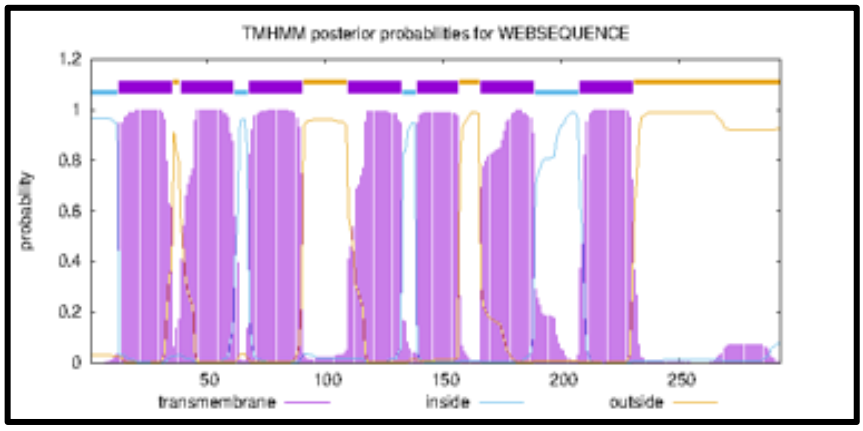

HCoV-OC43

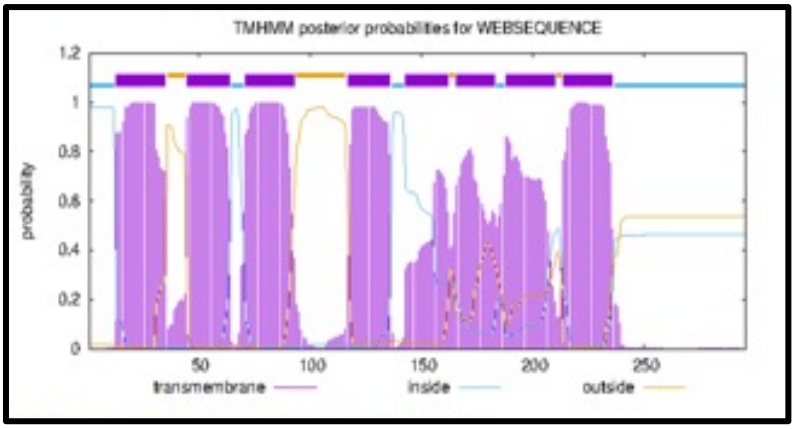

SARS-CoV-2

Figure 9: Transmembrane prediction analysis

The figure illustrates the predicted transmembrane regions of NSP6 from FCoV, HCoV-OC43, and SARS-CoV-2. The Protter tool (a) provides a visual topology of the helices, whilst the labelled graphs (DeepTMHMM, b, and TMHMM, c) depict the topology as markers.

3.3 Restriction digest cloning of NSP6 into a pCAGGS-mCherry vector

The gene encoding the fluorescent mCherry protein was successfully inserted into the pCAGGS vector by restriction ligation cloning using the restriction enzymes *EcoRI* and *KpnI* [figure 10a]. Two bands were detected on the agarose gel at approximately 900 bp and 4.6 kb. Presence of this insert was then confirmed by test digest with the same enzymes and DNA gel electrophoresis [figure 10b]. The resulting product of the cloning was 5476 bp. Genes encoding FCOV, HCoV-OC43 and SARS-CoV-2NSP6s were synthesized by GenScript then amplified from via PCR, with added linker regions and restriction sites. PCR amplification was confirmed by DNA gel electrophoresis [figure 10d] and NSP6 fragments were digested with corresponding restriction enzymes. Digested PCR fragments were then inserted into pCAGGS-mCherry vector by ligation and was confirmed through test digests. FCOV was digested with KpnI and NheI, whilst both HCoV-OC43 and SARS-CoV-2 were

digested with KpnI and XhoI. The resulting products of the digests are highlighted in figure 10c where the mCherry vector is observed around 5.4 kb and each insert observed around 900 bp. These results confirm the presence of each NSP6 construct within the pCAGGS-mCherry vector once both mini-prep and maxi-preps had been performed, providing a suitable construct for further protein expression analysis.

a)

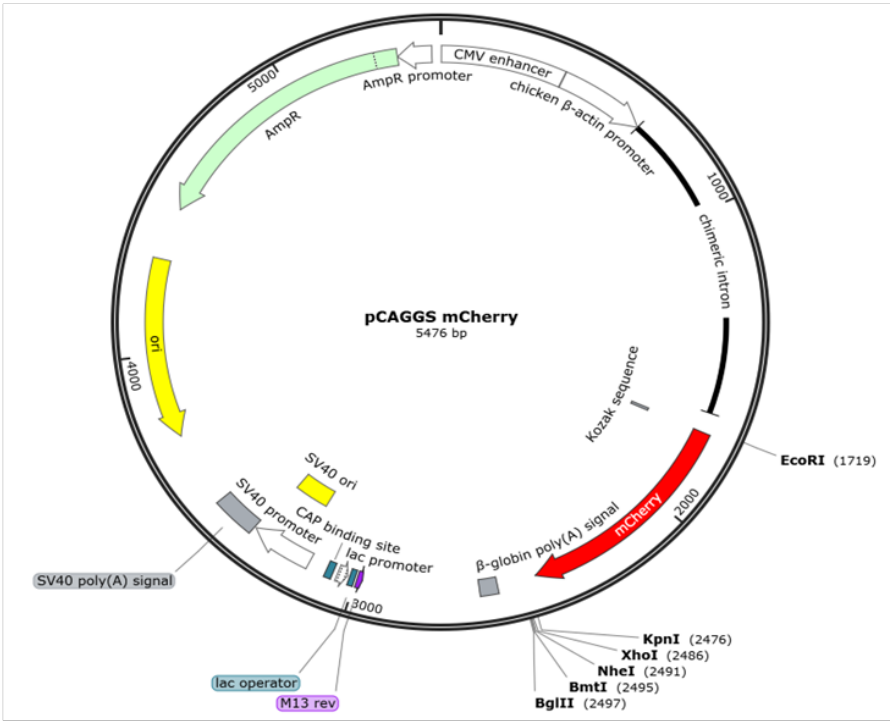
pCAGGS mCherry
5476 bp
5000
AmpR
AmpR promoter
CMV enhancer
chicken β-actin promoter
1000
chimeric intron
EcoRI (1719)
2000
mCherry
β-globin poly(A) signal
Kozak sequence
3000
KpnI (2476)
XhoI (2486)
NheI (2491)
BmtI (2495)
BglII (2497)
4000
ori
SV40 ori
SV40 promoter
CAP binding site
lac promoter
SV40 poly(A) signal
lac operator
M13 rev

b)

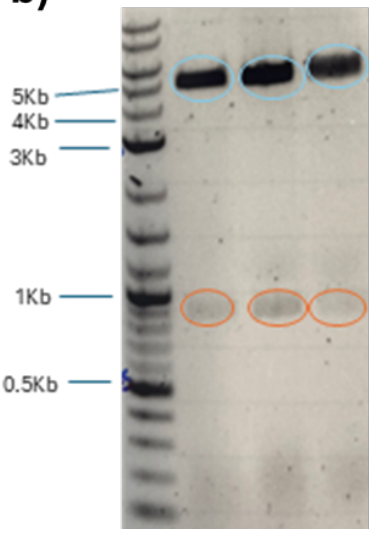
5Kb
4Kb
3Kb
1Kb
0.5Kb

c)

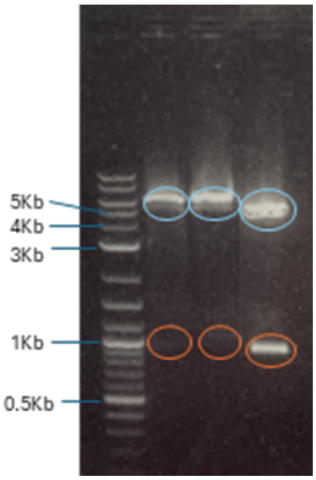
5Kb
4Kb
3Kb
1Kb
0.5Kb

d)

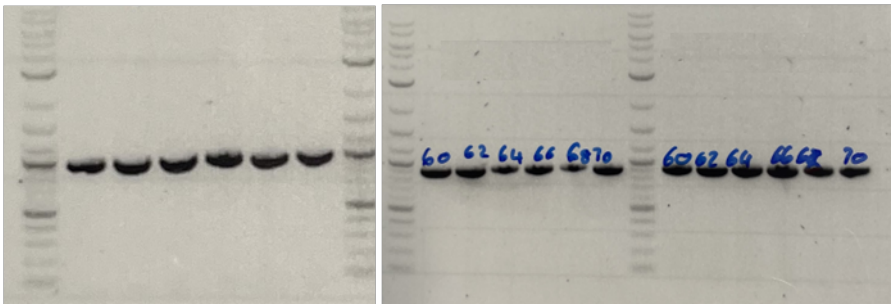

Figure 10: Preparation of mCherry-tagged NSP6 expression constructs

The process of cloning NSP6 sequences into the pCAGGS mCherry expression vector. **A)** pCAGGS mCherry plasmid map demonstrating the restriction sites present which were used for cloning NSP6 sequences into the vector. **B)** Agarose gel electrophoresis of three mini-prep repeats. In each case, vector and mCherry insert fragments were observed around 5.4 kb and <1 kb respectively, indicating successful insertion. **C)** Agarose gel electrophoresis of PCR amplification of NSP6 sequences. PCR was performed with a temperature gradient on the primer annealing step: lane 1=60°C to lane 6= 70°C. The amplified inserts contained added linker regions and restriction sites for further cloning and were observed <1 kb. **D)** Agarose gel electrophoresis of minipreps of pCAGGS-mCherry-FIP (lane 1), pCAGGS-mCherry-HCoV-OC43 (lane 2) and pCAGGS-mCherry-SARS-CoV-2 (lane 3) confirming successful insertion of NSP6 sequences.

3.4 Chemical manipulation of autophagy

3.5.1 Indirect immunofluorescence detection of autophagosomes

A549 cells were incubated with different drug compounds to monitor the induction of autophagy. Cells were incubated with: torin1, an mTOR inhibitor that upregulates autophagy, and/or CQ, which has pleiotropic effects including autophagosome accumulation and induction of CASM. This experiment also used a media only control, as well as a combination experiment with both drug treatments. Cells were fixed 4 hours post-treatment. Autophagosomes were detected by indirect immunofluorescence with an anti-LC3B antibody. As presented in figure 11, autophagy induction was confirmed by an increase in LC3B-positive punctae (green). The control group was observed to have lower levels of LC3B-positive punctae compared to the other images, indicative of the basal level of autophagy. Torin1 treatment gave an obvious increase in LC3B puncta, which is associated with

increased autophagosome production and overall greater autophagy induction. The pleiotropic effects of CQ cause an increased accumulation of larger LC3-positive punctae, indicating an increased amounts of autophagosome, but a potential block in canonical flux. Torin1 increases autophagy induction and CQ pleiotropically effects autophagosomes which blocks canonical flux, as such, treatment with both presented a significant increase in LC3-positive punctae. These observations demonstrate the ability to chemically manipulate autophagy and detect changes in levels of induction.

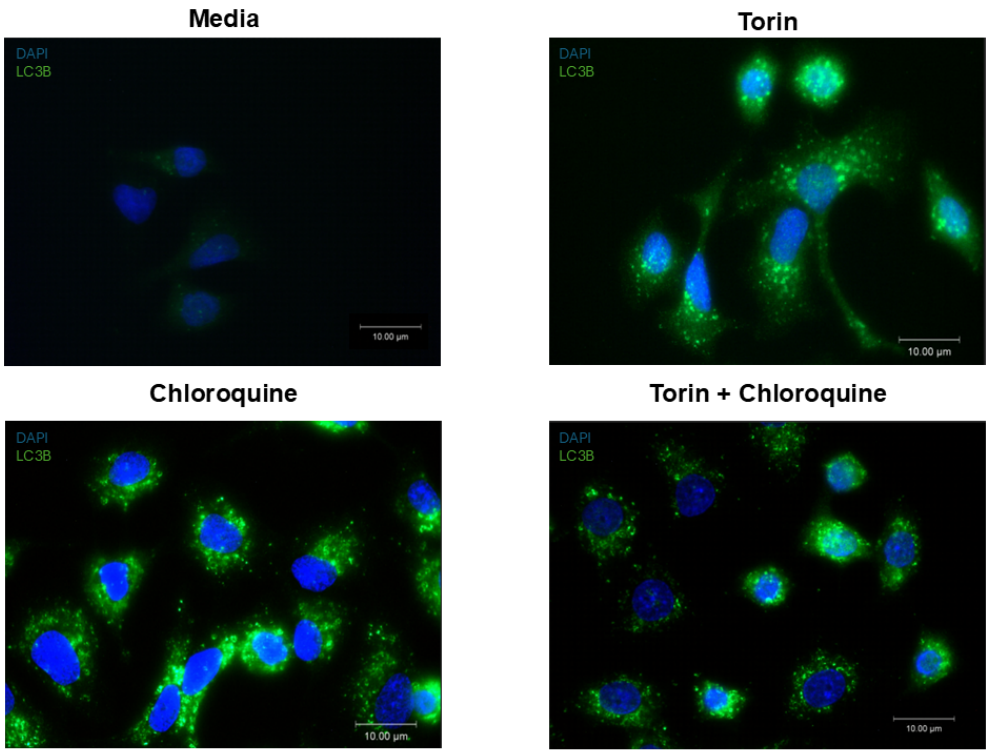

Figure 11: Indirect immunofluorescence of autophagy chemical manipulation

A549 cells were incubated with control media, 1 µM torin1, 100 µM Chloroquine, or combined torin1 and chloroquine, for 4 hours prior to fixing with 100% frozen methanol. Cells were labelled by indirect immunofluorescence with an anti-LC3B antibody (green), and nuclei were counterstained with DAPI (blue). Scale bars=10 µm.

3.5.2 Western blot analysis of autophagy

To assess the effect of known chemical modulators of autophagy, HEK293T cells were cultured in complete media prior to 4-hour incubation periods with: control

media, torin1, CQ and torin1+CQ. Cells were lysed with Laemmli buffer. Western blot analysis was performed with whole cell lysates to observe the effect of different drug treatments on the expression of key autophagy indicators, LC3B and p62/SQSTM1. Densitometric analysis was performed to provide a quantified ratio of lipidated LC3 (LC3-II) to LC3-I; the ratio was normalised to the hsp90 loading control and then made relative to the control. Similarly, anti-hsp90 was used as a loading control within densitometry analysis of p62/SQSTM1 to standardise the protein levels. As presented in figure 12, baseline levels of lipidated LC3 were relatively high, suggesting a significant level of pre-existing lipidation in unstimulated cells. This knowledge suggests that the A549 cells may have been in a stressed state prior to drug treatment, which may influence the observed results. In spite of this, torin1 treatment resulted in a further increase in lipidated LC3 (LC3-II) and overall LC3-II/LC3-I ratio, an indicator of increased autophagosome production. Also observed in torin1 incubated cells was a decrease in p62/SQSTM1 levels, which is indicative of increased autophagic flux.

CQ treatment resulted in the accumulation of both LC3-II and p62/SQSTM1, which typically demonstrates a blockage in autophagic flux, due to lysosomal fusion inhibition, which results in lower autophagosome degradation. Combination treatment with both torin1 and CQ gave a large increases in LC3-II and p62/SQSTM1 accumulation, respectively. The observed effect confirms the ability to chemically manipulate autophagy to observe autophagosome production and the effect on autophagic flux, however, these results must be interpreted with caution due to the elevated baseline lipidation levels of LC3-II.

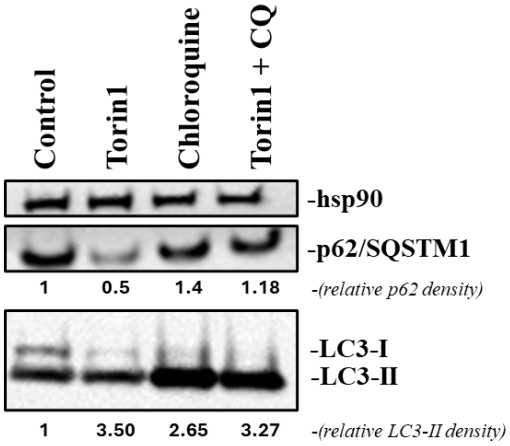

Figure 12: Chemical manipulation of autophagy western blot

Western blot analysis of A549 cells incubated with media (control), 1 μM torin1, 100 μM CQ, or combined torin1 and CQ, for 4 hours prior to lysate collection. Protein levels of hsp90 (loading control), p62/SQSTM1 and LC3B were assessed. Densitometric analysis is presented below each lane, with relative protein expression levels standardised to hsp90.

3.5 NSP6 enhances the accumulation of autophagosomes

3.5.1 Immunofluorescent analysis

Immunofluorescence was used to visualise the accumulation of autophagosomes in cells expressing each of the mCherry-NSP6 constructs. A549 cells were transiently co-transfected with a GFP-tagged LC3 (GFP-LC3) construct and one of the NSP6 variants: pCAGGS-mCherry-FIP, pCAGGS-mCherry-HCoV-OC43 or pCAGGS-mCherry-SARS-CoV-2. They were then fixed with 4% PFA 48 hours post-transfection and counterstained with DAPI to visualise the nuclei.

Figure 13 shows the widefield microscopy images obtained at 100x magnification. There was visual co-localisation between areas of increased GFP-LC3 punctae and mCherry-NSP6 expression in cells. Within cells transfected with the control (pCAGGS-mCherry vector) the GFP-LC3 appears more diffuse, suggesting a basal level of autophagosome production had occurred. In cells expressing FIP-NSP6, there

was a visually greater amount of GFP-LC3 punctae, potentially indicating a higher level of autophagosome production in these cells compared to the other variants. Across all NSP6 constructs was an increase in the intensity and abundance of GFP-LC3 punctae observed.

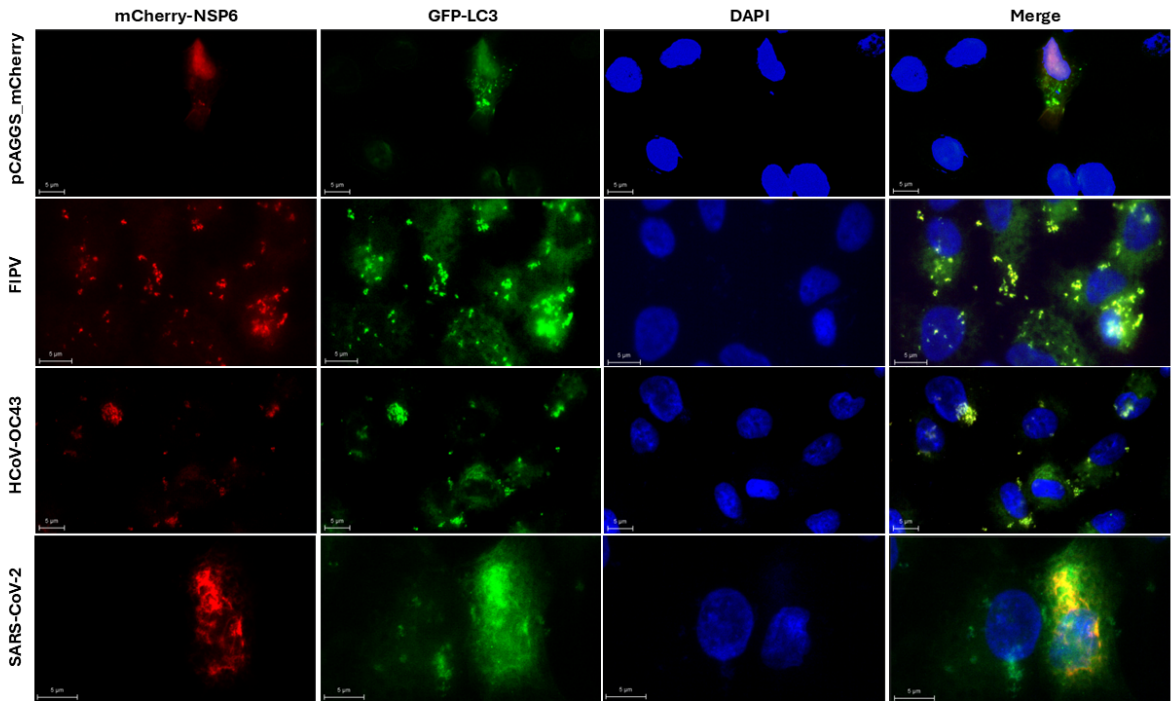

Figure 13: Immunofluorescent analysis of GFP-LC3 expression when co-transfected with mCherry-NSP6

A549 cells were co-transfected with mCherry-tagged NSP6 constructs and GFP-LC3 reporter construct. The cells were fixed 48 hours post-transfection with 4% PFA. Cells were counterstained with DAPI (blue) to visualise the nuclei. Scale bars=10µm.

3.6.2 Western blot results

To assess the effect of NSP6 on autophagosome production, A549 cells were transiently transfected with mCherry-tagged NSP6 constructs. To confirm the expression of NSP6-mCherry, fluorescence images at 20X magnification were obtained [figure 14a] prior to lysate collection. The cells were lysed 48 hours post-transfection and analysed by western blot with antibodies for hsp90 and LC3B. Densitometric analysis was performed to provide a quantified ratio of lipidated LC3 (LC3-II) to LC3-I; the ratio was normalised to the hsp90 loading control and then made relative to the control. The western blot results, observed in figure 14b, demonstrated an overall increase in LC3-II/LC3-I ratio when NSP6 was expressed, compared to the control. This observation was more pronounced in the human-CoVs, HCoV-OC43 and SARS-CoV-2, with a two-fold increase relative to the control. FIP still elicited an increase in autophagosome production, but this was lower than the human CoVs.

An increase in the relative LC3-II:LC3-I ratio is typically an indicator of increased autophagosome accumulation, as lipidated LC3-II is membrane-bound and directly associated as a marker of autophagosome production. Subsequently, autophagosome accumulation is a marker of increased autophagy levels.

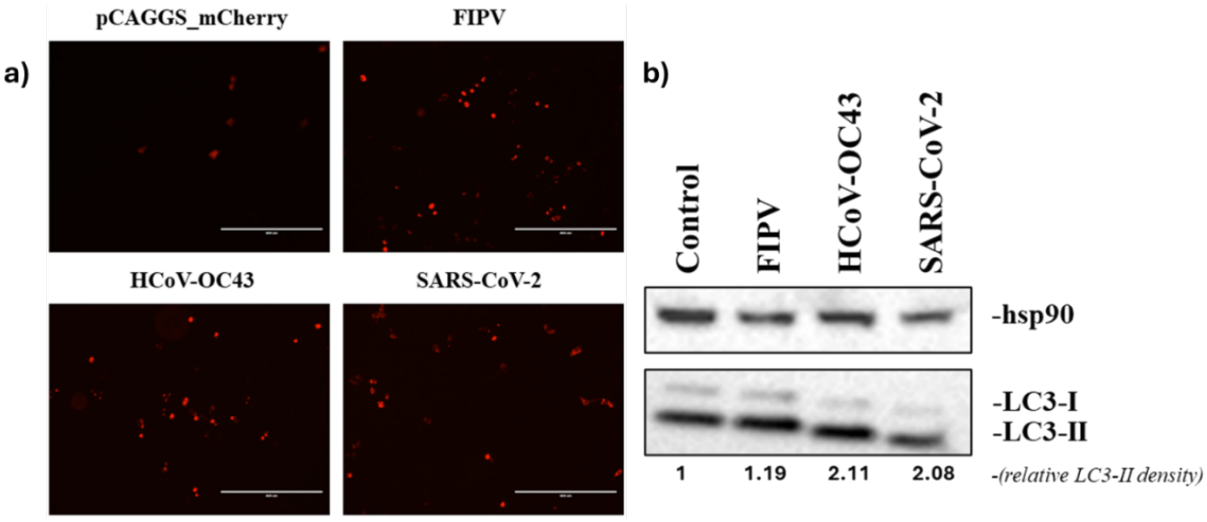

Figure 14: Western blot analysis of autophagosome accumulation when NSP6 transfected into cells

A) mCherry-NSP6 expression confirmed 48 hours post-transfection by fluorescence microscopy at 20x magnification. **B)** Western blot analysis of A549 cells transfected with mCherry-tagged NSP6 constructs for 48 hours prior to lysate collection. Anti-hsp90 (loading control) and anti-LC3B antibodies were incubated with the PVDF membrane to assess expression of these proteins. Densitometric analysis is presented below the LC3B panel, with the relative ratio of LC3-II:LC3-I being displayed. The ratio was normalised hsp90 loading control and made relative to the vector only control.

3.6 NSP6 overexpression interferes with autophagic flux

To investigate the impact that NSP6 has on autophagic flux, A549 cells were transiently transfected with mCherry-tagged NSP6 constructs. Protein levels of p62/SQSTM1 were analysed by western blot, as described above. Figure 15 demonstrates a clear accumulation of p62/SQSTM1 when NSP6 is expressed, compared to the control. The most significant increase in p62/SQSTM1 accumulation was observed in SARS-CoV-2, with a 4-fold increase after densitometry analysis. Expression of FIP and HCoV-OC43 resulted in a 3-fold increase in p62/SQSTM1 levels compared to the control, respectively.

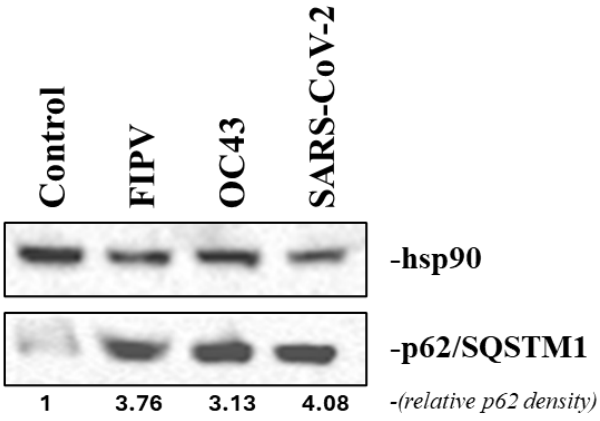

Figure 15: Western blot analysis of the effect NSP6 has on autophagic flux

Western blot analysis of A549 cells transfected with mCherry-tagged NSP6 constructs for 4hs prior to lysate collection. Anti-hsp90 (loading control) and anti-p62 antibodies were incubated with the PVDF membrane to assess expression of these proteins. Densitometric analysis is presented below p62/SQSTM1. The relative p62/SQSTM1 density was normalised to the hsp90 loading control and then made relative to the vector only control.

3.7 NSP6 modulates mTOR activity

To ascertain whether NSP6 elicits an effect on mTOR signalling, protein levels of P70S6K and phopsho-P70S6K were analysed by western blot as above. Western blot analysis was performed using anti-P70S6K and anti-phosphoP70S6K antibodies. Protein expression was quantified through densitometry analysis and normalised to hsp90. A relative ratio of phosphorylated P70S6k to total P70S6k was used to assess the effect of NSP6 on mTOR signalling. Whilst a reduction in relative phosphoP70S6K:P70S6K ratio was observed across all NSP6 constructs, the variation seen was subtle. The densitometry analysis suggested a general trend towards a decrease in the relative ratio of phosphoP70S6K:P70S6K, particularly in cells expressing HCoV-OC43 NSP6 and FIP NSP6, compared with the control [Figure 16]. Despite this, the differences observed were not substantial, and it remains unclear whether this suggests a reduction in the signalling activity of mTOR.

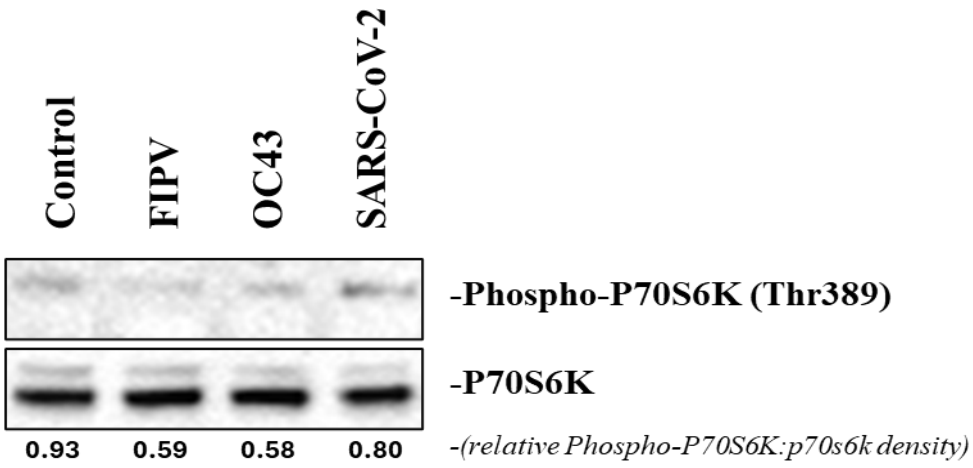

Figure 16: Western blot analysis of mTOR activity when NSP6 is expressed in cells

Western blot analysis of A549 cells transfected with mCherry-tagged NSP6 constructs for 4 hours prior to lysate collection. Anti-P70S6K and anti-phospho P70S6K antibodies were incubated with the PVDF membrane to assess expression of these proteins. Densitometric analysis is presented below the blot. The relative phosphor P70S6K: total P70S6K density was normalised to vector only control.

3.8 NSP6 co-localises with BST-2/Tetherin

To assess the effect NSP6 may have on the stability of BST-2/tetherin, A549 cells were co-transfected with mCherry-tagged NSP6 and BST-2-HA constructs. Indirect immunofluorescence was performed to visualise BST-2 expression within the cells. Counterstaining with DAPI was performed to observe the nuclei. Widefield microscopy analysis at 100x magnification, seen in figure 17, showed a distinct co-localisation pattern between NSP6 and BST-2. The yellowing colour observed in the merged panel shows an overlap of BST-2 and NSP6-mCherry, potentially indicating an interaction of the two proteins. Observed in the figure 18, there is a clear increase in the expression of BST-2 in the perinuclear region of the cells when NSP6 is expressed. The highest intensity signals were detected in intracellular compartments, where BST-2 is known to localise.

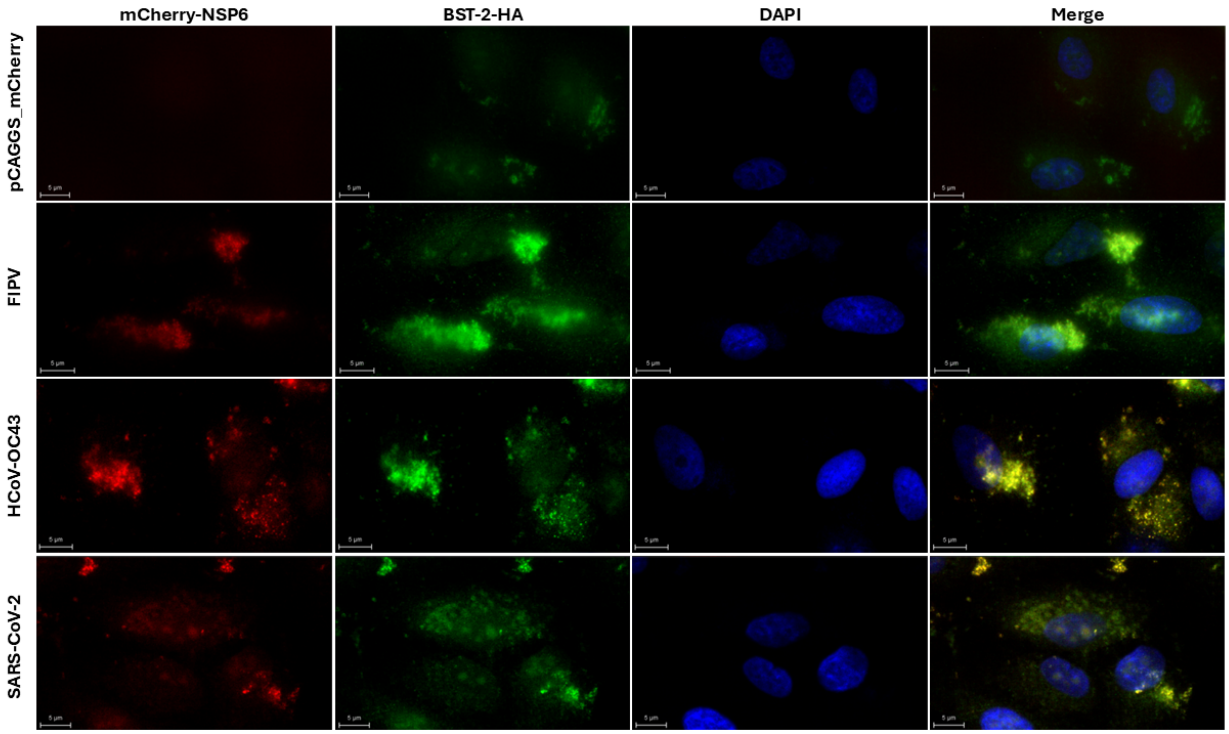

Figure 17: Indirect immunofluorescent analysis of BST-2-HA and mCherry-NSP6

A549 cells were co-transfected with mCherry-tagged NSP6 constructs and BST-2-HA. The cells were fixed 48 hours post-transfection with 4% PFA, and permeabilised with Triton-x100. Cells were labelled with an anti-HA antibody (green) to visualise BST-2. Cells were counterstained with DAPI (blue) to visualise the nuclei. Scale bars=10μm.

4 Discussion

4.1 Modulation of autophagy by NSP6 in coronavirus infection

The autophagy pathway has many key roles that aid in normal cellular processes and overall survival. NSP6 appears to play a critical role in modulating the autophagy pathway, perhaps in a bid to evade host cellular immune responses. The present study demonstrated that NSP6 of FIP, HCoV-OC43 and SARS-CoV-2 may upregulate autophagy. A modulation of the autophagy pathway in a similar way was previously observed in infection with the RNA virus, human immunodeficiency virus 1 (HIV-1). The virus is able to inhibit autophagy to prevent sequestration of HIV-1 proteins into autophagosomes, which prevents the lysosomal degradation stage of autophagy. Interactions with Beclin-1 within the PI3KC3 complex allow inhibition of autophagosome expansion (Choi *et al.*, 2018). This effect observed in HIV-1 could possibly be an area of future experiments to assess the modulation of NSP6 on Beclin-1 and the complete maturation of autophagosomes. Such work would provide knowledge of whether autophagic flux is affected before or during the lysosomal fusion process. The results obtained show that NSP6 may increase the production of autophagosomes and block the degradation of sequestered cargo. The effects are observed across the three CoV NSP6 variants. The results also align with results seen in infectious bronchitis virus (IBV) where the study utilised p62/SQSTM1 and LC3B immunofluorescence to visually observe the effects of IBV NSP6 on protein expression. Levels of p62/SQSTM1 and LC3B were visually increased, indicating increased autophagosome accumulation, and an interference with autophagic flux (Cottam *et al.*, 2011).

Despite this general conservation, there are a number of differences in the protein sequences of the NSP6 variants, which may result in the functional properties of coronavirus genera being different, with the beta-CoVs appearing to have a much-increased modulation of the autophagy pathway compared to FIP. The slightly lower

increase observed in FCoV, however, may be representative of the feline NSP6 construct being expressed in the human lung cell line, A549. The effect observed may have been, both, more representative and greater had the FCoV NSP6 construct been expressed in a feline-derived, enteric cell line. This would also have removed the subjectivity of tropism differences as beta-CoVs are predominantly human and affect the respiratory system, whereas FCoV is gastrointestinal in tropism.

4.2 Analysis of bioinformatics

4.2.1 Clustal Omega multiple alignment analysis of nucleotides

The Clustal Omega multiple sequence alignment analysis of NSP6 nucleotide sequences from FCoV, HCoV-OC43 and SARS-CoV-2 provided insight into the conservation of the NSP6 sequences. The alignment revealed an overall conservation of above 46%, with SARS-CoV-2 and HCoV-OC43 having a similarity score of 51%. This suggests greater conservation throughout the beta-CoVs. This is illustrated by the high conservation observed in an alignment between SARS-CoV-2 NSP6 and SARS-CoV NSP6, where an 87% conservation was detected (Bills, Xie, and Shi, 2023). However, the conservation of sequences alone doesn't necessarily imply functional equivalence, as post-translational modifications and structural folding can affect the activity of NSP6. Given the apparent role of NSP6 in the modulation of autophagy, identifying the conserved nucleotide regions may provide insights into potential regulatory elements that influence the action and/or stability of the protein. However, since protein function is a derivative of amino acid sequence and structural conformation, further analysis of NSP6 protein sequences is required to more clearly analyse the regions which are functionally important for the role of NSP6.

4.2.2 Clustal Omega multiple analysis of protein sequences

The Clustal Omega multiple protein sequence alignment analysis of NSP6 from FCoV, HCoV-OC43 and SARS-CoV-2 was performed to assess areas conservation across the protein sequences. The alignment highlighted relatively low conservation

throughout these CoVs, with SARS-CoV-2 and HCoV-OC43 sharing a similarity of around 32%, where FCoV showed around a 28% similarity with the beta-CoVs. This sequence divergence may play a role in functional differences in host immune interactions and modulation of autophagy.

Importantly, sequence alignment does not necessarily identify functional regions. Whilst only few conserved amino acid regions were identified, two stretches of three and one stretch of five, the role of these conserved sequences in the activity of NSP6 are unclear. The five amino acid conservation at the 5′ end of the alignment is located in the N-glycosylated site, which suggests a post-translational modification that may be crucial for the function of NSP6. Since N-glycosylation plays a pivotal role in protein stability, folding, and interactions, this conserved site could contribute to the ability of NSP6 to modulate host cell pathways (Wang *et al.*, 2018).

Given the prior work by Dr Coleman (unreleased data) has suggested that NSP6 localises to the ER and modulates autophagy, these areas of conservation may play a role in membrane interactions or the formation of DMVs, in a potential modulation of autophagy. Despite this, it is key to note that sequence conservation alone may not necessarily infer a functional region; protein activity often includes three-dimensional folding, where distant amino acids contribute to form functional domains.

4.2.3 Transmembrane prediction analysis

Transmembrane prediction analysis was performed using DeepTMHMM, TMHMM and Protter tools to analyse the topology of the NSP6 sequences. All three programmes predicted multiple transmembrane helices, which supported their role in membrane-associated functions. Despite this, some discrepancies in the prediction of the exact number of helices in each CoV NSP6 exists. In FCoV, there was one less transmembrane helix predicted by DEEPTMHMM. Whereas, in both HCoV-OC43 and SARS-CoV-2 there was an additional transmembrane helix predicted by DEEPTMHMM when compared to the Protter tool. The additional domain found in

beta-CoVs suggests a potential enhanced interaction with autophagy-related proteins. However, the methodological uncertainties associated with these transmembrane prediction tools necessitate experimental validation to establish more conclusive claims. There are some precedents for targeting transmembrane domains in drug development. However, it is unclear whether NSP6 is a viable target for this approach. More research is needed to explore this possibility. This idea has been previously suggested in work on NSP3 in SARS-CoV-2. Researchers mapped the transmembrane regions to understand the domains and identify potential therapeutic targets (Babot *et al.*, 2024). Additionally, targeting NSP6 has been investigated using natural products and drug repurposing. Some molecular dynamics data suggests that certain drugs may have potential in vivo testing (Abdelkader *et al.,* 2022).

4.3 Restriction digest cloning of NSP6 into a mammalian expression vector

The foundation of this study relied on the cloning of FIP, HCoV-OC43 and SARS-CoV-2 NSP6 sequences into a, previously engineered, pCAGGS_mCherry vector. This provided constructs which could be used to analyse the functional effects of NSP6 in cellular protein expression. The pCAGGS_mCherry vector was initially produced by using a mammalian expression vector, pCAGGS, and performing a restriction digest to clone mCherry as an insert. The successful cloning was confirmed by restriction digestion using enzymes and whole genome sequencing. Subsequently, the nucleotide sequence encoding the NSP6 of each CoV was amplified from a puc57 vector and restriction sites added by PCR. Each NSP6 was inserted into the pCAGGS_mCherry vector, and a mini-prep was performed to purify the plasmid. Each of these newly designed clones was confirmed by Sanger sequencing and restriction digestions to ensure NSP6 was present and that the mCherry tag was in frame for fluorescent expression. However, some challenges arose throughout the cloning process, particularly when the addition of a HA tag was attempted. The

previously made clones of pCAGGS_mCherry were amplified with added HA tags on the C-terminal end of the sequence. Whilst this was successful for FIP and HCoV-OC43, SARS-CoV-2 was not able to be cloned, likely due to the required melting temperature being too high. InFusion cloning was attempted with SARS-CoV-2; however, restriction digestion experiments confirmed the HA was not in frame and the decision was made to proceed with further experiments using mCherry-tagged NSP6 only.

4.4 Protein expression analysis

4.4.1 Chemical manipulation of autophagy in A549 cells

To provide contextual knowledge of cellular autophagy regulation and induction in A549 cells, chemical manipulation using Torin1 and CQ was performed. Torin1, is a potent mTOR inhibitor, and upregulates autophagy, observed by the increase in LC3B punctae (immunofluorescence) and increase in relative LC3-II/LC3-I ratio (immunoblotting). Both of these observations confirmed an increase in autophagosome production, a key indicator of increased autophagy.

CQ, commonly described as a potent inhibitor of lysosomal fusion, led to an accumulation of LC3B and p62/SQSTM1, which typically means there has been a block in autophagic flux. However, CQ is known to have pleiotropic effects, including the induction of CASM, which is a noncanonical LC3 lipidation pathway (Durgan *et al.*, 2021). This knowledge demonstrates that the increase in LC3B levels observed after CQ treatment may not solely imply an inhibition of lysosomal fusion, and further clarification would be required to differentiate between the mechanisms.

For normalisation of the western blot, hsp90 was used as a loading control across various cellular conditions. There is some evidence to suggest that β-actin and/or GAPDH may be influenced by cellular stress responses, whereas hsp90 remains stable in these conditions. This evidence could that affect protein turnover (Xu *et al.,* 2010).

The choice made ensured that there was a reliable control for standardisation of protein expression analyses.

The combination of both Torin1 and CQ further demonstrated that autophagosome production could be induced and that the canonical autophagic flux could be effectively blocked in the A549 cells. Despite this, the high baseline levels of LC3-II suggest pre-stressed conditions in the cells prior to drug treatment. This pre-existing lipidation of LC3-II makes interpretation of the effects of CQ harder to interpretate as it is possible that noncanonical autophagy may have caused a portion of the blockage effects seen. To mitigate this in future experiments, an alternative cell line, such as HEK293T, which exhibit lower baseline autophagy activity could give a clearer understanding of the drug effects (Klinosky *et al.*, 2021).

The results achieved highlight the need for further experimental clarification to understand the foundation mechanisms driving the lipidation of LC3B. Such assays would include WIPI2 (a marker for early phagophore formation; Dooley *et al.*, 2014), ATG12-ATG3 (a marker for CASM induction), and lysosomal activity assays to give a clearer picture of canonical and noncanonical LC3B lipidation. Despite this, these treatments confirmed that we were able to measure an increase in autophagy in A549 cells with the methods outlined, providing a baseline for subsequent analysis and observations of overexpression effects of autophagy in NSP6 transfected cells.

4.4.2 NSP6 influences the accumulation of autophagosomes

The primary aim of this study was to establish if NSP6 modulates the autophagy pathway to provide a more favourable environment for viral replication; assessing whether this effect was conserved across different CoV. Immunofluorescent and western blot analyses NSP6 of FIP, HCoV-OC43 and SARS-CoV-2 both saw autophagosome accumulation was increased where NSP6 was expressed. This effect was observed by the increase in GFP-LC3 punctae and the rise in relative LC3-II/LC3-I ratio. This suggests that NSP6 is a potential promoter of autophagosome

formation and suggests that this could generate a more favourable environment for the replication of the virus.

Despite this, a key consideration from this analysis is whether the GFP intensity was equivalent across the control and variants; differences observed here may suggest modifications in protein turnover rather than an increase in punctae. If NSP6 modulates autophagic flux differently, this may cause the change in GFP intensity, which could cause an accumulation rather than autophagic flux. This, coupled with the knowledge of results observed in analysis, composes the question of why these results were observed when the western blot results of LC3B appear relatively consistent throughout the control and variants. Confirmation of this autophagosome accumulation or degradation activity would require treatments with other lysosomal inhibitors to analyse the effects on autophagic flux. A different explanation for this intensity is that the plasmid preps may not have been entirely purified, which allows for contaminants to potentially cause the variability observed.

The increase in autophagosome accumulation without a clear increase in autophagic flux, as indicated by the increased p62/SQSTM1 levels observed in other experiments, indicates that there a potential modulatory effect on upstream activities by NSP6; possibly by interactions with Beclin-1 and/or the PI3KC3 complex. This effect is consistent with the hypothesis that NPS6 hijacks the autophagy pathway to enhance the replication process and survival of CoVs, as suggested in hepatitis C virus and SARS-CoV-2 previously, where both viruses were observed to hijack factors, such as Atg5, Atg12 and VPS34 which are key in the expansion of autophagosomes (Twu *et al.*, 2021). The conserved effect observed among the three variants of NSP6, despite their sequential differences that lead to the accumulation of autophagosomes, suggests that the underlying mechanism is maintained throughout the viruses and could potentially serve as an active enhancer of replication. Previous studies concluded that NSP6 induces induction of smaller autophagosomes, making the degradation process less efficient (Lv *et al.*, 2024). Together with this study, indicating a reduction in

autophagic flux, provides a better insight that NSP6 may be inhibiting the expansion of autophagosomes, blocking maturation and overall degradation. The observed accumulation of GFP-LC3 punctae also indicates a potential impact NPS6 has on autophagosome maturation or a potential blockage of autophagic flux.

These results indicate that NSP6 may play a role in enhancing autophagosome accumulation, however, without lysosomal inhibitors, it is not clear whether this increase is indicative of increased autophagosome production or a block in autophagic flux. Given the immunofluorescence analysis suggests a possible change in GFP-LC3 turnover, the similar levels of LC3B observed in the western blot analysis may indicate that NSP6 promotes autophagosome formation, but the impact on degradation of autophagosomes is still a question. Bafilomycin A1 is an inhibitor of vacuolar H^+-ATPase (V-ATPase), which disrupts acidification of lysosomes and prevents autolysosomal fusion, it blocks the degradation stage of autophagy causing an accumulation of LC3-II (Mauvezin and Neufeld, 2015). This would help to distinguish between an increase in autophagosome formation or a block of autophagic flux in NSP6. The different levels of autophagy induction by NSP6 suggest that human-CoVs may be more potent modulators of the pathway. The overall increase in autophagosome accumulation supports the hypothesis that NSP6 enhances autophagosome production and drives increased autophagy levels.

Analysing autophagosome size using immunofluorescence visualisation, comparing the effects of various NSP6 variants and mutants on autophagic flux, could provide a future perspective. Protein expression analysis suggests that NSP6 may modulate mTOR, LC3B lipidation, and p62 degradation. Targeted mutagenesis of NSP6 transmembrane regions could identify crucial interacting motifs responsible for subsequent interactions. Transmembrane prediction analysis revealed structural differences among CoV NSP6 variants, varying in the number and position of predicted helices. These structural variations may correlate to autophagic activity, potentially identifying key transmembrane domains mediating host autophagy

modulation. Multiple sequence alignments highlighted conserved regions, which could correspond to functional domains crucial in autophagy modulation; removal of these sites would help to confirm their potential function. Immunoprecipitation could provide insights into whether these conserved regions directly interact with autophagy-related proteins like LC3B, p62, and upstream mTOR components.

4.4.3 NSP6 interferes with autophagic flux

Interference with autophagic flux by NSP6 was an effect that this study expected to observe, but the accumulation of p62/SQSTM1 implied a blockage in canonical degradation of autophagosomes. The effect was previously described in IBV immunofluorescent analysis where an increase in p62/SQSTM1 punctae was observed in cells expressing NSP6 (Cottam *et al.*, 2011). In this study, the effect of NSP6 was demonstrated by the accumulation of LC3-II and p62/SQSTM1 in immunoblotting analysis. The accumulation of p62/SQSTM1, which is a prominent marker of interference with autophagic degradation, may indicate that NSP6 elicits an effect on the autophagy process in a mechanism that may enhance viral replication, through the inhibition of degradation processes. The fact that the effect was conserved across the three CoV NSP6 variants, could imply that NSP6 is key for modulating autophagy to provide a more favourable viral environment, rich with nutrients for better replication.

4.4.4 Modulation of mTOR activity by NSP6

The accumulation of p62/SQSTM1 and LC3B indicates that a blockage in autophagic flux is occurring, potentially leading to an effect on the induction of autophagy taking place. However, as seen in the analysis of LC3B, there is an implication that NSP6 may also influence autophagosome production, which would indicate a broader effect on the autophagy pathway. Suppression of mTOR signalling is known to be an active upregulator of the autophagy pathway and may also support the increased levels of autophagosome production. The potential modulation of this mTOR signalling pathways was assessed by observing of the effect of NSP6 construct (of FIP, HCoV-

OC43, and SARS-CoV-2) on Phospho-s6k and p70s6k, which allowed a relative ratio to be produced. While a decrease in Phospho-s6k and p70s6k was observed when NSP6 was expressed, the differences were subtle. The general trend suggests that NSP6 may have some effect mTOR activity, but a more definitive extent of this inhibition remains unclear.

Despite this, the increased accumulation of autophagosomes and influence on autophagic flux by NSP6 suggests that the protein may create a favourable environment for viral replication by preventing cargo degradation and building a reservoir of autophagosomes. As observed in a previous study, NSP6 binds to the sigma receptor 1 which is involved in endoplasmic reticulum stress response (Abdelkader *et al.*, 2022). Such a mechanism could be assessed in future work to establish a more local interaction that NSP6 elicits on upstream targets of mTOR.

This dual effect that appears to be elicited by the NSP6 variants supports the hypothesis that the effect on autophagy is pan-CoV and that this mechanism has key role in CoV pathogenesis. Given the variability in the densitometry data, and the lack of definitive statistical analyses, further experiments (with increased replicates) would be required to draw conclusions and confirm a direct effect on mTOR by NSP6, or whether an effect upstream of mTOR drives this process. Utilising previously described experimental approaches, such as those employed in assessing the modulation of mTOR in HCV, could give an idea of the potential targets for NSP6. While, HCV does not contain an NSP6 protein, it has been observed to induces the autophagy pathway by interacting with RAB5A and PIK3C3, which are key autophagy regulators that NSP6 may potentially interact with (Su *et al.*, 2011).

4.4.5 Co-localisation of NSP6 with BST-2/Tetherin

Another hypothesis made for this research was that NSP6 elicits an effect on the immunomodulatory protein, BST-2/Tetherin. Observation of this effect was made through immunofluorescent protein expression analysis. A co-localisation of

mCherry-tagged NSP6 and BST-2 (GFP) was seen throughout the images obtained. This possible interaction between NSP6 and BST-2 indicates a potential modulation of the antiviral function of BST-2, possibly being sequestered into the autophagy pathway. The presence of increased BST-2 punctae when cells expressed NSP6 suggests that NSP6 may influence the localisation and/or stability of BST-2. This would support the hypothesis that NSP6 interacts with the host immune pathway, potentially modulating the activity of BST-2 in a pro-viral manner, possibly by sequestering BST-2 into intracellular compartments. BST-2 is a key preventative mechanism that restricts viral egress, modulation of this activity by NPS6 could aid the replication and spread of virus. This observation is supported by the knowledge that the spike protein of SARS-CoV-2 of the Omicron variant interacts with BST-2 to down-regulate its effect. BST-2 is ubiquitinated into the lysosomal pathway to inhibit and potentially degrade the antiviral protein (Shi *et al.*, 2024). The exact interaction between the spike protein and BST-2 has not been fully described, but it suggests a possibility that NSP6 is creating the favorable environment to sequester BST-2 into lysosomes for downstream degradation.

This interaction of NSP6 with BST-2 seemingly occurs to inhibit the tethering effect that BST-2 has on the release of progeny virus particles in response to viral infection. Such interaction and modulation may allow for greater/easier release of virions, increasingly the ability of the virus to spread from cell to cell and perhaps increasing the pathogenesis of CoVs. This effect was conserved throughout the three NSP6 variants examined suggesting a vital function in the survival and viral propagation of CoVs.

Further investigations are required to determine the exact mechanism that NSP6 interacts with BST-2 and whether the increase in autophagosome production and/or block of autophagic flux is employed by NSP6 in this modulation.

4.5 Broader implications of autophagy and immune modulation by NSP6 in coronaviruses

The findings from this study may have implications in understanding the role NSP6 has in modulating host cell process and defences in CoV pathogenesis. Demonstrating the role that NSP6 of different CoV variants have in the modulation of autophagy, such as potentially increasing autophagosome production and interfering with mTOR signalling/autophagic flux, alongside the potential interaction with BST-2; this research has highlighted a few strategies that may be employed in CoV pathogenesis. The increase observed in autophagosome accumulation, coupled with a potential interference with autophagic flux, suggest that NSP6 could play a role in creating a favourable cellular environment for viral replication. The increase in autophagosome number was observed in IBV and also mouse hepatitis virus (MHV), where protein expression analysis showed that replication of the viruses was significantly decreased in autophagy-deficient cell lines, indicating the critical importance of autophagosomes in the replication process (Prentice *et al.*, 2004; Cottam, Whelband and Wileman, 2014). The disruption of autophagic flux potentially creates a cellular environment of stress, which also suppresses mTOR activity. Alongside the function that NSP6 has on autophagosome accumulation and autophagic flux, the interference with mTOR activity suggests a broader action on cellular metabolism and defence pathways. mTOR is a critical regulator of cell proliferation and metabolism; inhibition by NSP6 could alter could interfere with cellular energy, which could enhance viral takeover of cells. The elicited effect on mTOR activity by NSP6 could be significant in CoVs with increased pathologies, such as SARS-CoV-2, where dysregulation of metabolic pathways could increase the pathological alterations associated with infection (Chen *et al.*, 2023). Suppression of mTOR signalling was also observed in Chikungunya virus, where the inhibition of mTORC1 enhanced the translation of viral proteins in the eIF4E pathway, which is upstream of mTOR, rather than being a utiliser of

autophagy (Joubert *et al.*, 2015). Assessing the expression of eIF4E may be a useful tool in identifying whether a direct modulation of mTORC1 occurs in CoV infection in adding to s6k phosphorylation. The interaction that was observed between NSP6 and BST-2 is potentially significant in the host-immune evasion by CoVs. Establishing whether NSP6 directly targets BST-2 to be degraded or whether the modulation is mediated by other pathways remains a question, but understanding this role will be critical in uncovering the immune evasion and viral propagation by CoVs.

4.6 Future directions

Previous studies have identified a role that NSP6 may play in the restriction of host immune factors. In order to distinguish whether NSP6 redirects BST-2 into the autophagy pathway, immunofluorescence using mCherry_NSP6 constructs, LC3B and BST-2 staining would be performed to visually detect co-localisation within transfected cells. A presence of co-localisation between NSP6, BST-2 and LC3B would be a strong indicator of an interaction between these proteins, and a possible mechanism of immune evasion by NSP6. Increased autophagosome accumulation, indicated by LC3B punctae, and a decrease in BST-2 punctae would be expected if NSP6 is modulating or sequestering BST-2 into the autophagy pathway. This effect on the restriction factor was indicated in HIV-1 studies where ATG-5 has been observed as a trigger to drive an unconventional autophagy pathway, that directed BST-2 into a degradation pathway (Judith *et al.*, 2023). The effect observed in this study indicates that NSP6 expression may increase autophagosome numbers to modulate the function of, and potentially degrade, BST-2; perhaps in a mechanism to enhance CoV pathogenesis. Assessing this effect in a complete experiment would provide better understanding of possible interactions, which could be investigated by immunoprecipitation to identify interacting partners. Another critical direction to assess is the modulation of mTOR activity by NSP6. The demonstration of autophagosome accumulation and block of autophagic flux in the study appear to be a

mechanism that NSP6 employs to subvert host-immune responses and modulate metabolic processes. Despite this, it would be invaluable to assess whether increased autophagosome accumulation leads to greater viral replication or whether it is an intrinsic effector of immune pathways. The use of autophagy-deficient cell lines, such as ATG5 KO cells would provide a method for assessing whether increased autophagosome accumulation and/or the decrease in autophagic flux is entirely dependent on the autophagy pathway. This would allow for more valuable conclusions to be drawn on the influence of NSP6 on the autophagy pathway. In addition, utilising other NSP6 variants beside those that have been previously studied would provide a better knowledge of whether the effect of NSP6 is conserved pan-CoV; coupled with additional bioinformatics data, this could lead to novel targets for therapeutic treatments in the future.

5. Conclusion

This study has demonstrated that NSP6 of FCoV, HCoV-OC43 and SARS-CoV-2 may have the ability to modulate autophagy, disrupt canonical autophagic flux and interfere with mTOR signalling. Successful cloning and subsequent protein expression analysis suggested that NSP6 had a role in inducing autophagosome accumulation and also indicated a potential interaction with BST-2, which could influence the ability of coronaviruses to evade host immune processes. While these findings are important in improving our knowledge of coronavirus pathogenesis and replication in hosts, further studies are required to determine the mechanisms by which NSP6 effects on autophagy and to explore the broader implications of NSP6 interacting with immune proteins. Such studies would provide greater numbers of replicates for analysis, which would allow for statistical analyses and more informed conclusions to be drawn. This would give key knowledge on NSP6 in viral pathogenesis and immune evasion; potentially providing a route for novel therapies.

References

Abdelkader, A. *et al.* (2022) '*In-Silico* targeting of SARS-CoV-2 NSP6 for drug and natural products repurposing', *Virology*, 573, pp. 96–110. Available at: https://doi.org/10.1016/j.virol.2022.06.008.

Akira, S., Uematsu, S. and Takeuchi, O. (2006) 'Pathogen recognition and innate immunity', *Cell*, 124(4), pp. 783–801. Available at: https://doi.org/10.1016/j.cell.2006.02.015.

Atluri, K., Aimlin, I. and Arora, S. (2022) 'Current Effective Therapeutics in Management of COVID-19', *Journal of Clinical Medicine*, 11(13), p. 3838. Available at: https://doi.org/10.3390/jcm11133838.

Babot, M. *et al.* (2024) 'Oligomeric assembly of the C-terminal and transmembrane region of SARS-CoV-2 nsp3', *Journal of Virology*, 98(4), pp. e01575-23. Available at: https://doi.org/10.1128/jvi.01575-23.

Baranov, P.V. *et al.* (2005) 'Programmed ribosomal frameshifting in decoding the SARS-CoV genome', *Virology*, 332(2), pp. 498–510. Available at: https://doi.org/10.1016/j.virol.2004.11.038.

Baric, R.S. and Yount, B. (2000) 'Subgenomic Negative-Strand RNA Function during Mouse Hepatitis Virus Infection', *Journal of Virology*, 74(9), pp. 4039–4046. Available at: https://doi.org/10.1128/jvi.74.9.4039-4046.2000.

Bayati, A. *et al.* (2021) 'SARS-CoV-2 infects cells after viral entry via clathrin-mediated endocytosis', *The Journal of Biological Chemistry*, 296, p. 100306. Available at: https://doi.org/10.1016/j.jbc.2021.100306.

Belouzard, S. *et al.* (2012) 'Mechanisms of Coronavirus Cell Entry Mediated by the Viral Spike Protein', *Viruses*, 4(6), pp. 1011–1033. Available at: https://doi.org/10.3390/v4061011.

Bergsbaken, T., Fink, S.L. and Cookson, B.T. (2009) 'Pyroptosis: host cell death and inflammation', *Nature Reviews. Microbiology*, 7(2), pp. 99–109. Available at: https://doi.org/10.1038/nrmicro2070.

Bianchi, M. *et al.* (2021) 'SARS-Cov-2 ORF3a: Mutability and function', *International Journal of Biological Macromolecules*, 170, pp. 820–826. Available at: https://doi.org/10.1016/j.ijbiomac.2020.12.142.

Bills, C., Xie, X. and Shi, P.-Y. (2023) 'The multiple roles of nsp6 in the molecular pathogenesis of SARS-CoV-2', *Antiviral Research*, 213, p. 105590. Available at: https://doi.org/10.1016/j.antiviral.2023.105590.

Broadbent, D.G. *et al.* (2023) 'Quantitative analysis of autophagy reveals the role of ATG9 and ATG2 in autophagosome formation', *The Journal of Cell Biology*, 222(7), p. e202210078. Available at: https://doi.org/10.1083/jcb.202210078.

Cameroni, E. *et al.* (2022) 'Broadly neutralizing antibodies overcome SARS-CoV-2 Omicron antigenic shift', *Nature*, 602(7898), pp. 664–670. Available at: https://doi.org/10.1038/s41586-021-04386-2.

Cascella, M. *et al.* (2024) 'Features, Evaluation, and Treatment of Coronavirus (COVID-19)', in *StatPearls*. Treasure Island (FL): StatPearls Publishing. Available at: http://www.ncbi.nlm.nih.gov/books/NBK554776/ (Accessed: 3 August 2024).

Castillo, G. *et al.* (2023) 'Molecular mechanisms of human coronavirus NL63 infection and replication', *Virus Research*, 327, p. 199078. Available at: https://doi.org/10.1016/j.virusres.2023.199078.

Chan, K., Sharif, S. and Rochwerg, B. (2021) 'Is dexamethasone an effective treatment for severe COVID-19 patients: Journal Club review', *Cjem*, 23(2), pp. 159–161. Available at: https://doi.org/10.1007/s43678-020-00033-3.

Chang, C.K., Hou, M.H., Chang, C.F., Hsiao, C.D. and Huang, T.H., 2014. The SARS coronavirus nucleocapsid protein–forms and functions. *Antiviral research*, *103*, pp.39-50.

Charles A Janeway, J. *et al.* (2001) 'Principles of innate and adaptive immunity', in *Immunobiology: The Immune System in Health and Disease. 5th edition*. Garland Science. Available at: https://www.ncbi.nlm.nih.gov/books/NBK27090/ (Accessed: 2 August 2024).

Chen, D.-Y. *et al.* (2023) 'Spike and nsp6 are key determinants of SARS-CoV-2 Omicron BA.1 attenuation', *Nature*, 615(7950), pp. 143–150. Available at: https://doi.org/10.1038/s41586-023-05697-2.

Chen, J.S. *et al.* (2020) 'Cyclooxgenase-2 is induced by SARS-CoV-2 infection but does not affect viral entry or replication', *bioRxiv: The Preprint Server for Biology*, p. 2020.09.24.312769. Available at: https://doi.org/10.1101/2020.09.24.312769.

Chen, P. *et al.* (2023) 'Metabolic alterations upon SARS-CoV-2 infection and potential therapeutic targets against coronavirus infection', *Signal Transduction and Targeted Therapy*, 8(1), pp. 1–23. Available at: https://doi.org/10.1038/s41392-023-01510-8.

Chen, Q. *et al.* (2021) 'Prefused lysosomes cluster on autophagosomes regulated by VAMP8', *Cell Death & Disease*, 12(10), pp. 1–10. Available at: https://doi.org/10.1038/s41419-021-04243-0.

Chernomordik, L.V. *et al.* (1998) 'The Pathway of Membrane Fusion Catalyzed by Influenza Hemagglutinin: Restriction of Lipids, Hemifusion, and Lipidic Fusion Pore Formation', *Journal of Cell Biology*, 140(6), pp. 1369–1382. Available at: https://doi.org/10.1083/jcb.140.6.1369.

Choi, S., Houdek, X. and Anderson, R.A. (2018) 'Phosphoinositide 3-Kinase Pathways and Autophagy Require Phosphatidylinositol Phosphate Kinases', *Advances in biological regulation*, 68, p. 31. Available at: https://doi.org/10.1016/j.jbior.2018.02.003.

Choi, W.-I. *et al.* (2021) 'Comparison of the clinical characteristics and mortality of adults infected with human coronaviruses 229E and OC43', *Scientific Reports*, 11(1), p. 4499. Available at: https://doi.org/10.1038/s41598-021-83987-3.

Choi, Y., Bowman, J.W. and Jung, J.U. (2018) 'Autophagy during viral infection — a double-edged sword', *Nature Reviews Microbiology*, 16(6), pp. 341–354. Available at: https://doi.org/10.1038/s41579-018-0003-6.

Corman, V.M. *et al.* (2018) 'Hosts and Sources of Endemic Human Coronaviruses', *Advances in Virus Research*, 100, pp. 163–188. Available at: https://doi.org/10.1016/bs.aivir.2018.01.001.

Cottam, E.M. *et al.* (2011) 'Coronavirus nsp6 proteins generate autophagosomes from the endoplasmic reticulum via an omegasome intermediate', *Autophagy*, 7(11), pp. 1335–1347. Available at: https://doi.org/10.4161/auto.7.11.16642.

Cottam, E.M., Whelband, M.C. and Wileman, T. (2014) 'Coronavirus NSP6 restricts autophagosome expansion', *Autophagy*, 10(8), pp. 1426–1441. Available at: https://doi.org/10.4161/auto.29309.

Croft, M. (2009) 'The role of TNF superfamily members in T-cell function and diseases', *Nature reviews. Immunology*, 9(4), pp. 271–285. Available at: https://doi.org/10.1038/nri2526.

Dagon, Y. *et al.* (2012) 'p70S6 Kinase Phosphorylates AMPK on Serine 491 to Mediate Leptin's Effect on Food Intake', *Cell Metabolism*, 16(1), pp. 104–112. Available at: https://doi.org/10.1016/j.cmet.2012.05.010.

Denison, M.R. and Perlman, S. (1986) 'Translation and processing of mouse hepatitis virus virion RNA in a cell-free system', *Journal of Virology*, 60(1), pp. 12–18. Available at: https://doi.org/10.1128/jvi.60.1.12-18.1986.

Ebel, H., Benecke, T. and Vollmer, B. (2022) 'Stabilisation of Viral Membrane Fusion Proteins in Prefusion Conformation by Structure-Based Design for Structure Determination and Vaccine Development', *Viruses*, 14(8), p. 1816. Available at: https://doi.org/10.3390/v14081816.

Dooley, H.C., Razi, M., Polson, H.E., Girardin, S.E., Wilson, M.I. and Tooze, S.A., 2014. WIPI2 links LC3 conjugation with PI3P, autophagosome formation, and pathogen clearance by recruiting Atg12–5-16L1. *Molecular cell*, *55*(2), pp.238-252.

Durgan, J., Lystad, A.H., Sloan, K., Carlsson, S.R., Wilson, M.I., Marcassa, E., Ulferts, R., Webster, J., Lopez-Clavijo, A.F., Wakelam, M.J. and Beale, R., 2021. Non-canonical autophagy drives alternative ATG8 conjugation to phosphatidylserine. *Molecular Cell*, *81*(9), pp.2031-2040.

Fang, P. *et al.* (2021) 'Functions of Coronavirus Accessory Proteins: Overview of the State of the Art', *Viruses*, 13(6), p. 1139. Available at: https://doi.org/10.3390/v13061139.

Gaunt, E.R. *et al.* (2010) 'Epidemiology and Clinical Presentations of the Four Human Coronaviruses 229E, HKU1, NL63, and OC43 Detected over 3 Years Using a Novel Multiplex Real-Time PCR Method', *Journal of Clinical Microbiology*, 48(8), pp. 2940–2947. Available at: https://doi.org/10.1128/JCM.00636-10.

Gea-Mallorquí, E. (2021) 'Mapping host restriction of SARS-CoV-2', *Nature Reviews Immunology*, 21(1), pp. 3–3. Available at: https://doi.org/10.1038/s41577-020-00482-y.

Gogesch, P. *et al.* (2021) 'The Role of Fc Receptors on the Effectiveness of Therapeutic Monoclonal Antibodies', *International Journal of Molecular Sciences*, 22(16), p. 8947. Available at: https://doi.org/10.3390/ijms22168947.

Gorkhali, R. *et al.* (2021) 'Structure and Function of Major SARS-CoV-2 and SARS-CoV Proteins', *Bioinformatics and Biology Insights*, 15, p. 11779322211025876. Available at: https://doi.org/10.1177/11779322211025876.

Graat, J.M. *et al.* (2003) 'A prospective, community-based study on virologic assessment among elderly people with and without symptoms of acute respiratory infection', *Journal of Clinical Epidemiology*, 56(12), pp. 1218–1223. Available at: https://doi.org/10.1016/S0895-4356(03)00171-9.

Guillén, J. *et al.* (2005) 'Identification of the Membrane-Active Regions of the Severe Acute Respiratory Syndrome Coronavirus Spike Membrane Glycoprotein Using a 16/18-Mer Peptide Scan: Implications for the Viral Fusion Mechanism', *Journal of Virology*, 79(3), pp. 1743–1752. Available at: https://doi.org/10.1128/jvi.79.3.1743-1752.2005.

Hallgren, J. *et al.* (2022) 'DeepTMHMM predicts alpha and beta transmembrane proteins using deep neural networks'. bioRxiv, p. 2022.04.08.487609. Available at: https://doi.org/10.1101/2022.04.08.487609.

Helmy, Y.A. *et al.* (2020) 'The COVID-19 Pandemic: A Comprehensive Review of Taxonomy, Genetics, Epidemiology, Diagnosis, Treatment, and Control', *Journal of Clinical Medicine*, 9(4), p. 1225. Available at: https://doi.org/10.3390/jcm9041225.

Hoffmann, M., Kleine-Weber, H., Schroeder, S., Krüger, N., Herrler, T., Erichsen, S., Schiergens, T.S., Herrler, G., Wu, N.H., Nitsche, A. and Müller, M.A., 2020. SARS-CoV-2 cell entry depends on ACE2 and TMPRSS2 and is blocked by a clinically proven protease inhibitor. *cell*, *181*(2), pp.271-280.

Hooper, K.M., Jacquin, E., Li, T., Goodwin, J.M., Brumell, J.H., Durgan, J. and Florey, O., 2022. V-ATPase is a universal regulator of LC3-associated phagocytosis and non-canonical autophagy. *Journal of Cell Biology*, *221*(6), p.e202105112.

Hm, L., Jw, S. and Ms, D. (2019) 'Shared and Distinct Functions of Type I and Type III Interferons', *Immunity*, 50(4). Available at: https://doi.org/10.1016/j.immuni.2019.03.025.

Huang, X.-Y. *et al.* (2023) 'A pangolin-origin SARS-CoV-2-related coronavirus: infectivity, pathogenicity, and cross-protection by preexisting immunity', *Cell Discovery*, 9(1), pp. 1–13. Available at: https://doi.org/10.1038/s41421-023-00557-9.

Izes, A.M. *et al.* (2020) 'Current status on treatment options for feline infectious peritonitis and SARS-CoV-2 positive cats', *The Veterinary Quarterly*, 40(1), pp. 322–330. Available at: https://doi.org/10.1080/01652176.2020.1845917.

Javorsky, A., Humbert, P.O. and Kvansakul, M. (2021) 'Structural basis of coronavirus E protein interactions with human PALS1 PDZ domain', *Communications Biology*, 4(1), pp. 1–8. Available at: https://doi.org/10.1038/s42003-021-02250-7.

Joubert, P.-E. *et al.* (2015) 'Inhibition of mTORC1 Enhances the Translation of Chikungunya Proteins via the Activation of the MnK/eIF4E Pathway', *PLoS Pathogens*, 11(8). Available at: https://doi.org/10.1371/journal.ppat.1005091.

Judith, D. *et al.* (2023) 'ATG5 selectively engages virus-tethered BST2/tetherin in an LC3C-associated pathway', *Proceedings of the National Academy of Sciences*, 120(20), p. e2217451120. Available at: https://doi.org/10.1073/pnas.2217451120.

Kandasamy, M. (2021) 'NF-κB signalling as a pharmacological target in COVID-19: potential roles for IKKβ inhibitors', *Naunyn-Schmiedeberg's Archives of Pharmacology*, 394(3), pp. 561–567. Available at: https://doi.org/10.1007/s00210-020-02035-5.

Karsli-Uzunbas, G. *et al.* (2014) 'Autophagy is Required for Glucose Homeostasis and Lung Tumor Maintenance', *Cancer discovery*, 4(8), pp. 914–927. Available at: https://doi.org/10.1158/2159-8290.CD-14-0363.

Khaminets, A., Behl, C. and Dikic, I., 2016. Ubiquitin-dependent and independent signals in selective autophagy. *Trends in cell biology*, *26*(1), pp.6-16.

Kim, H., Webster, R.G. and Webby, R.J. (2018) 'Influenza Virus: Dealing with a Drifting and Shifting Pathogen', *Viral Immunology*, 31(2), pp. 174–183. Available at: https://doi.org/10.1089/vim.2017.0141.

Kim, Y.-M. and Shin, E.-C. (2021) 'Type I and III interferon responses in SARS-CoV-2 infection', *Experimental & Molecular Medicine*, 53(5), pp. 750–760. Available at: https://doi.org/10.1038/s12276-021-00592-0.

Kistler, K.E. and Bedford, T. (2021) 'Evidence for adaptive evolution in the receptor-binding domain of seasonal coronaviruses OC43 and 229e', *eLife*, 10, p. e64509. Available at: https://doi.org/10.7554/eLife.64509.

Klionsky, D.J., Abdel-Aziz, A.K., Abdelfatah, S., Abdellatif, M., Abdoli, A., Abel, S., Abeliovich, H., Abildgaard, M.H., Abudu, Y.P., Acevedo-Arozena, A. and Adamopoulos, I.E., 2021. Guidelines for the use and interpretation of assays for monitoring autophagy. *autophagy*, *17*(1), pp.1-382.

Klos, A. *et al.* (2009) 'The Role of the Anaphylatoxins in Health and Disease', *Molecular immunology*, 46(14), pp. 2753–2766. Available at: https://doi.org/10.1016/j.molimm.2009.04.027.

Kuma, A. *et al.* (2002) 'Formation of the ~350-kDa Apg12-Apg5·Apg16 Multimeric Complex, Mediated by Apg16 Oligomerization, Is Essential for Autophagy in Yeast*', *Journal of Biological Chemistry*, 277(21), pp. 18619–18625. Available at: https://doi.org/10.1074/jbc.M111889200.

Kumar, A., Kumar, P., Saumya, K.U. and Giri, R., 2021. Investigating the conformational dynamics of SARS-CoV-2 NSP6 protein with emphasis on non-transmembrane 91–112 & 231–290 regions. *Microbial Pathogenesis*, *161*, p.105236.

Lemmermeyer, T. *et al.* (2016) 'Characterization of monoclonal antibodies against feline coronavirus accessory protein 7b', *Veterinary Microbiology*, 184, pp. 11–19. Available at: https://doi.org/10.1016/j.vetmic.2015.12.009.

Li, A. *et al.* (2023) 'SARS-CoV-2 nsp13 Restricts Episomal DNA Transcription without Affecting Chromosomal DNA', *Journal of Virology*, 97(7), p. e0051223. Available at: https://doi.org/10.1128/jvi.00512-23.

Liang, S. *et al.* (2021) 'Autophagy in Viral Infection and Pathogenesis', *Frontiers in Cell and Developmental Biology*, 9, p. 766142. Available at: https://doi.org/10.3389/fcell.2021.766142.

Littler, D.R. *et al.* (2020) 'Crystal Structure of the SARS-CoV-2 Non-structural Protein 9, Nsp9', *iScience*, 23(7). Available at: https://doi.org/10.1016/j.isci.2020.101258.

Liu, C. *et al.* (2021) 'Cytokines: From Clinical Significance to Quantification', *Advanced Science*, 8(15), p. 2004433. Available at: https://doi.org/10.1002/advs.202004433.

Liu, D.X., Liang, J.Q. and Fung, T.S. (2021) 'Human Coronavirus-229E, -OC43, -NL63, and -HKU1 (Coronaviridae)', *Encyclopedia of Virology*, pp. 428–440. Available at: https://doi.org/10.1016/B978-0-12-809633-8.21501-X.

Lu, R. *et al.* (2020) 'Genomic characterisation and epidemiology of 2019 novel coronavirus: implications for virus origins and receptor binding', *Lancet (London, England)*, 395(10224), pp. 565–574. Available at: https://doi.org/10.1016/S0140-6736(20)30251-8.

Luckheeram, R.V. *et al.* (2012) 'CD4+T Cells: Differentiation and Functions', *Clinical and Developmental Immunology*, 2012, p. 925135. Available at: https://doi.org/10.1155/2012/925135.

Lv, X. *et al.* (2024) 'NSP6 inhibits the production of ACE2-containing exosomes to promote SARS-CoV-2 infectivity', *mBio*, 15(3), pp. e03358-23. Available at: https://doi.org/10.1128/mbio.03358-23.

M, H. *et al.* (2013) 'Autophagosomes form at ER-mitochondria contact sites', *Nature*, 495(7441). Available at: https://doi.org/10.1038/nature11910.

Ma, Y. *et al.* (2015) 'Structural basis and functional analysis of the SARS coronavirus nsp14-nsp10 complex', *Proceedings of the National Academy of Sciences of the United States of America*, 112(30), pp. 9436–9441. Available at: https://doi.org/10.1073/pnas.1508686112.

Madeira, F., Madhusoodanan, N., Lee, J., Eusebi, A., Niewielska, A., Tivey, A.R., Lopez, R. and Butcher, S., 2024. The EMBL-EBI Job Dispatcher sequence analysis tools framework in 2024. *Nucleic acids research*, *52*(W1), pp.W521-W525.

Masters, P.S. (2006) ‘The Molecular Biology of Coronaviruses’, in *Advances in Virus Research*. Academic Press, pp. 193–292. Available at: https://doi.org/10.1016/S0065-3527(06)66005-3.

Mauvezin, C. and Neufeld, T.P., 2015. Bafilomycin A1 disrupts autophagic flux by inhibiting both V-ATPase-dependent acidification and Ca-P60A/SERCA-dependent autophagosome-lysosome fusion. *Autophagy*, *11*(8), pp.1437-1438.

McEwan, D.G. *et al.* (2015) ‘PLEKHM1 regulates autophagosome-lysosome fusion through HOPS complex and LC3/GABARAP proteins’, *Molecular Cell*, 57(1), pp. 39–54. Available at: https://doi.org/10.1016/j.molcel.2014.11.006.

Miguez-Rey, E. *et al.* (2022) ‘Monoclonal antibody therapies in the management of SARS-CoV-2 infection’, *Expert Opinion on Investigational Drugs*, pp. 1–18. Available at: https://doi.org/10.1080/13543784.2022.2030310.

Miller, W.A. and Koev, G. (2000) ‘Synthesis of Subgenomic RNAs by Positive-Strand RNA Viruses’, *Virology*, 273(1), pp. 1–8. Available at: https://doi.org/10.1006/viro.2000.0421.

Najjar-Debbiny, R. *et al.* (2023) ‘Effectiveness of Paxlovid in Reducing Severe Coronavirus Disease 2019 and Mortality in High-Risk Patients’, *Clinical Infectious Diseases: An Official Publication of the Infectious Diseases Society of America*, 76(3), pp. e342–e349. Available at: https://doi.org/10.1093/cid/ciac443.

Nakayama, M. (2014) ‘Antigen Presentation by MHC-Dressed Cells’, *Frontiers in Immunology*, 5, p. 672. Available at: https://doi.org/10.3389/fimmu.2014.00672.

Namy, O. *et al.* (2006) ‘A mechanical explanation of RNA pseudoknot function in programmed ribosomal frameshifting’, *Nature*, 441(7090), pp. 244–247. Available at: https://doi.org/10.1038/nature04735.

Natoli, G. and Ostuni, R. (2019) ‘Adaptation and memory in immune responses’, *Nature Immunology*, 20(7), pp. 783–792. Available at: https://doi.org/10.1038/s41590-019-0399-9.

Neil, S.J.D., Zang, T. and Bieniasz, P.D. (2008) ‘Tetherin inhibits retrovirus release and is antagonized by HIV-1 Vpu’, *Nature*, 451(7177), pp. 425–430. Available at: https://doi.org/10.1038/nature06553.

Neuman, B.W. *et al.* (2011) ‘A structural analysis of M protein in coronavirus assembly and morphology’, *Journal of Structural Biology*, 174(1), pp. 11–22. Available at: https://doi.org/10.1016/j.jsb.2010.11.021.

Nikolaus, J. *et al.* (2011) ‘The Pathway to Membrane Fusion through Hemifusion*’, in L.V. Chernomordik and M.M. Kozlov (eds) *Current Topics in Membranes*. Academic Press, pp. 1–32. Available at: https://doi.org/10.1016/B978-0-12-385891-7.00001-5.

Nutt, S.L. *et al.* (2015) ‘The generation of antibody-secreting plasma cells’, *Nature Reviews. Immunology*, 15(3), pp. 160–171. Available at: https://doi.org/10.1038/nri3795.

Otter, C.J. *et al.* (2024) ‘SARS-CoV-2 nsp15 endoribonuclease antagonizes dsRNA-induced antiviral signaling’, *Proceedings of the National Academy of Sciences*, 121(15), p. e2320194121. Available at: https://doi.org/10.1073/pnas.2320194121.

Peter M., Howley and DM, Knipe (2020) ‘Fields Virology: Emerging Viruses’, *Wolters Kluwer*. Available at: https://www.lww.co.uk/9781975112547/fields-virology-emerging-viruses/ (Accessed: 2 August 2024).

Petersen, E. *et al.* (2020) ‘Comparing SARS-CoV-2 with SARS-CoV and influenza pandemics’, *The Lancet Infectious Diseases*, 20(9), pp. e238–e244. Available at: https://doi.org/10.1016/S1473-3099(20)30484-9.

Plant, E.P. *et al.* (2010) 'Achieving a Golden Mean: Mechanisms by Which Coronaviruses Ensure Synthesis of the Correct Stoichiometric Ratios of Viral Proteins', *Journal of Virology*, 84(9), pp. 4330–4340. Available at: https://doi.org/10.1128/jvi.02480-09.

Platanias, L.C. (2005) 'Mechanisms of type-I- and type-II-interferon-mediated signalling', *Nature Reviews Immunology*, 5(5), pp. 375–386. Available at: https://doi.org/10.1038/nri1604.

Prentice, E. *et al.* (2004) 'Coronavirus Replication Complex Formation Utilizes Components of Cellular Autophagy', *The Journal of Biological Chemistry*, 279(11), pp. 10136–10141. Available at: https://doi.org/10.1074/jbc.M306124200.

Read, J.M. *et al.* (2021) 'Hospital-acquired SARS-CoV-2 infection in the UK's first COVID-19 pandemic wave', *The Lancet*, 398(10305), pp. 1037–1038. Available at: https://doi.org/10.1016/S0140-6736(21)01786-4.

Rock, K.L., Reits, E. and Neefjes, J. (2016) 'Present Yourself! By MHC Class I and MHC Class II Molecules', *Trends in immunology*, 37(11), pp. 724–737. Available at: https://doi.org/10.1016/j.it.2016.08.010.

Rodrigues, T.S. *et al.* (2021) 'Inflammasomes are activated in response to SARS-CoV-2 infection and are associated with COVID-19 severity in patients', *The Journal of Experimental Medicine*, 218(3), p. e20201707. Available at: https://doi.org/10.1084/jem.20201707.

Ruben J. G. Hulswit and et al (2018) *Human coronaviruses OC43 and HKU1 bind to 9-O-acetylated sialic acids via a conserved receptor-binding site in spike protein domain A | PNAS*. Available at: https://www.pnas.org/doi/10.1073/pnas.1809667116 (Accessed: 2 August 2024).

Rus, H., Cudrici, C. and Niculescu, F. (2005) 'The role of the complement system in innate immunity', *Immunologic Research*, 33(2), pp. 103–112. Available at: https://doi.org/10.1385/IR:33:2:103.

Satarker, S. *et al.* (2020) 'JAK-STAT Pathway Inhibition and their Implications in COVID-19 Therapy', *Postgraduate Medicine*, p. 1. Available at: https://doi.org/10.1080/00325481.2020.1855921.

Satarker, S. and Nampoothiri, M. (2020) 'Structural Proteins in Severe Acute Respiratory Syndrome Coronavirus-2', *Archives of Medical Research*, 51(6), pp. 482–491. Available at: https://doi.org/10.1016/j.arcmed.2020.05.012.

Sathe, A. and Cusick, J.K. (2024) 'Biochemistry, Immunoglobulin M', in *StatPearls*. Treasure Island (FL): StatPearls Publishing. Available at: http://www.ncbi.nlm.nih.gov/books/NBK555995/ (Accessed: 3 August 2024).

Schneider, C.A., Rasband, W.S. and Eliceiri, K.W. (2012) 'NIH Image to ImageJ: 25 years of image analysis', *Nature Methods*, 9(7), pp. 671–675. Available at: https://doi.org/10.1038/nmeth.2089.

Schroeder, H.W. and Cavacini, L. (2010) 'Structure and function of immunoglobulins', *The Journal of Allergy and Clinical Immunology*, 125(2 Suppl 2), pp. S41-52. Available at: https://doi.org/10.1016/j.jaci.2009.09.046.

Shah, K. *et al.* (2021) 'T cell receptor (TCR) signaling in health and disease', *Signal Transduction and Targeted Therapy*, 6, p. 412. Available at: https://doi.org/10.1038/s41392-021-00823-w.

Shekhar, R. *et al.* (2021) 'COVID-19 Vaccine Booster: To Boost or Not to Boost', *Infectious Disease Reports*, 13(4), pp. 924–929. Available at: https://doi.org/10.3390/idr13040084.

Sherding, R.G. (2006) ‘Feline Infectious Peritonitis (Feline Coronavirus)’, *Saunders Manual of Small Animal Practice*, pp. 132–143. Available at: https://doi.org/10.1016/B0-72-160422-6/50012-7.

Shi, Y. *et al.* (2024) ‘Mutations accumulated in the Spike of SARS-CoV-2 Omicron allow for more efficient counteraction of the restriction factor BST2/Tetherin’, *PLoS pathogens*, 20(1), p. e1011912. Available at: https://doi.org/10.1371/journal.ppat.1011912.

Sil, P., Muse, G. and Martinez, J. (2018) ‘A ravenous defense: canonical and non-canonical autophagy in immunity’, *Current opinion in immunology*, 50, pp. 21–31. Available at: https://doi.org/10.1016/j.coi.2017.10.004.

Stewart, H. *et al.* (2022) ‘Tetherin antagonism by SARS-CoV-2 enhances virus release: multiple mechanisms including ORF3a-mediated defective retrograde traffic’, *bioRxiv*, p. 2021.01.06.425396. Available at: https://doi.org/10.1101/2021.01.06.425396.

Su, W.-C. *et al.* (2011) ‘Rab5 and Class III Phosphoinositide 3-Kinase Vps34 Are Involved in Hepatitis C Virus NS4B-Induced Autophagy’, *Journal of Virology*, 85(20), p. 10561. Available at: https://doi.org/10.1128/JVI.00173-11.

Suffredini, A.F. *et al.* (1999) ‘New insights into the biology of the acute phase response’, *Journal of Clinical Immunology*, 19(4), pp. 203–214. Available at: https://doi.org/10.1023/a:1020563913045.

Sun, X., Liu, Y., *et al.* (2022) ‘SARS-CoV-2 non-structural protein 6 triggers NLRP3-dependent pyroptosis by targeting ATP6AP1’, *Cell Death and Differentiation*, 29(6), pp. 1240–1254. Available at: https://doi.org/10.1038/s41418-021-00916-7.

Sun, X., Yu, J., *et al.* (2022) ‘SARS-CoV-2 targets the lysosome to mediate airway inflammatory cell death’, *Autophagy*, 18(9), pp. 2246–2248. Available at: https://doi.org/10.1080/15548627.2021.2021496.

Tavares, M.R. *et al.* (2015) ‘The S6K protein family in health and disease’, *Life Sciences*, 131, pp. 1–10. Available at: https://doi.org/10.1016/j.lfs.2015.03.001.

Tekes, G. and Thiel, H.-J. (2016) ‘Feline Coronaviruses’, *Advances in Virus Research*, 96, pp. 193–218. Available at: https://doi.org/10.1016/bs.aivir.2016.08.002.

Thau, L., Asuka, E. and Mahajan, K. (2024) ‘Physiology, Opsonization’, in *StatPearls*. Treasure Island (FL): StatPearls Publishing. Available at: http://www.ncbi.nlm.nih.gov/books/NBK534215/ (Accessed: 2 August 2024).

Torii, S. *et al.* (2016) ‘Identification of PPM1D as an essential Ulk1 phosphatase for genotoxic stress-induced autophagy’, *EMBO Reports*, 17(11), pp. 1552–1564. Available at: https://doi.org/10.15252/embr.201642565.

Tung, Y.-T. *et al.* (2010) ‘The evolutionarily conserved interaction between LC3 and p62 selectively mediates autophagy-dependent degradation of mutant huntingtin’, *Cellular and Molecular Neurobiology*, 30(5), pp. 795–806. Available at: https://doi.org/10.1007/s10571-010-9507-y.

Twu, W.-I. *et al.* (2021) ‘Contribution of autophagy machinery factors to HCV and SARS-CoV-2 replication organelle formation’, *Cell Reports*, 37(8). Available at: https://doi.org/10.1016/j.celrep.2021.110049.

Vidarsson, G., Dekkers, G. and Rispens, T. (2014) ‘IgG Subclasses and Allotypes: From Structure to Effector Functions’, *Frontiers in Immunology*, 5, p. 520. Available at: https://doi.org/10.3389/fimmu.2014.00520.

Virgin, H.W. and Levine, B. (2009) ‘Autophagy genes in immunity’, *Nature immunology*, 10(5), pp. 461–470. Available at: https://doi.org/10.1038/ni.1726.

V'kovski, P. *et al.* (2021) 'Coronavirus biology and replication: implications for SARS-CoV-2', *Nature Reviews Microbiology*, 19(3), pp. 155–170. Available at: https://doi.org/10.1038/s41579-020-00468-6.

Wang, N. *et al.* (2020) 'Subunit Vaccines Against Emerging Pathogenic Human Coronaviruses', *Frontiers in Microbiology*, 11. Available at: https://www.frontiersin.org/articles/10.3389/fmicb.2020.00298 (Accessed: 14 December 2023).

Wang, H., Li, S., Wang, J., Chen, S., Sun, X.L. and Wu, Q., 2018. N-glycosylation in the protease domain of trypsin-like serine proteases mediates calnexin-assisted protein folding. *Elife*, *7*, p.e35672.

Wang, X. *et al.* (2022) 'The role of IL-6 in coronavirus, especially in COVID-19', *Frontiers in Pharmacology*, 13, p. 1033674. Available at: https://doi.org/10.3389/fphar.2022.1033674.

Wang, Y. *et al.* (2016) 'SNARE-mediated membrane fusion in autophagy', *Seminars in Cell & Developmental Biology*, 60, pp. 97–104. Available at: https://doi.org/10.1016/j.semcdb.2016.07.009.

Wang, Y. *et al.* (2020) 'Remdesivir in adults with severe COVID-19: a randomised, double-blind, placebo-controlled, multicentre trial', *Lancet (London, England)*, 395(10236), pp. 1569–1578. Available at: https://doi.org/10.1016/S0140-6736(20)31022-9.

White, J.M. and Whittaker, G.R. (2016) 'Fusion of Enveloped Viruses in Endosomes', *Traffic*, 17(6), pp. 593–614. Available at: https://doi.org/10.1111/tra.12389.

Wiemken, T.L. *et al.* (2023) 'Seasonal trends in COVID-19 cases, hospitalizations, and mortality in the United States and Europe', *Scientific Reports*, 13(1), p. 3886. Available at: https://doi.org/10.1038/s41598-023-31057-1.

Wilson, L., Mckinlay, C., Gage, P. and Ewart, G., 2004. SARS coronavirus E protein forms cation-selective ion channels. *Virology*, *330*(1), pp.322-331.

Wu, J. *et al.* (2021) 'SARS-CoV-2 ORF9b inhibits RIG-I-MAVS antiviral signaling by interrupting K63-linked ubiquitination of NEMO', *Cell Reports*, 34(7), p. 108761. Available at: https://doi.org/10.1016/j.celrep.2021.108761.

Wu, W., Cheng, Y., Zhou, H., Sun, C. and Zhang, S., (2023). The SARS-CoV-2 nucleocapsid protein: its role in the viral life cycle, structure and functions, and use as a potential target in the development of vaccines and diagnostics. *Virology journal*, *20*(1), p.6.

Xia, B., Shen, X., He, Y., Pan, X., Liu, F.L., Wang, Y., Yang, F., Fang, S., Wu, Y., Duan, Z. and Zuo, X., 2021. SARS-CoV-2 envelope protein causes acute respiratory distress syndrome (ARDS)-like pathological damages and constitutes an antiviral target. *Cell research*, *31*(8), pp.847-860.

Xia, H. *et al.* (2020) 'Evasion of Type I Interferon by SARS-CoV-2', *Cell Reports*, 33(1), p. 108234. Available at: https://doi.org/10.1016/j.celrep.2020.108234.

Xie, C.B., Jane-Wit, D. and Pober, J.S. (2020) 'Complement Membrane Attack Complex', *The American Journal of Pathology*, 190(6), pp. 1138–1150. Available at: https://doi.org/10.1016/j.ajpath.2020.02.006.

Xu, Y.Z., Thuraisingam, T., de Lima Morais, D.A., Rola-Pleszczynski, M. and Radzioch, D., 2010. Nuclear translocation of β-actin is involved in transcriptional regulation during macrophage differentiation of HL-60 cells. *Molecular biology of the cell*, *21*(5), pp.811-820.

Yang, L. *et al.* (2021) 'The signal pathways and treatment of cytokine storm in COVID-19', *Signal Transduction and Targeted Therapy*, 6(1), pp. 1–20. Available at: https://doi.org/10.1038/s41392-021-00679-0.

Yewdell, J.W. (2021) 'Antigenic drift: Understanding COVID-19', *Immunity*, 54(12), pp. 2681–2687. Available at: https://doi.org/10.1016/j.immuni.2021.11.016.

Yim, W.W.-Y. and Mizushima, N. (2020) 'Lysosome biology in autophagy', *Cell Discovery*, 6, p. 6. Available at: https://doi.org/10.1038/s41421-020-0141-7.

Youle, R.J. and Narendra, D.P., 2011. Mechanisms of mitophagy. *Nature reviews Molecular cell biology*, *12*(1), pp.9-14.

Zanna, M.Y. *et al.* (2021) 'Review of Dendritic Cells, Their Role in Clinical Immunology, and Distribution in Various Animal Species', *International Journal of Molecular Sciences*, 22(15), p. 8044. Available at: https://doi.org/10.3390/ijms22158044.

Zhang, N. and Bevan, M.J. (2011) 'CD8+ T Cells: Foot Soldiers of the Immune System', *Immunity*, 35(2), pp. 161–168. Available at: https://doi.org/10.1016/j.immuni.2011.07.010.

Zhu, C. *et al.* (2021) 'Molecular biology of the SARs-CoV-2 spike protein: A review of current knowledge', *Journal of Medical Virology*, 93(10), pp. 5729–5741. Available at: https://doi.org/10.1002/jmv.27132.

Ziebuhr, J., Snijder, E.J. and Gorbalenya, A.E. (2000) 'Virus-encoded proteinases and proteolytic processing in the Nidovirales', *Journal of General Virology*, 81(4), pp. 853–879. Available at: https://doi.org/10.1099/0022-1317-81-4-853.